Modeling of V^2 Control with Composite Capacitors And Average Current Mode Control

Feng Yu

Thesis submitted to the Faculty of the Virginia Polytechnic Institute and State University in partial fulfillment of the requirements for the degree of

Master of Science

in

Electrical Engineering

Fred C. Lee, Chairman

Dushan Boroyevich

Paolo Mattavelli

May 2nd, 2011

Blacksburg, Virginia

Keywords: V^2 control, ripple based control, composite capacitors, modeling, describing function, average current mode control

Modeling of V^2 Control with Composite Capacitors And Average Current Mode Control

Feng Yu

Abstract

Various types of current mode control are being used in different applications. Model for current mode control is indispensable for proper system design. Since 1980s, modeling of current mode control has been a hot topic in power electronics field. In current mode control, sub-harmonic oscillation is a common issue, especially for constant frequency current mode control: like peak current mode control, valley current mode control, or average current mode control.

Recently V^2 control is becoming more and more popular due to its simple implementation ad super fast transient response. V^2 control can also run into sub-harmonic oscillation just as current mode control. Efforts have been devoted to modeling of V^2 control.

A common property of different types of current mode control and V^2 control is that they are all multi-loop structures and the inner loops are all highly nonlinear. Due to the nonlinearity of the inner loops, modeling of these structures is extremely difficult. Up to now, there are two main problems which haven't been solved: 1. modeling of average current mode control; 2. modeling of V^2 control with composite capacitors.

This thesis tries to solve these two problems and starts with V^2 control. For V^2 control with single type of bulk capacitors, an accurate model has been proposed

previously. In this thesis, an equivalent circuit model is proposed to get better physical understanding. This method makes use of previous current mode control modeling result and relates V^2 control with current mode control.

To model V^2 control with composite capacitors, capacitor currents and output voltage time domain waveforms are analyzed. Based on describing function method, transfer function from control to output is derived. The modeling result shows that with more parallel ceramic capacitors, system has smaller stability margin.

For average current mode control, the structure is compared with V^2 control. Similarity between the structures of current compensator in average current mode and output capacitor network in V^2 control is identified. V^2 model is utilized for average current mode control. The modeling derivation process is simplified. For the current compensator in average current mode control, it is not desired to have a high frequency pole from stability point of view.

As a conclusion, a circuit model for V^2 control with bulk capacitors is proposed and another two problems are examined: modeling of V^2 control with composite capacitors and modeling of average current mode control. It has been demonstrated that there is similarity between these two structures. The modeling results are verified through simulation and experiments.

Acknowledgements

First I would like to express my sincere gratitude to my advisor, Dr. Fred C. Lee. It is him who leads me into the world of power electronics. I have learned a lot from his extensive knowledge and his rigorous research attitude during the past three years. I can never forget those days of struggling and learning. None of the results showing here would be possible without his help.

I am also grateful to my other committee members: Dr. Dushan Boroyevich and Dr. Paolo Mattavelli. Dr. Boroyevich's incisive view always gives us a hard time and inspires us a lot. For Dr. Mattavelli, I would like to thank you for all the discussions and all the great suggestions.

I would also like to thank all the great staff in CPES: Ms. Teresa Shaw, Ms. Linda Gallagher, Ms. Marianne Hawthorne, Ms. Teresa Rose, Ms Linda Long and Mr. Bob Martin.

It takes courage to be here in CPES and it also takes courage to leave here for the coming future. The last three years was not easy for me because of all the frustrations and all the struggling. I am proud that I make it to this point but I also feel sorry that I cannot stay any longer. It has been such a pleasure to work in Center for Power Electronics Systems (CPES) and it is such an honor to be part of the great family. I would like to thank all the people that have been part of my life: Dr. Ming Xu, Dr. Shuo Wang, Dr. Pengju Kong, Dr. Jian Li, Dr. Julu Sun, Dr. Chuanyun Wang, Dr. Yan Dong, Dr. Dianbo Fu, Dr. Yan Jiang, Dr. Yan Liang, Dr. Rixin Lai, Dr. Honggang Sheng, Dr. Michele Lim, Dr. Di Zhang, Dr. Puqi Ning, Dr. Brian Cheng, Dr. Xiaoyong Ren, Dr. Fang Luo, Mr.

Doug Sterk, Mr. Yi Sun, Mr. Qiang Li, Mr. David Reusch, Mr. Xiao Cao, Mr. Shu Ji, Mr. Igor Cvetkovic, Mr. Zheng Luo, Mr. Pengjie Lai, Mr. Qian Li, Mr. Daocheng Huang, Mr. Zijian Wang, Mr. Zhiyu Shen, Mr. Dong Jiang, Mr. Ruxi Wang, Ms. Zheng Zhao, Ms. Ying Lu, Mr. Dong Dong, Mr. Zheng Chen, Ms Sara Ahmad, Mr. Mingkai Mu, Mr. Haoran Wu, Mr. Yingyi Yan, Mr. Chanwit Prasantanakorn, Ms. Yiying Yao, Mr. Jing Xue, Ms. Zhuxian Xu, Mr. Yipeng Su, Mr. Marko Jaksic, Mr. Milisav Danilovic, Mr. Hemant Bishnoi, Mr. Weiyi Feng, Mr. Bo Wen, Mr. Wei Zhang, Mr. Shuilin Tian, Mr. Li Jiang, Mr Xuning Zhang, Mr. Jin Li, Mr. Pei-Hsin Liu, Mr. Zhiqiang Wang, Mr. Lingxiao Xue, Mr. Yin Wang, Mr. Zhemin Zhang, Mr. Bo Zhou, Mr. Tao Tao.

Last but not least, I want to thank my family, my father Mingquan Yu, my brother Mingrong Wang and my brother Yang Yu. Thank you for the support over these years.

This work was supported by the power management consortium(AcBel Polytech, Chicony Power, Crane Aerospace, Delta Electronics, Emerson Network Power, Huawei Technologies, International Rectifier, Intersil Corporation, Linear Technology, Lite-On Technology, Monolithic Power Systems, National Semiconductor, NXP Semiconductors, Richtek Technology and Texas Instruments), and the Engineering Research Center Shared Facilities supported by the National Science Foundation under NSF Award Number EEC-9731677. Any opinions, findings and conclusions or recommendations expressed in this material are those of the author and do not necessarily reflect those of the National Science Foundation.

This work was conducted with the use of SIMPLIS software, donated in kind by Transim Technology of the CPES Industrial Consortium.

Table of Contents

List of Figures

Chapter 1. Introduction

1.1 Current mode control

Current mode control has been widely used in power converter design for several decades. Current mode control has many advantages over traditional voltage mode control, such as good dynamic performance, inherent current limiting, and current sharing abilities. However, current mode control may run into stability issue: sub-harmonic oscillation. Ever since the born of current mode control, attempts to model current mode control haven't stopped. As early as 1980s, many papers are devoted to the modeling of peak current mode control [1][2][3][4][5][6]. Since then, many modeling approaches have been proposed. Although many industry products have been made and used, further understanding about current mode control is still critical to improve converter design.

The fundamental difference between voltage mode control and current mode control is the PWM modulator. Starting from voltage mode control, as shown in Figure 1.1, a ramp signal is needed to compare with control signal and to decide the switch action instant. In voltage mode control, this ramp signal is coming from an artificial ramp generator. Figure 1.1 gives an example of constant frequency saw-tooth ramp. Usually there is only one loop in voltage mode control.

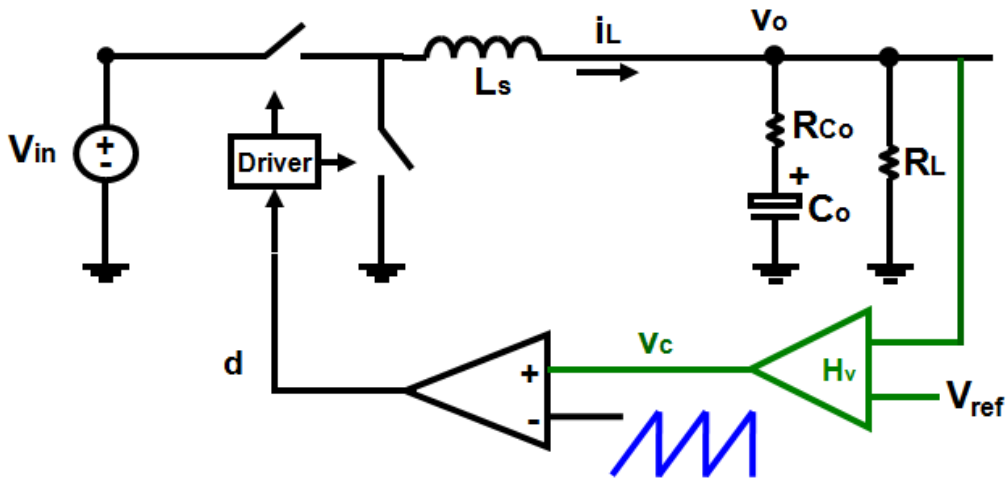

(a)

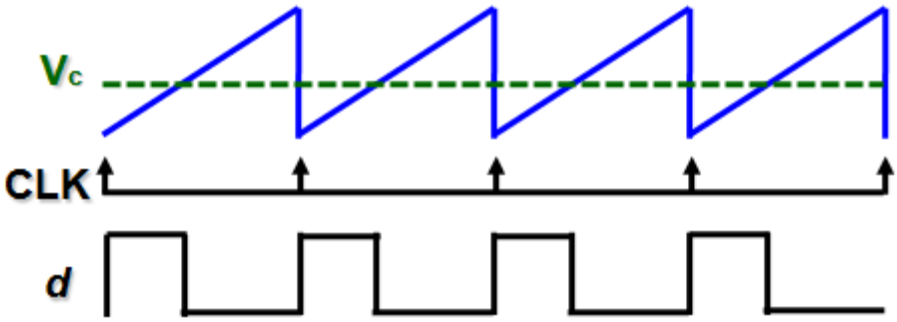

(b)

Figure 1. 1 Voltage Mode Control: (a) control structure (b) modulation principle

As shown in Figure 1.1, in constant frequency voltage mode control, the top switch on instant is triggered by clock signal. The top switch is turned off when the saw-tooth ramp overtakes control signal.

For current mode control, the most widely used structure is peak current mode control. The peak current mode control structure is shown in Figure 1.2.

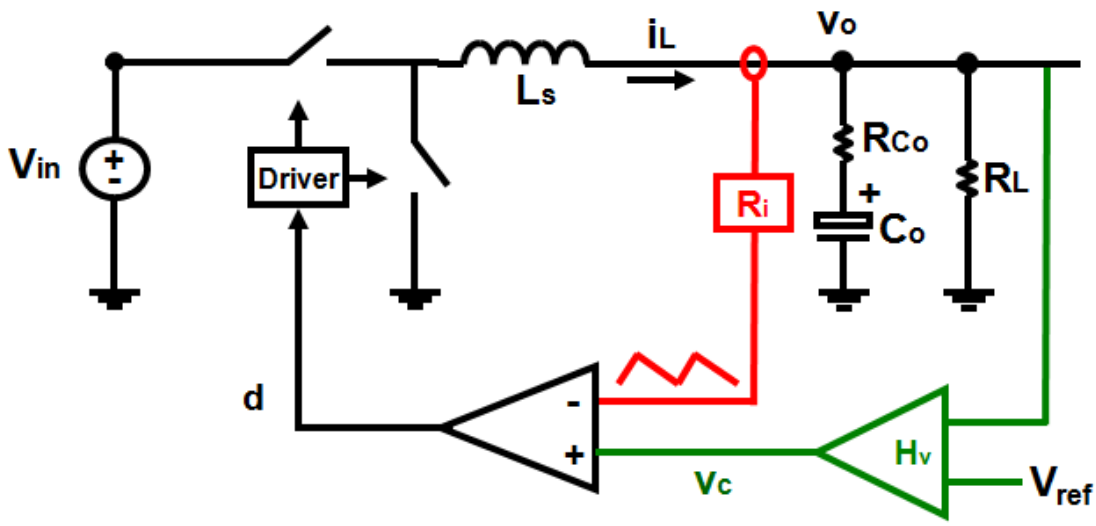

(a)

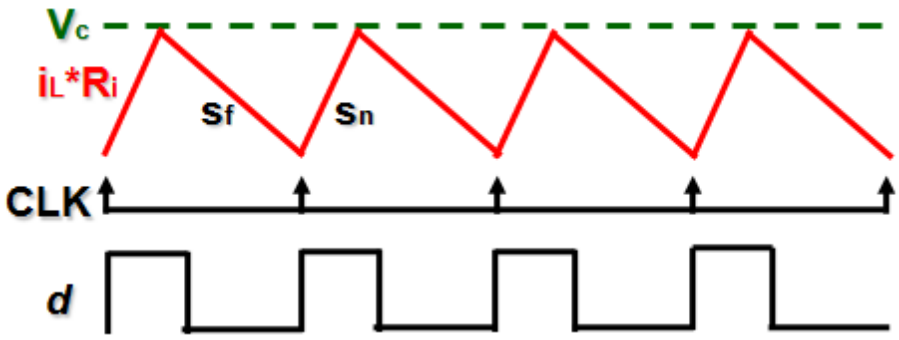

(b)

Figure 1. 2 Peak Current Mode Control: (a) control structure (b) modulation principle

From Figure 1.2, the inductor current is sensed using a proportional gain. Different from voltage mode control, in peak current mode control, the sensed inductor current ramp is used instead of an artificial ramp. The inductor current usually has a triangular waveform. The top switch on instant is also triggered by clock signal. The sensed inductor current waveform is compared with control signal to decide the switch off time

instant. The inductor current feedback is indispensable for the PWM modulator. For current mode control, two-loop structure is generally used. Besides the current loop, another outer voltage loop is needed to regulate the output voltage.

Many different schemes of current mode control have been proposed, including peak current mode control, valley current mode control, constant on-time current mode control, constant off-time current mode control, charge control and average current mode control [8].

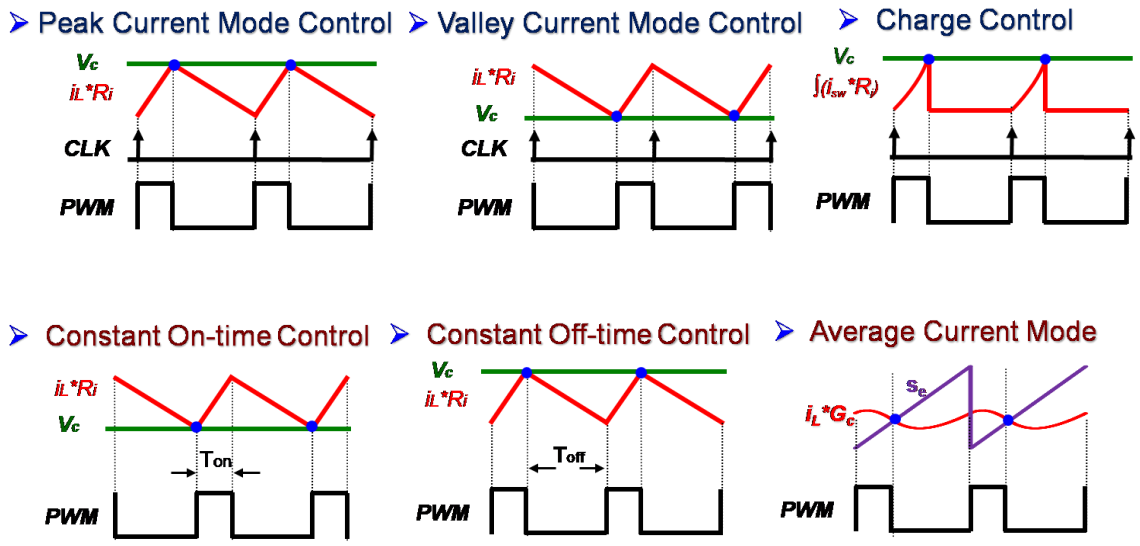

Figure 1. 3 Different modulation schemes of current mode control

For the many current mode control schemes list here, peak current mode, valley current, constant on time and constant off time sense the inductor current using a proportional gain and send the triangular current waveform to the modulator. Charge control and average current mode control manipulate the sensed current information. As shown in Figure 1.3, current waveforms at the input of PWM modulator for charge control or average current mode control are not triangular. For all these current mode

structures, external ramp can be used to increase the ramp signal and hence enhance system stability.

From switching frequency point of view, peak current, valley current and charge control are constant frequency cases; while constant on time and constant off time current mode control are variable frequency cases. For average current mode control, it can be either constant frequency or variable frequency.

For all these current mode control schemes, they have been examined somewhere in history. It is always difficult to model current mode control as the current loop is of high bandwidth and usually is highly nonlinear. In the current feedback loop, all the sideband frequencies as well as switching harmonics are fed back to the PWM modulator. The feedback information of a typical peak current mode control is shown in Figure 1.4.

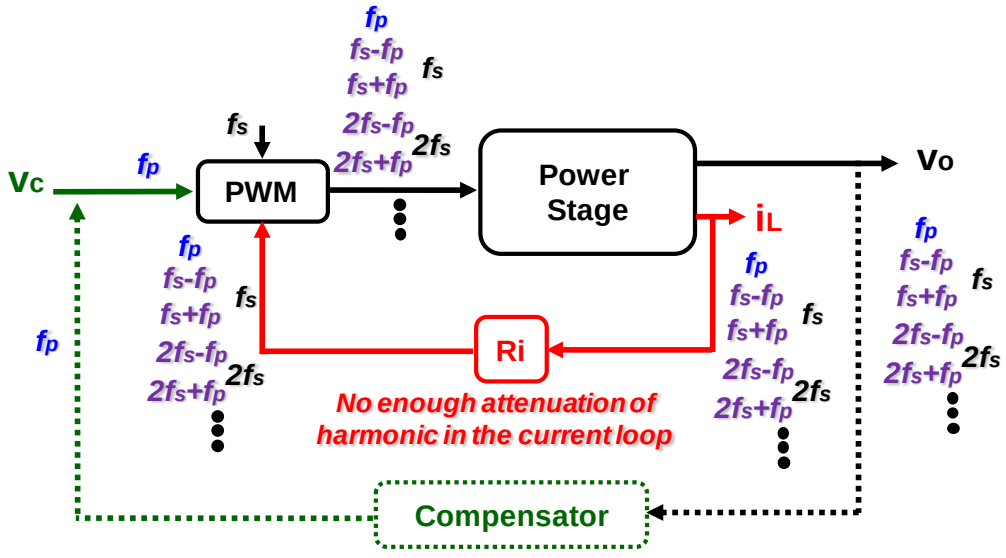

Figure 1. 4 Feedback information in peak current mode control

Due to the switch actions of the PWM modulator, sideband frequencies as well as switching harmonics are generated. All these information will pass through the current

feedback loop and reach the modulator again. The reason why average modeling concept fails is that it only considers the fundamental modulation frequency and ignores all the sideband information.

The most popular model for peak (valley) current mode control is proposed by Dr. R. Ridley in 1990s based on the so called sample and hold concept [9]. The sample and hold term ***He(s)*** is used to capture all the sideband related information and hence to predict the sub-harmonic oscillation. The modeling concept is shown as in Figure 1.5.

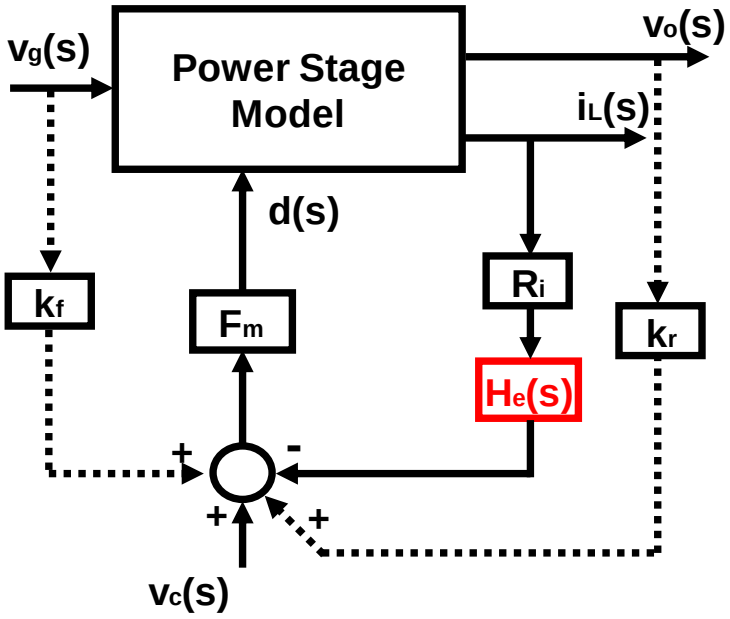

Figure 1. 5 Sample and hold concept in peak current mode control

Dr. Ridley also attempted to model constant on time (off-time) current mode control using the same concept [10]. Later on, the sample and hold concept is inherited and extended to charge control and average current mode control by Dr. Wei Tang [11][12]. However, whether the sample and hold concept can be used in variable frequency modulation and average current mode control is not well justified.

Recently all the previous modeling results are examined with great care from a brand new view angle: time domain describing function method by Dr. Jian Li from CPES, Virginia Tech [13][14]. By using describing function method, all of the structures in Figure 1.3 except average current mode control have been solved perfectly. The results show the limitation of using the sample and hold concept in variable frequency current mode schemes. The describing function method used for peak current mode control is shown as in Figure 1.6.

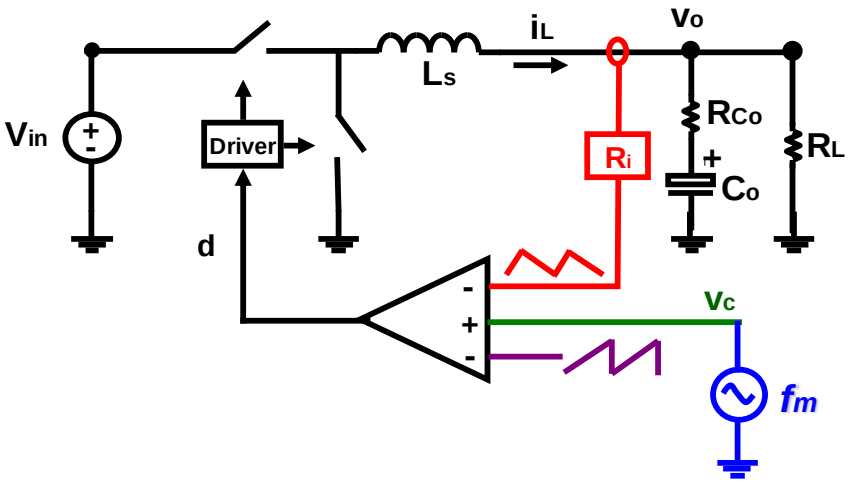

Figure 1. 6 Describing function for peak current mode control

A small signal sinusoidal perturbation is injected at the control signal. Based on the control law, the duty cycle variation as well as the inductor current variation are calculated in time domain. The time domain relation between control signal and inductor current is transferred into frequency domain using Fourier analysis and hence the transfer function can be derived. Describing function method takes account into all the frequency components shown in Figure 1.4.

The modeling results show that in small signal sense the current feedback will turn the converter into a current source with certain impedance. The small signal model is summarized using an equivalent circuit as shown in Figure 1.7.

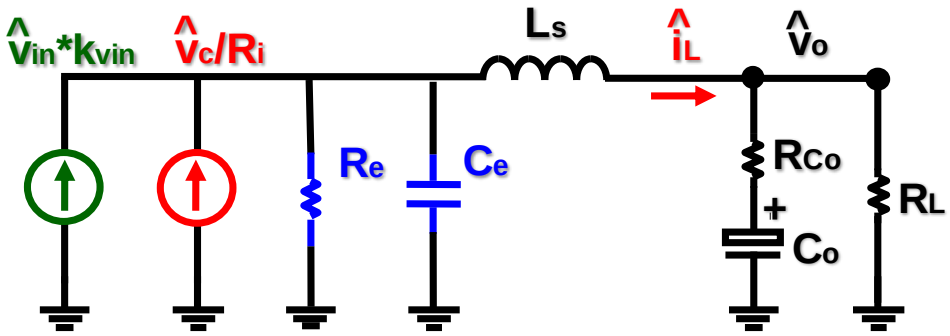

$$k_{vin} = \frac{k_1}{R_i} = \frac{D}{L_s}\left[\frac{1}{Q_2\omega_2} - \frac{T_{off}}{2}\right]$$

$$C_e = \frac{1}{L_s\omega_2^2} = \frac{T_{sw}^2}{L_s\pi^2} \qquad R_e = L_sQ_2\omega_2 = L_s/\left[T_{sw}\left(\frac{s_n + s_e}{s_n + s_f} - 0.5\right)\right]$$

Figure 1. 7 Equivalent circuit for peak current mode control

The equivalent circuit model can be accurate up to switching frequency. The equivalent circuit in Figure 1.7 can be extended to other types of current mode controls by changing the parameters as shown in [14]. However, the work done in [14] still leaves us average current mode control unsolved.

Average current mode control has been widely used for PFC, automotive, battery charger, LED and point of load applications [26][27]. In voltage regulator application, the active droop function to achieve adaptive positioning is also another example of average current mode control. The only difference for active droop function is that the current loop and voltage loop share the same compensator.

The structure of average current mode control is shown as in Figure 1.8. The sensed current information will pass through a compensation network and compare with external ramp to determine the duty cycle.

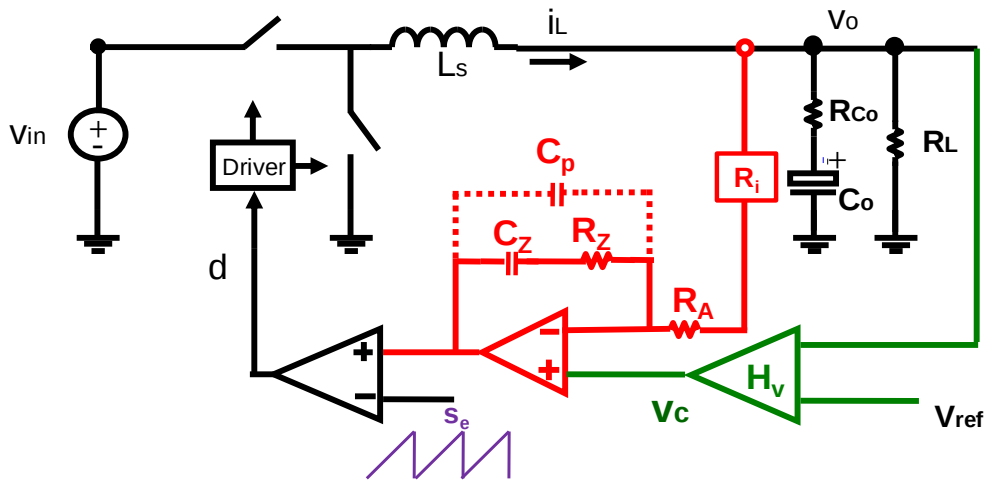

Figure 1. 8 Structure of average current mode control

Many papers have been devoted to the modeling of average current mode control [12][26][43-50]. A simple way of dealing with average current mode control is to treat the current loop similarly as voltage loop in voltage mode control and apply average modeling concept. The average modeling concept assumes that the current compensator works as a good low pass filter so that only the modulation frequency needs to be considered. The modeling concept is shown as in Figure 1.9. This concept is effective only when the current loop bandwidth is relatively low: say below $F_{sw}/5$. When the current loop bandwidth is beyond one third of the switching frequency and approaching half of switching frequency, the current loop is becoming more and more nonlinear. Then the average modeling concept will fail as large amount of current ripple including

switching frequency information and sideband frequency information will remain after the current compensator.

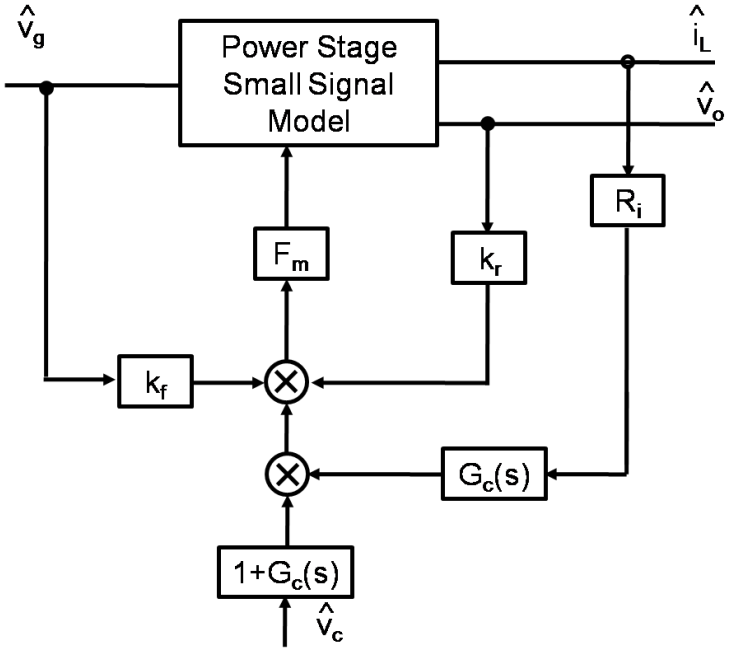

Figure 1. 9 Average modeling concept for average current mode control

However in applications where we need to push the current loop bandwidth by designing the current compensator or reducing the external ramp magnitude, the average modeling concept fails to predict sub-harmonic oscillation in average current mode control.

In the middle 90s, after Dr. R. Ridley proposed the famous sample and hold concept for peak current mode control [9], Dr. Wei Tang applied the sample and hold concept to average current mode control [12]. It is over debate that whether it is valid to use sample hold concept in average current mode control as the current waveform has been greatly changed after the current compensator. The modeling result is also questioned by some other authors [47][48].

The modeling concept in [12] is shown as in Figure 1.10. The sample and hold term is used in the current feedback loop.

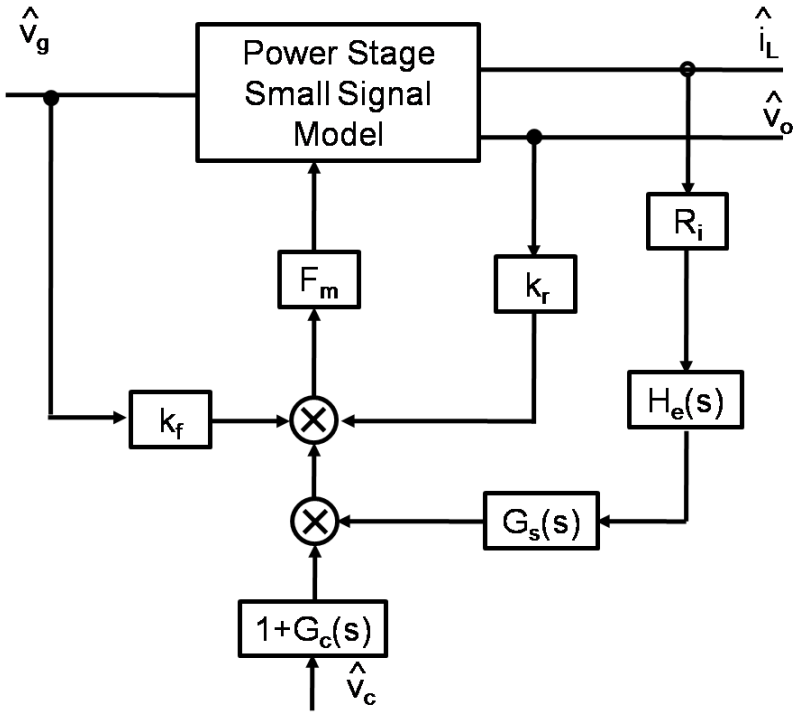

Figure 1. 10 Modeling concept adopting sample and hold term

In Figure 1.10, $G_c(s)$ is the transfer function of the current compensator. For $G_s(s)$, it is the current compensator transfer function without considering the high frequency pole. It was claimed that the high frequency pole will not impact the current feedback loop in [12]. However, this point has been theoretically justified.

The two main drawbacks of this modeling concept are: 1. the sample and hold term is used without justification; 2. the current compensator expression is forced to be different in current loop and in voltage loop.

A good model for average current mode control is indispensable for proper design. This thesis will try to solve average current mode control and complete the modeling work for different current mode control schemes.

1.2 V^2 Control and Ripple Based Control

Recently a structure called V^2 control is gaining more and more attention, especially for low power applications with stringent transient requirement. Main IC companies like Maxim, Texas Instruments, National Semiconductor, Intersil ,Onsemiconductor, International Rectifier etc. are all making similar products [21][22][23][24][25]. This structure is mainly used in point of load application or mobile VR application. In all these applications, simple implementation, no need for compensation and fast transient performance are very important merits.

V^2 control can be implemented as constant frequency modulation or variable frequency modulation. The constant on time V^2 control structure is shown in Figure 1.11. This is an example of V^2 control with single type of output capacitors. Later on, V^2 control with composite output capacitors will be discussed.

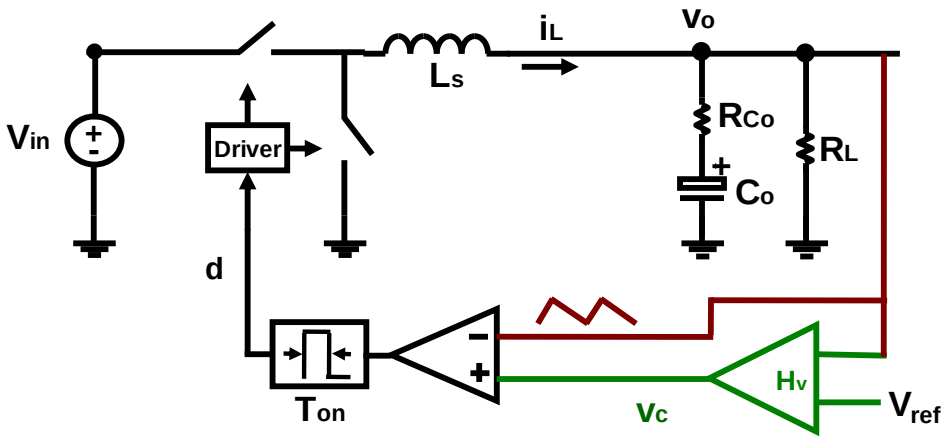

Figure 1. 11 Constant on-time V^2 control

Originally V^2 control is proposed in 1990s to provide ultra-fast transient performance in [15][16]. In V^2 control, the output voltage is used to generate the error signal (control signal) and to work as the ramp signal. There are two voltage feedback loops. The inner loop is a direct voltage feedback loop: the voltage ripple signal is directly fed to the modulator. The outer loop is slower than inner loop: the voltage feedback will go through a compensation network to generate the control signal. As when transient happens, the modulator will directly see the voltage drop over the output capacitor, V^2 control can provide much better transient performance.

Figure 1.12 gives a typical transient waveform of constant on time V^2 control. In Figure 1.12, the top curve is the load current, the middle one is the output voltage while the bottom one is duty cycle. When load current steps, the ESR voltage of the output capacitor will change immediately. The ESR voltage step will also be seen from the PWM comparator so that the duty cycle will also response rapidly. From Figure 1.12, it can be seen the output voltage transient can settle down in around two or three switching cycles.

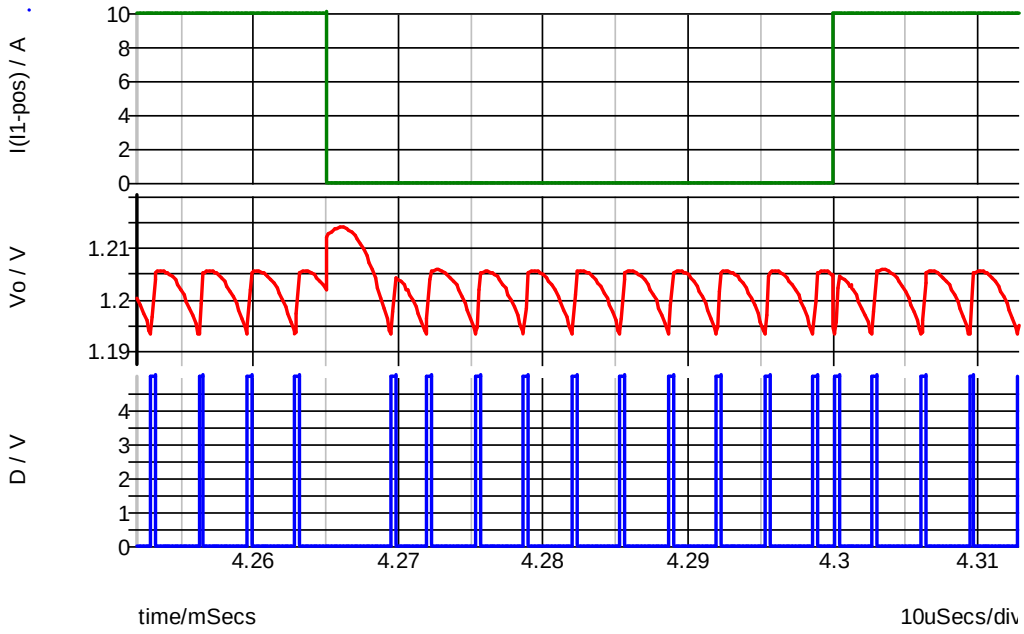

Figure 1. 12 1Typical transient waveform of constant on time V^2 control

In V^2 implementation, the inner voltage feedback contains two parts: ESR voltage and capacitance voltage as shown in Figure 1.13. The ESR voltage as shown is the triangular waveform. It is formed by capacitor current flowing through the ESR of output capacitors. As in DC/DC converters, the load resistor is usually large, almost all of the AC portion of inductor current flows through the output capacitor. So the ESR voltage has similar waveform as inductor current. The other part in Figure 1.13 is the voltage over the pure capacitance. This voltage is formed by integration of the capacitor current over the output capacitance. The ESR ripple and capacitor ripple together form the total output voltage ripple. The switch turning on instant is determined by the intersection of output voltage ripple and control signal as shown in Figure 1.13.

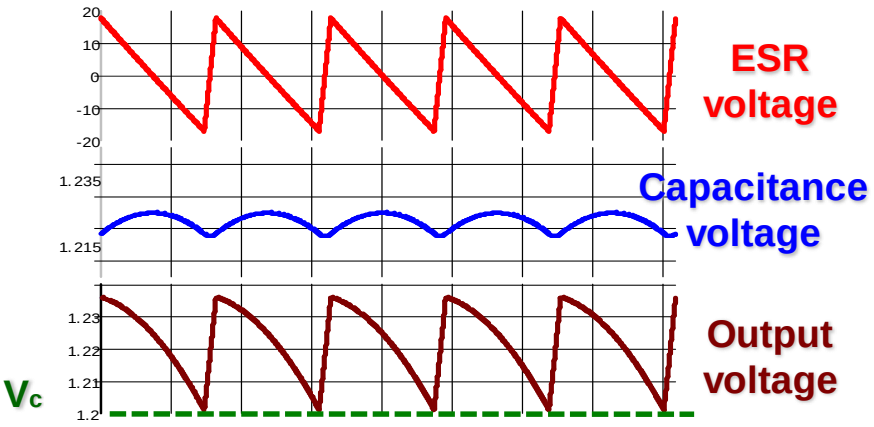

Figure 1. 13 Feedback information of V^2 control

The ESR voltage information is similar as inductor current feedback information in current mode control. However, the additional voltage over the pure capacitance makes V^2 control different from current mode control. As the capacitance voltage is formed by integration of the capacitor current, this waveform contains larger phase lag than the ESR voltage. This is also referred as delay effect of the capacitance voltage. If the capacitance voltage ripple is strong in the total feedback information, the system might be unstable due to the excessive delay. This unstable phenomenon is the so called sub-harmonic oscillation in V^2 control.

For V^2 control with pure ceramic capacitor case, the ESR of the output capacitor is small and capacitance voltage ripple is strong. The excessive delay of capacitance voltage makes the system unstable. Figure 1.14 shows the sub-harmonic oscillation of constant on time V^2 control with ceramic capacitors.

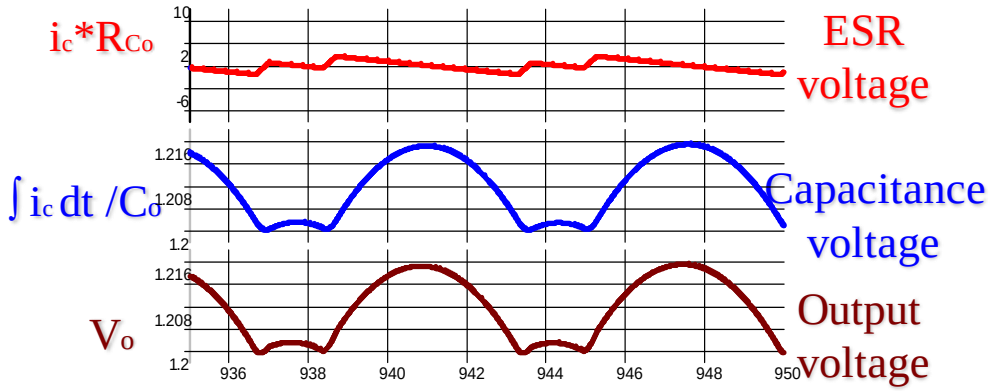

Figure 1. 14 Sub-harmonic oscillation with ceramic capacitors

The early modeling concept for V^2 control always consider V^2 similarly as current mode control and many papers directly adopt the sample and hold term in peak current mode control in the inner voltage feedback loop without further justification [17][18]. However, later on it is realized in industry that the output capacitors characteristic play an important role in system stability. The importance of output capacitor characteristic cannot be fully explained using previous modeling results.

Actually this approach of using sample and hold concept ignores an essential difference between V^2 control and current mode control. In V^2 control, the feedback information (output voltage) is formed by inductor current flowing into output RC network. The output RC network can not only process output power in the power stage but also performs as a low pass filter in the inner voltage feedback loop.

In peak current mode control, there is no low pass filter function in the current loop from inductor current to the input of modulator. The sample and hold term has its origin in the sample data analysis [32]. The sample data analysis is based on discrete time domain describing function. In this modeling approach, all the sideband frequencies are

considered as shown in Figure 1.4. That means the sample and hold in Ridley's model actually includes all the sideband frequencies [9].

When there is a low pass filter in the feedback loop, with certain amount of sideband frequencies attenuated, the sample and hold term cannot be directly used. Moreover, the sample and hold term is usually used in constant frequency case, it is still over debate whether it can be used for variable frequency control [14][30][31].

Recently Dr. Jian Li used the describing function method to handle the V^2 control model [14][19]. The modeling concept will be further explained in Chapter 2. The modeling result gives the relation between control signal and output voltage. This result reveals the effect of output capacitor characteristic and is very accurate and easy to use.

V^2 control is an example of ripple based control with two voltage feedback loops. A close relative of V^2 control is even more popular. The structure is shown in Figure 1.15.

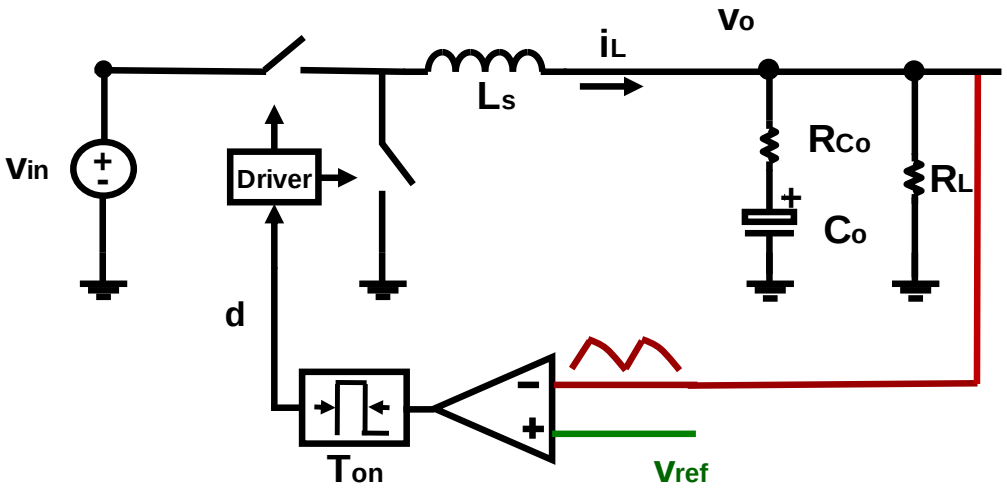

Figure 1. 15 Ripple based control: constant on-time control

In this structure, output voltage is fed back to the modulator and compared with the reference voltage. It is even simpler than V^2 control due to the lack of outer voltage loop. This ripple based control structure is often referred as constant on time control if constant on time modulation scheme is used [20][23]. All the benefits of V^2 control are kept except that this structure will introduce a steady state voltage error which is related with half of output voltage switching ripple. Previous Jian Li's modeling result [14][19] can also be applied to this structure. The previous control signal to output voltage relation is now reference voltage to output voltage relation in this structure. The stability criterion is the same.

V^2 control or constant on time control are both examples of ripple based control. The output voltage ripple works as the ramp signal at the input of modulator comparator. It's important to keep certain amount of ripple magnitude and certain slope magnitude for proper duty cycle determination. When the slope at the decision point is smaller, the system has a greater chance to run into instability. That also means for V^2 control (or constant on time control), the output capacitor should have relatively large ESR to get the desired slope rate.

In industry, it is common practice to parallel certain amount of high quality ceramic capacitors together with output bulk capacitors. The ceramic capacitor branch can effectively reduce the output impedance. The output voltage ripple will be much smaller. However, smaller output voltage ripple is not necessarily good for the whole system when ripple based control is used. In V^2 control, the ceramic capacitor branch reduces the feedback signal magnitude and may cause problem. Figure 1.16 shows the structure of V^2

control with composite output capacitors. R_{C1} and C_{o1} are ESR and capacitance of bulk capacitors and R_{C2} and C_{o2} are ESR and capacitance of the ceramic capacitors.

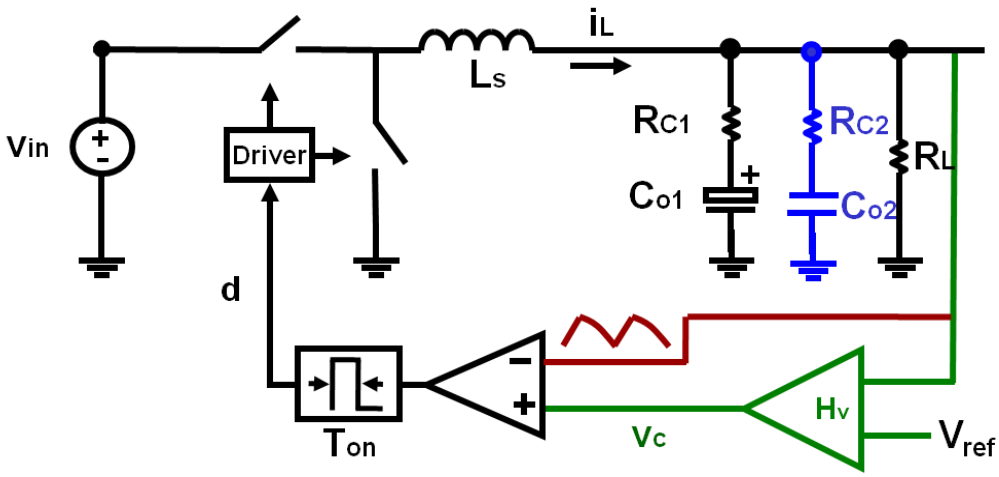

Figure 1. 16 V^2 control with composite output capacitors

It is noticed that for V^2 control, with more ceramic capacitance in parallel, the originally stable system may run into subharmonic oscillation. Examples are shown in Figure 1.17. The one with too many ceramic capacitors runs into oscillation. That means the additional ceramic branch will change the small signal behavior of the system.

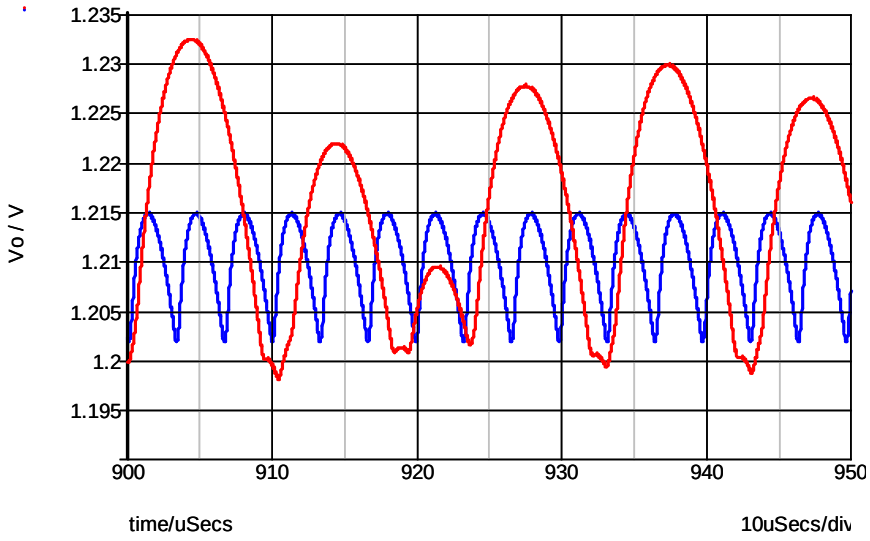

Figure 1. 17 Output voltage ripple (Blue curve: R_{c1}=3mΩ, C_{o1}=660μF, R_{C2}=100mΩ, C_{o2} =300μF; Red curve: R_{c1} =3mΩ, C_{o1}=660μF, R_{C2}=33mΩ, C_{o2}=900μF)

With certain amount of ceramic capacitors in parallel, the feedback information of output voltage is changed. Still looking at the voltage over the bulk capacitors, the feedback information also contains two parts: ESR voltage and capacitor voltage. However, the waveforms of these two parts are totally different from previous single type of output capacitor case. The time domain waveforms are shown in Figure 1.18.

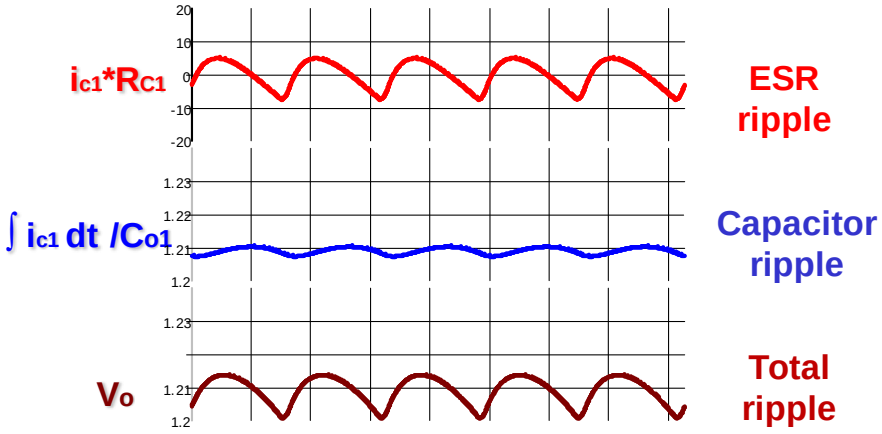

Figure 1. 18 Voltage waveforms of the bulk capacitor

Comparing Figure 1.18 with Figure 1.13, we can see the capacitor current flowing through the same bulk capacitor branch is changed. Not only the total ripple magnitude is smaller but also the slope at the switch action decision point (end of off time) is smaller. So the small signal behavior for composite capacitors is changed.

Previously Dr. Jian Sun employs the Krylov-Bogoliubov-Mitropolsky (KBM) ripple estimation technique to solve the model for current mode control and V^2 control [31][37]. For V^2 control with single type capacitors, this modeling method looks into the detail of output voltage time domain waveform. A time domain equation of duty ratio constraint relates duty cycle and control signal. Based on perturbation and linearization of the duty ratio constraint, small signal model can be derived. However, the transfer function from control signal to output voltage is complicated and a stability criterion hasn't been provided in explicit form.

The KBM method can also be used to solve V^2 control with composite output capacitors. As the KBM method of recovering switching ripple is very complicated, to simplify the calculation, the composite output capacitor network is simplified as in Figure 1.19. The bulk capacitors are modeled with their ESR and the ceramic capacitors are modeled with their pure capacitance. Certain amount of accuracy has been lost due to this approximation. Moreover, simplified transfer function and stability criterion haven't been provided. This makes the modeling result very uneasy to use.

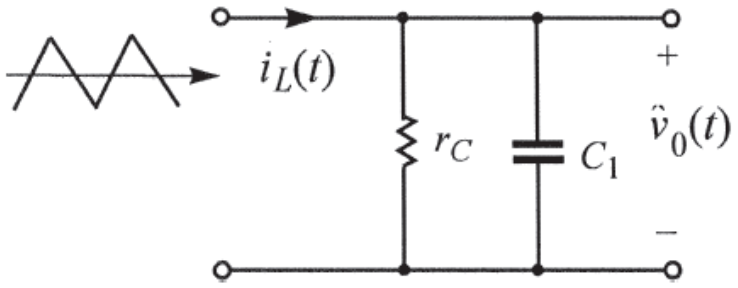

Figure 1. 19 Simplified composite output capacitor network

Up to now no good model has been provided for V^2 control with composite capacitors. This gives us new challenge for modeling this structure of V^2 control with composite capacitors. By adding another ceramic capacitor branch the modeling complexicity is increased dramatically. This thesis will try to tackle the problem in Chapter 3.

1.3 Thesis Outline

For all the existing current mode alike control methods, sub-harmonic oscillation is a potential problem. Modeling of these control methods is indispensable for proper design. With the development of modeling technique, most of the control structures have been solved and well understood with only a few exceptions. This thesis tries to solve two of the remaining problems which haven't been fully solved: V^2 control and average current mode control. Chapter 1 introduces these two control methods.

For V^2 control with single type of output capacitors, previously a very accurate model based on describing function method has been proposed [19]. In Chapter 2, this structure is examined from a different angle. The inner voltage loop feedback information

is separated into two parts and treated one by one. The final result is in an equivalent circuit form which is much easier to use. The relation between V^2 control and current mode control is explained using the circuit model. The limitations of the modeling concept are also explained.

For V^2 control with composite output capacitors, no mature model has been established. It is important to predict the instability problem caused by adding parallel ceramic capacitor branch. Detailed modeling process based on describing function method is shown in Chapter 3. The additional ceramic capacitor branch will form a current divider circuit with original bulk capacitor branch. The effect of previous bulk capacitor ESR is reduced and hence the stability margin is decreased. An additional high frequency pole is also introduced by the additional capacitor branch.

Average current mode control is widely used in various applications. By looking into the time domain waveforms, similarity between average current mode control and V^2 control is discovered and utilized. Previous modeling result for V^2 control is applied to average current mode control. Two commonly used current compensation structures are discussed in Chapter 4. Accurate model for average current mode control is derived for the first time. From the modeling result, the high frequency pole of the current compensator will decrease system stability margin.

Chapter 5 summarizes the conclusions and proposes ideas for future work.

Chapter 2. Circuit Model for V^2 Control with Bulk Capacitors

2.1 Previous Model for V^2 Control

Describing function method is widely used for modeling of nonlinear systems [33][34][35]. Recently V^2 control is modeled based on describing function method by Dr. Jian Li [14][19]. In order to capture the nonlinearity of the system, the power stage as well as the inner voltage feedback is considered as a single entity. So the feedback loop concept is gone. Based on this modeling concept, we cannot examine the inner voltage loop gain for V^2 control. The modeling concept is shown as in Figure 2.1. A small signal sinusoidal perturbation is injected at the control signal, and the time domain output voltage variation is calculated. After we get the time domain relation between control signal perturbation and output voltage variation, the time domain relation is transferred into frequency domain using Fourier analysis.

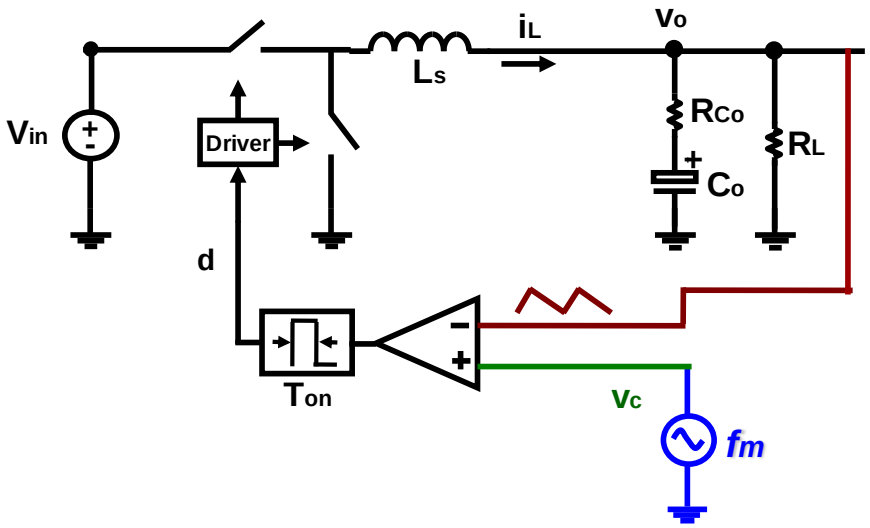

Figure 2. 1 Modeling concept based on describing function method

The describing function method considers all the frequency components in the inner voltage feedback loop. So the final result is very accurate. The accuracy of transfer function without any simplification is not limited by switching frequency. The frequency components considered by describing function are shown in Figure 2.2.

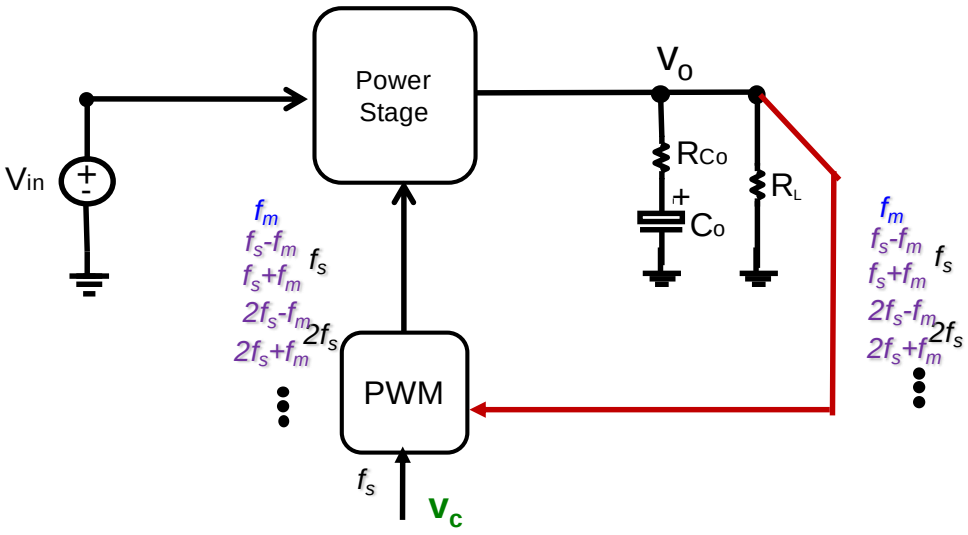

Figure 2. 2 Frequency components considered in describing function method

The final transfer function from control signal to output voltage can be simplified into polynomial form and a stability criterion is provided. The modeling result reveals that the RC time constant of the output capacitors plays a critical role for system stability. The control signal to output voltage transfer function for constant on-time V^2 control is:

$$\frac{v_o(s)}{v_c(s)} = \frac{R_{Co}C_o s + 1}{1 + \frac{s}{Q\omega_2} + \frac{s^2}{\omega_2^2}} \tag{2.1}$$

In which $Q = T_{sw} / [(R_{Co}C_o - T_{on}/2)\pi]$, $\omega_2 = \pi / T_{sw}$.

The stability criterion is to maintain a positive quality factor, so that all the eigenvalues of the characteristic equation will be in the left half plane. The critical condition for stability is $R_{Co}C_o > T_{on}/2$, which clearly shows the influence of the output capacitor characteristic.

Based on equation (2.1), the control to output transfer function has a double pole located at half of the switching frequency. The Q factor is not only related to the on-time T_{on} but also related to capacitor parameters. The critical condition $R_{Co}C_o > T_{on}/2$ reflects the interaction between the ESR and the capacitance of the output capacitors. It means that those two parameters must be considered at the same time. When the switching frequency is F_{sw} =300 kHz, and duty cycle is D≈0.1, the parameters of the OSCON capacitors (560μF/6mΩ) meet the critical condition. So the system is stable. However, the parameters of the ceramic capacitors (100μF/1.4mΩ) cannot meet the critical condition, so sub-harmonic oscillation happens.

The control signal to output voltage transfer function is verified using Simplis simulation in Figure 2.3. The parameters for the simulation setup is: switching frequency F_{sw} =300kHz, duty cycle D=0.1. The simplified model in equation (2.1) can be accurate above half of switching frequency. The effect of output capacitors is shown in Figure 2.4, in which it is clearly shown smaller RC time constant will introduce higher peaking indicating smaller stability margin.

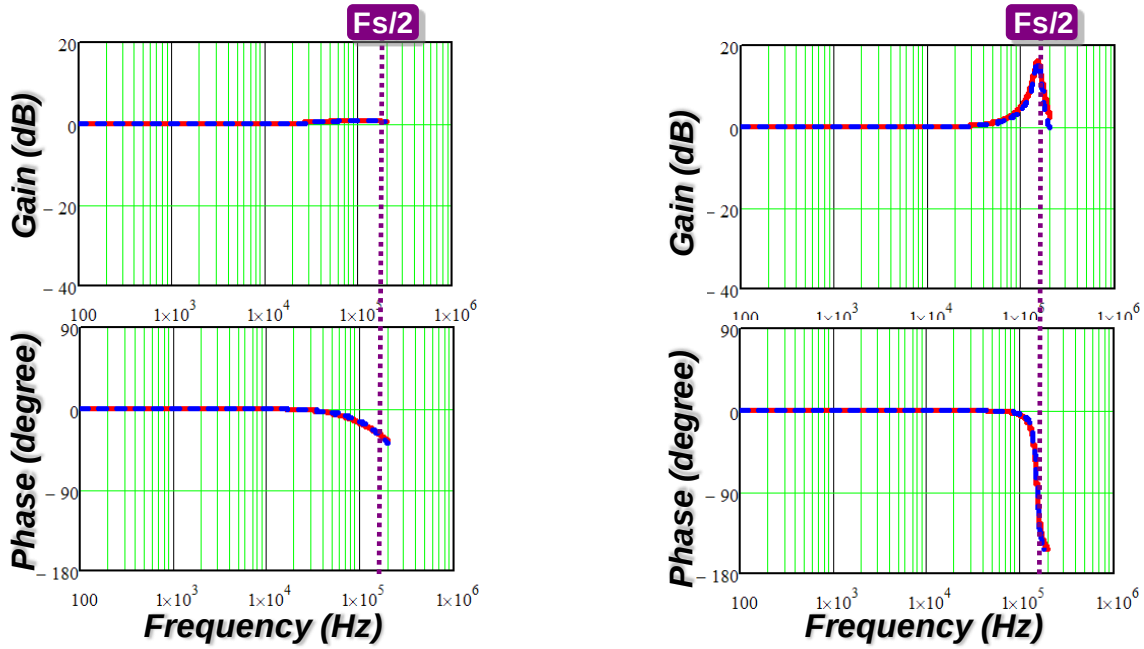

(a) (b)

Red curve: Model; Blue curve: Simplis simulation

Figure 2. 3 Control to output transfer function comparison: (a) output capacitor (560µF/6mΩ), (b) output capacitor (56µF/6mΩ)

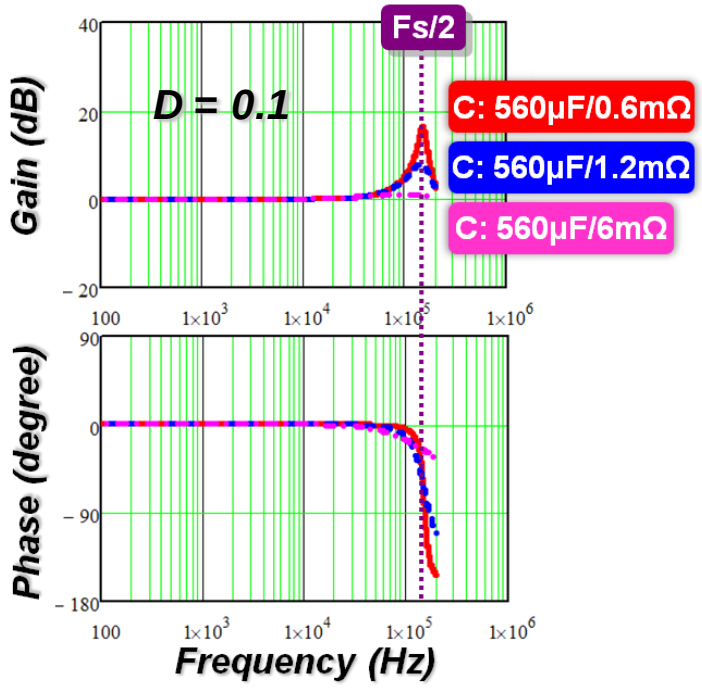

Figure 2. 4 Control to output voltage transfer function comparison

As shown in Figure 2.3, based on describing function method, very accurate small signal transfer function can be derived. The describing function method is a quite general modeling approach and is not limited by control methods or modulation schemes. It can apply to current mode control or V^2 control. The power stage and the inner feedback loop are considered together as a "black box". Although we can see the similarity between the feedback waveforms of current mode control and V^2 control, this modeling approach treats them individually. The relation between V^2 and current mode control is unrevealed.

2.2 Proposed Simplified Circuit Model

This chapter tries to model V^2 control from a different angle. The new proposed modeling method tries to separate different information in the inner voltage feedback loop and treat them separately [36]. As stated before, the inner voltage feedback

information includes two parts as shown in Figure 2.5 (same as Figure 1.13). The ESR voltage ripple contains the AC inductor current information which is more nonlinear comparing with capacitance voltage information. As the ESR voltage information is actually current information feedback, previous current mode control modeling result can be used. As the capacitance voltage is formed by inductor current flowing through a low pass filter, the capacitance voltage loop is considered using average modeling concept and only the fundamental modulation frequency is considered.

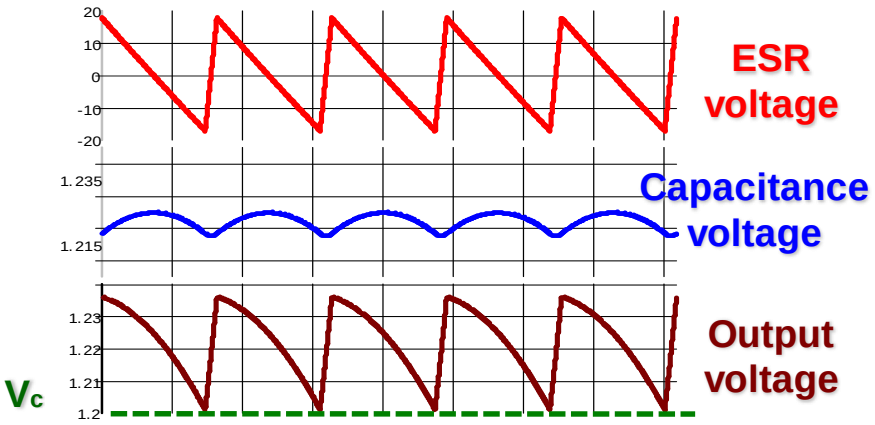

Figure 2. 5 Feedback information of V^2 control

The concept of separating feedback information is shown in Figure 2.6. This section is based on constant on time V^2 control example. However, the modeling concept can also be applied to constant frequency V^2 control.

In Figure 2.6 the structure (b) is equivalent to the original V^2 structure (a). Based on structure (b) the original V^2 inner loop is separated into two loops. The first one is AC inductor current feedback loop with a sensing gain equal to ESR of output capacitors; the second loop is capacitance voltage feedback loop. Of course the original outer voltage loop still remains.

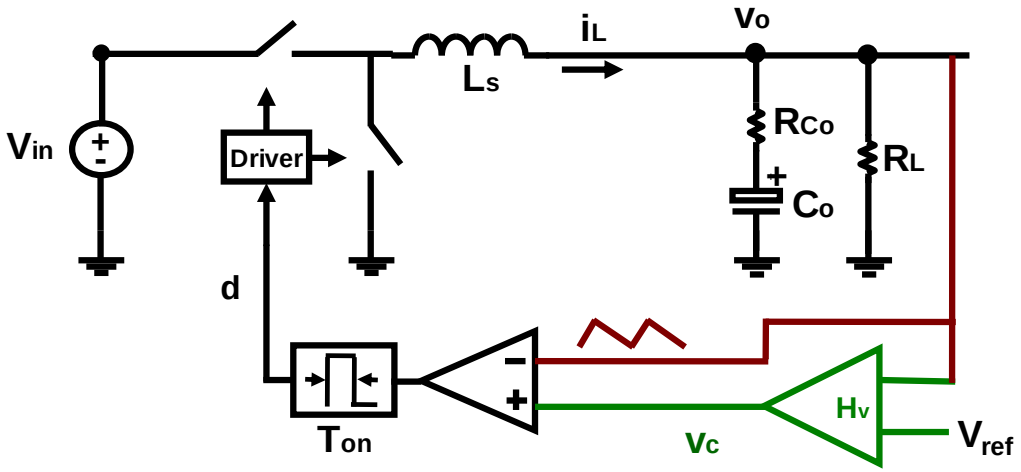

(a)

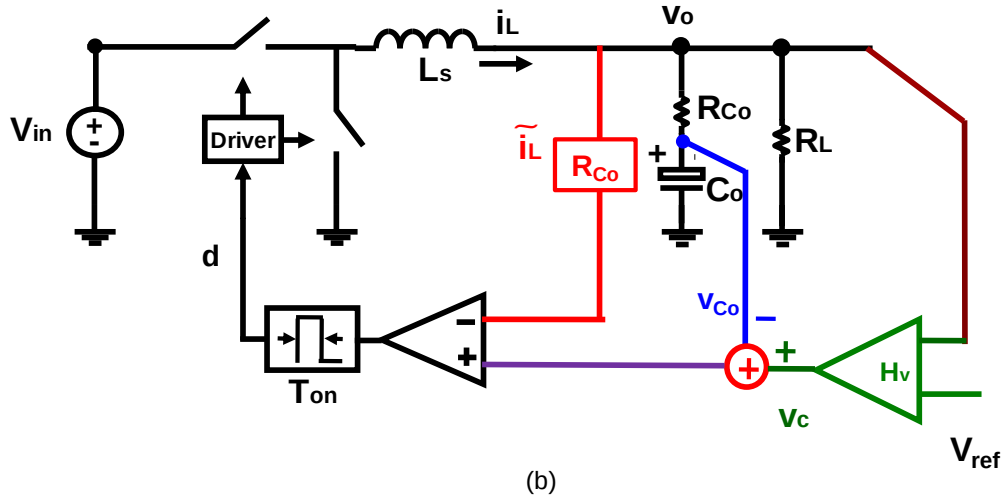

(b)

Figure 2. 6 (a):Original V^2 structure (b) Separation of inner voltage feedback information

The two parts of different information in the voltage feedback loop can be handled differently. The ESR voltage ripple which is a triangular waveform contains a lot of frequency information, including switching frequency, switching harmonics, modulation frequency and sideband frequencies. All these frequency components should be considered to capture the high frequency characteristic. Comparing with ESR voltage

ripple, the capacitance voltage ripple is less nonlinear, because the waveform is nearly sinusoidal as shown in Figure 2.5. The reason is that the transfer function from inductor current to capacitor voltage actually has a low pass filter function. When the output capacitor has a relatively low frequency ESR zero, the switching frequency, switching harmonics as well as sideband frequencies are highly damped. For simplicity we only consider one component which is the modulation frequency in the capacitance voltage information. Then we can use average concept to get the loop gain of capacitance voltage feedback. The frequency components considered in this modeling concept is shown in Figure 2.7.

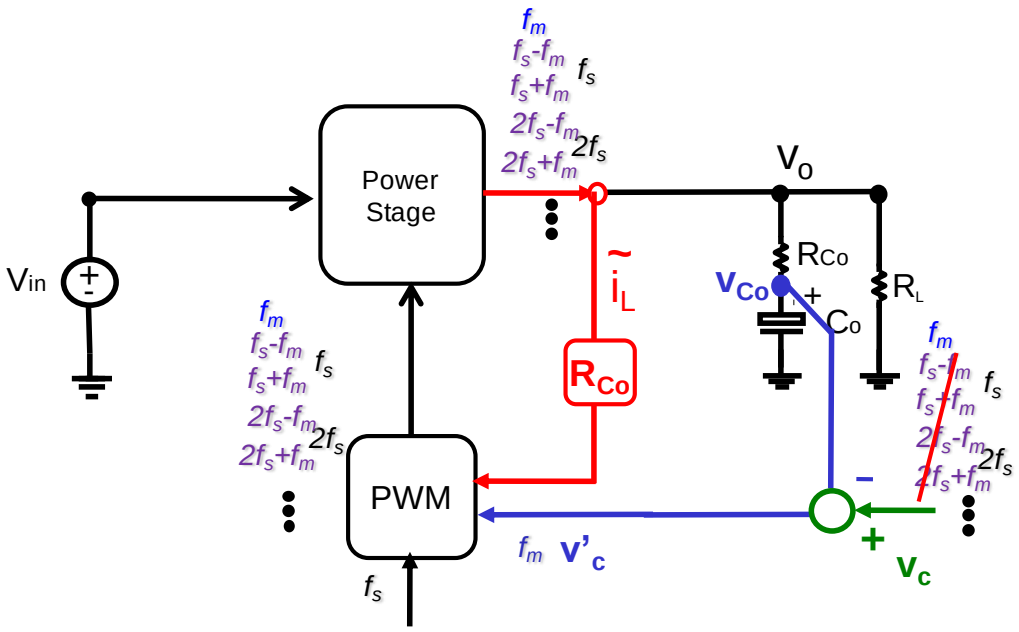

Figure 2. 7 Frequency components in different feedback loops (only f_m is considered in capacitor voltage feedback loop; valid up to half of switching frequency)

Comparing with Figure 2.2, the new modeling concept as shown in Figure 2.7 is an approximation which ignores some information especially in the capacitance voltage

feedback loop. This approximation is good only under certain conditions. That is when we have a good low pass filter in the capacitance voltage feedback loop. The switching frequency ripple ignored in the capacitance voltage feedback loop actually will impact the PWM modulator gain. By ignoring the switching frequency ripple, the modulator gain we use is larger than it is supposed to be. On the other hand, the sideband frequencies will impact the high frequency behavior for the capacitance voltage feedback loop. By ignoring the sideband frequencies in the capacitance voltage feedback loop, the final result will show less phase drop than real case. However, with bulk capacitors with relatively low ESR zero, the approximations are reasonable. The modeling concept cannot be applied to ceramic capacitor case. it is only good for OSCON cap, SP cap or POS cap cases. By recognizing the limit of this modeling concept, we can make full use of the simplified model as well as gain enough accuracy for our design purpose.

As shown in Figure 2.6, we can first consider the AC inductor current feedback loop and then consider the capacitance voltage feedback loop. For the AC inductor current feedback loop, the feedback information is the same as current mode control "SCM" implementation [2]. Previous modeling result for current mode control can be borrowed for the inner AC current feedback loop. For the outer capacitance voltage feedback loop, loop gain model is very easy to get based on average modeling concept.

2.2.1 Equivalent Circuit for Current Mode Control

The proposed modeling concept considers the inner voltage feedback as two separate loops. For the AC inductor current feedback loop, previous modeling result for current mode control can be used. Among many modeling approaches for current mode control,

equivalent circuit model can give us better physical meaning and necessary accuracy. This section will review previous equivalent circuit models for current mode control.

The easiest equivalent circuit model is based on the "current source" concept [1]. Based on this concept, the inductor current is treated as a well-controlled current source as shown in Figure 2.8. Figure 2.8 gives an example of peak current mode control. Actually this concept cannot differentiate different current mode control modulation schemes. The circuit model in Figure 2.8 (b) is also applicable for constant on-time current mode control case.

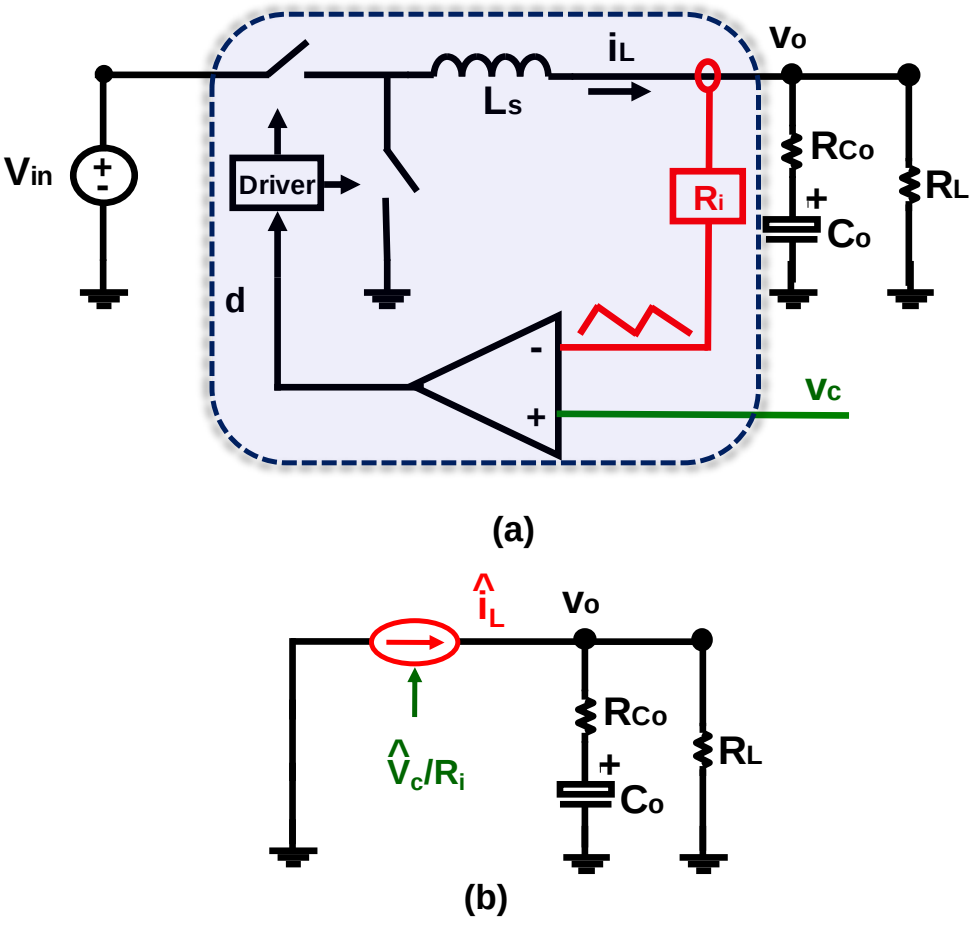

Figure 2. 8 "Current source" concept for current mode control

The "current source" concept provides very good insight to power supply designers. However, this model is too simple to predict sub-harmonic oscillations.

To further improve this equivalent circuit model, paper [13] gives a more accurate circuit model. The equivalent circuit is shown as in Figure 2.9 (same as Figure 1.7).

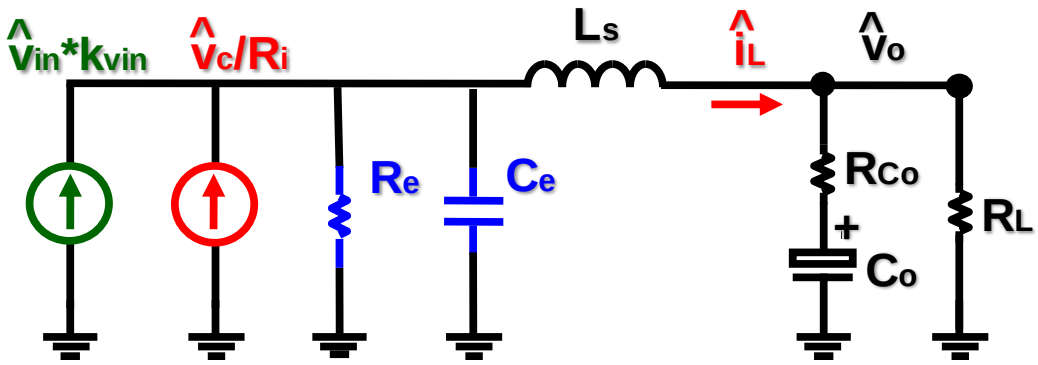

Figure 2. 9 Equivalent circuit model for current mode control (valid up to switching frequency)

Comparing with Figure 2.8, the new proposed equivalent model takes into account of the perturbation coming from input voltage. Moreover, two components are added in parallel with the controlled current source. The parameters of the two components are used to describe the high frequency effect of the transfer function. In high frequency range, based on different modulation schemes and different external ramp magnitude, C_e can possibly resonance with inductor L_s and form a double pole. Figure 2.9 shows that for current mode control. previous "current source " concept is modified. The effect of current loop is equivalent to controlling the inductor current as a current source with a certain impedance.

The equivalent circuit can be used for constant frequency current mode control or variable frequency current mode control based on different R_e and C_e parameters. The parameters are listed as below in Table 2.1:

Constant on-time control	Constant off-time control
$R_e = L_s Q_1 \omega_1$	$R_e = L_s Q_1 \omega_3$
$C_e = 1/(L_s \omega_1^2)$	$C_e = 1/(L_s \omega_3^2)$
$k_{vin} = \frac{T_{on}}{2L_s}$	$k_{vin} \approx 0$
Constant frequency peak current-mode control	Constant frequency valley current-mode control
$R_e = L_s Q_2 \omega_2$	$R_e = L_s Q_2' \omega_2$
$C_e = 1/(L_s \omega_2^2)$	$C_e = 1/(L_s \omega_2^2)$
$k_{vin} = \frac{D}{L_s}[\frac{1}{Q_2 \omega_2} - \frac{T_{off}}{2}]$	$k_{vin} = \frac{D}{L_s}[\frac{1}{Q_2' \omega_2} + \frac{T_{off}}{2}]$

Table 2. 1 Parameters for current mode equivalent circuit

In Table 2.1, $Q_1=2/\pi$, $Q_2=1/\{\pi[(s_n+s_e)/(s_n+s_f)-0.5]\}$, $Q'_2=1/\{\pi[(s_f+s_e)/(s_n+s_f)-0.5]\}$, $\omega_1 =\pi/T_{on}$, $\omega_2 = \pi/T_{sw}$, $\omega_3 = \pi/T_{off}$.

2.2.2 Equivalent Circuit Model for V^2 Control

When we only consider the AC current information feedback in V^2 control, we can see the control law is the same as current mode control. The comparison is shown in Figure 2.10 and Figure 2.11.

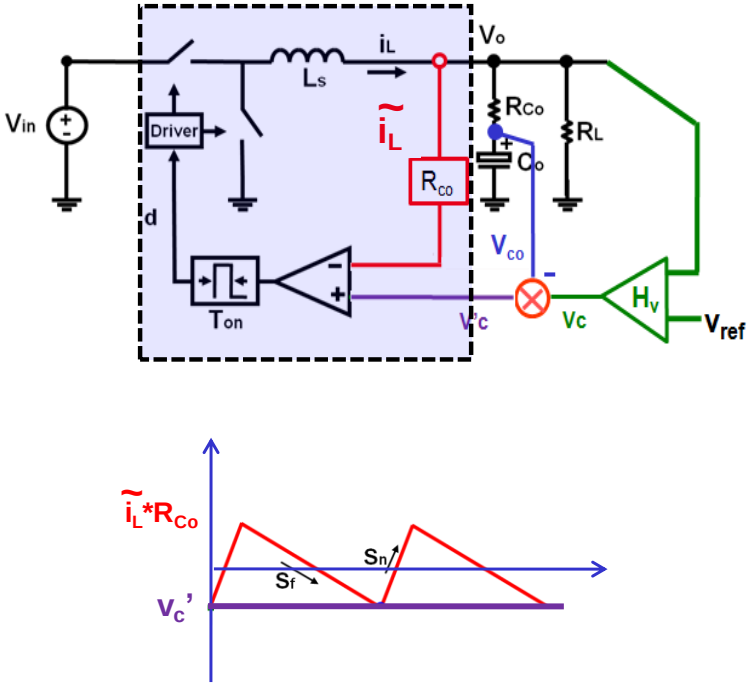

Figure 2. 10 AC inductor current feedback in V^2 control

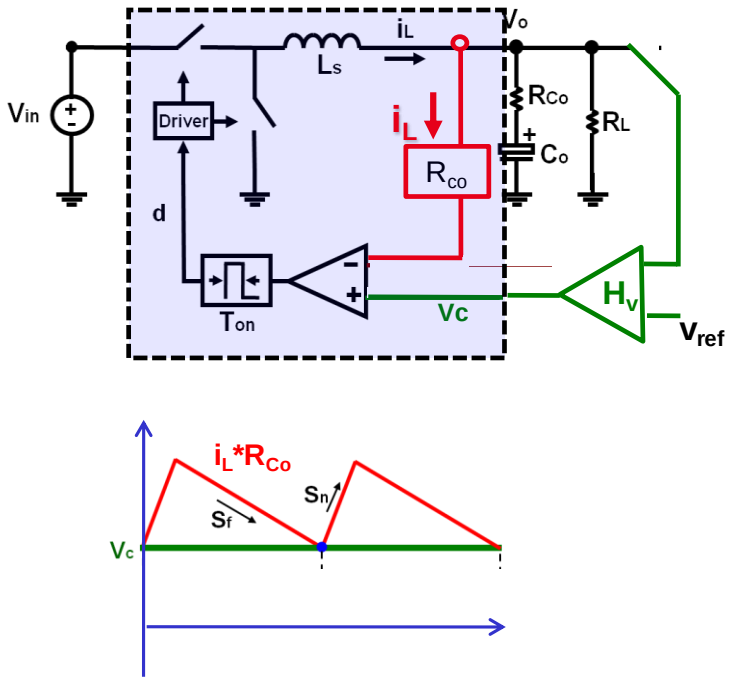

Figure 2. 11 Inductor current feedback in current mode control

In V^2 control, we consider capacitance voltage is a slow varying waveform, then it can be combined together with output voltage loop compensator output v_c , and form a new control voltage v_c' to control the AC inductor current feedback as shown in Figure 2.10.

Comparing Figure 2.10 and Figure 2.11, in the two shaded areas, the only difference is that in current mode control we feedback not only AC current but also DC current. Nevertheless, the DC offset will not impact the small signal behavior. So we can directly use previous current mode control modeling result for V^2 control inner current feedback. We plug in the small signal equivalent circuit in Figure 2.9 into V^2 structure. The result is shown as in Figure 2.12, which gives an equivalent circuit for V^2 control. Based on this structure we can see actually V^2 control can be considered as current mode control with a

direct voltage feedback loop from capacitance voltage. However, we should remember, this is an approximation by ignore high frequency sideband information in the capacitance voltage feedback loop as shown in Figure 2.7.

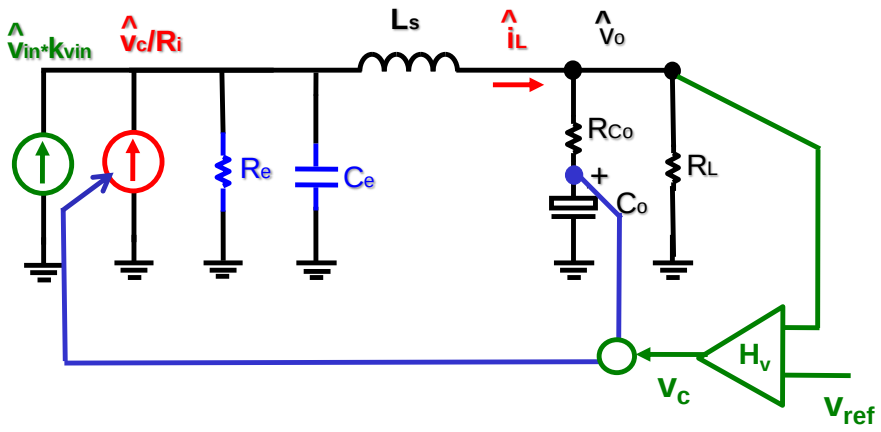

Figure 2. 12 Equivalent circuit model for V^2 control (valid up to half of switching frequency)

The equivalent circuit in Figure 2.12 is suitable for various V^2 modulation schemes based on the parameters shown in Table 2.1.

As mentioned before, the approximation for the capacitance voltage loop is justified with a low pass filter, which means the ESR zero frequency of the output capacitor should not be very high. That means the model can apply to output capacitors with large ESR like OSCON capacitor, SP cap, or POS cap cases when the switching frequency is in several hundred kHz range. Based on the equivalent circuit for V^2 control, we can easily get the loop gain model for capacitance voltage feedback.

For constant on-time V^2 control example,

$$T(s) = \frac{i_L(s)}{v_c(s)} \cdot \frac{v_{Co}(s)}{i_L(s)}$$

$$\approx \frac{1}{R_{Co}} \cdot \frac{1}{1 + \frac{s}{Q_1 \omega_1} + \frac{s^2}{\omega_1^2}} \cdot \frac{R_L}{(R_L + R_{Co}) C_o s + 1} \tag{2.2}$$

where,

$$Q_1 = \frac{2}{\pi}, \quad \omega_1 = \frac{\pi}{T_{on}}.$$

When we consider applications where duty cycle is relatively small, so the double pole in equation (2.2) is at very high frequency. As load resistor is much larger than ESR of output capacitors, we can further simplify loop gain transfer function as

$$T(s) \approx \frac{1}{R_{Co} C_o s} \tag{2.3}$$

So the bandwidth for capacitance voltage feedback loop actually is very simple.

$$BW \approx \frac{1}{R_{Co} C_o} \tag{2.4}$$

By simplified the capacitance voltage feedback loop transfer function, we can see bandwidth for this loop is predetermined by the output capacitor time constant. For OSCON capacitors the bandwidth is around 50kHz; for SP cap the bandwidth can be around or higher than 60kHz. In both cases the bandwidth is much lower than half of the switching frequency when the system runs at frequencies of several hundreds of kHz.

That means the outer voltage loop does work as a low pass loop and attenuate all the switching frequencies and sideband frequencies.

For a given example, the switching frequency is chosen as 300kHz and the duty cycle is 0.1. With OSCON output capacitors, the OSCON capacitor parameters are: R_{Co}=6mΩ, C_o =560μF. The ESR zero of the output capacitors is around 47kHz. Simplis simulation of the capacitor voltage feedback loop is shown as in Figure 2.13. The simulation indicates that the crossover frequency is around the ESR zero position. It is also shown that around the crossover frequency, we still have around 90° phase margin. So this loop is very stable. There is no sub-harmonic issue for constant on-time V^2 control with OSCON capacitors. For SP capacitors, similar conclusion can be made.

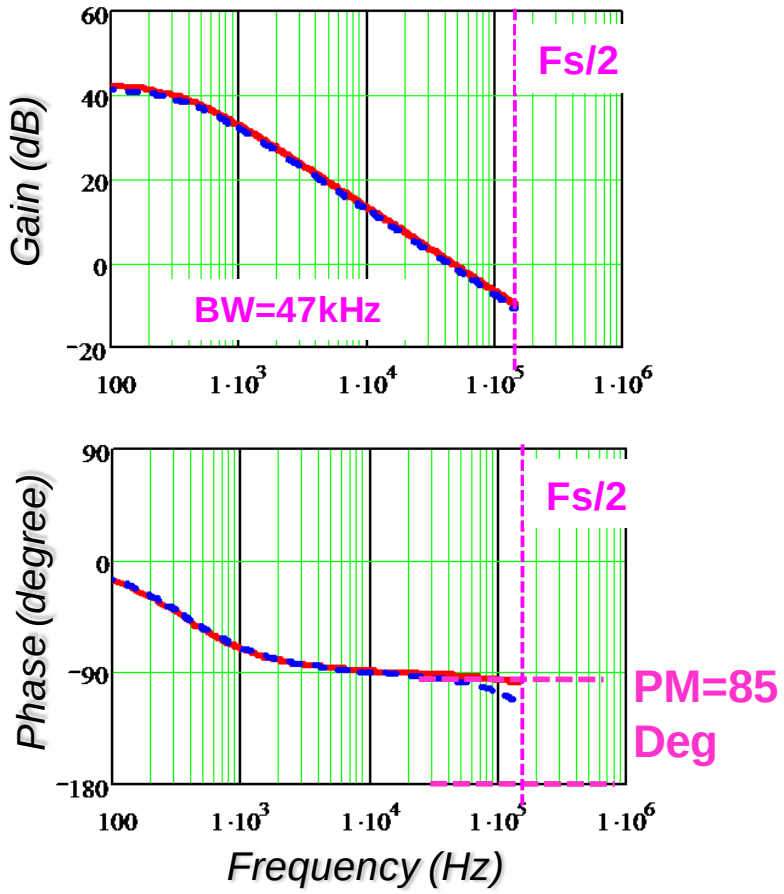

Figure 2. 13 Capacitance voltage loop gain verification

Based on the equivalent circuit as shown in Figure 2.12, control signal to output voltage transfer function with capacitance voltage loop closed can be easily derived.

$$\frac{v_o(s)}{v_c(s)} = \frac{G_{c2vo}(s)}{1+T(s)} \tag{2.5}$$

in which $G_{c2vo}(s)$ is the transfer function from control to output with capacitance voltage loop open. We can compare the difference of $G_{c2vo}(s)$ and $T(s)$. The difference

between these two actually is the transfer function from output voltage v_o to capacitor voltage v_{co}.

$$G_{c2vo}(s) = \frac{1}{R_{Co}} \cdot \frac{1}{1 + \frac{s}{Q_1 \omega_1} + \frac{s^2}{\omega_1^2}} \cdot \frac{R_L (R_{Co} C_o s + 1)}{(R_L + R_{Co}) C_o s + 1} \tag{2.6}$$

Figure 2.14 is used to compare the bode plots of $G_{c2vo}(s)$ and $T(s)$.

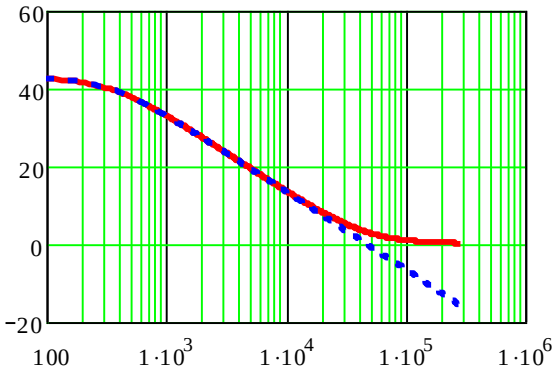

—Red: open loop control to output voltage G_{c2vo}

---Blue: Capacitor voltage feedback loop gain T

Figure 2. 14 Bode plot comparison of G_{c2vo} and T

From Figure 2.14, it is shown that at low frequency when T is far larger than 1, denominator and numerator are the same. So equation (2.5) equals to 1. At high frequency, T will be very small, so equation (2.5) equals to G_{c2vo} and also equals to 1 as shown in Figure 2.14. Equation (2.5) can be simplified as below:

$$\frac{v_o(s)}{v_c(s)} \approx \frac{R_L(R_{Co}C_o s+1)}{R_{Co}[(R_L+R_{Co})C_o s+1]+R_L} \approx 1 \tag{2.7}$$

The Simplis simulation verification is shown in Figure 2.15.

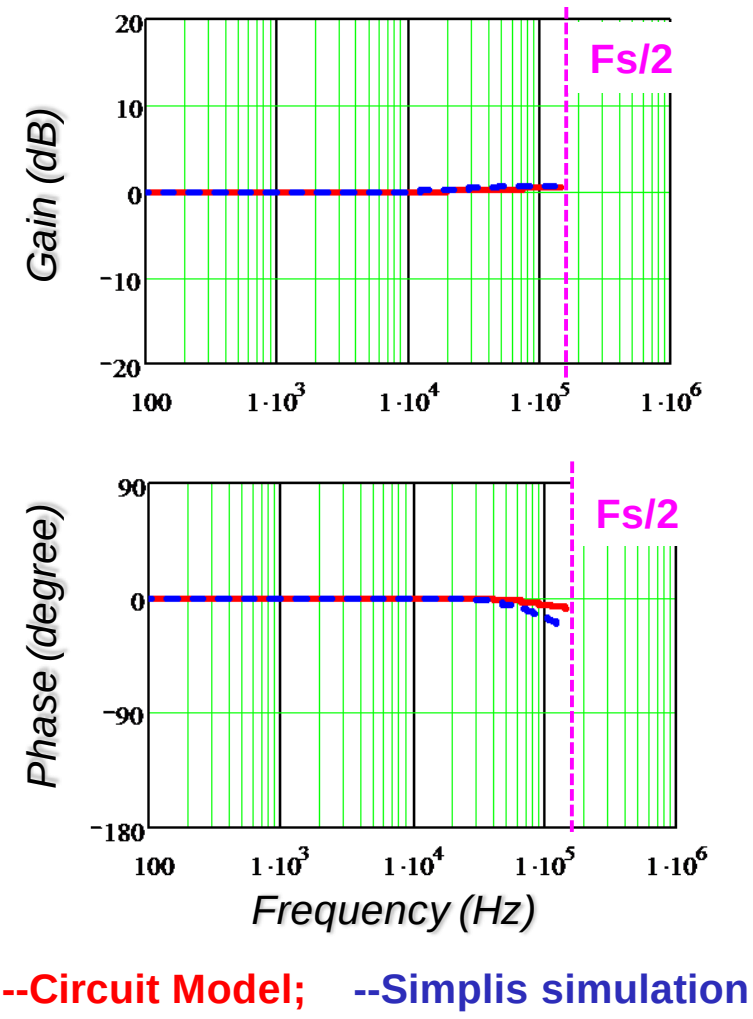

Figure 2. 15 Control to output voltage verification

From Figure 2.13, we can notice that around high frequency range, simulation result shows larger phase drop. However, the difference is very small and will not impact practical design. The phase difference is because the simplified circuit model ignores the

impact of high frequency sideband information which can introduce additional phase drop.

As aforementioned, the equivalent circuit can only be applied to capacitors with low ESR zero. That is because with low ESR zero type of output capacitor, the capacitor voltage feedback loop bandwidth is low so that high frequency sideband information can be ignored as shown in Figure 2.7.

If the loop gain model of equation (2.2) is applied to ceramic capacitors, the capacitor voltage feedback loop gain is shown as below:

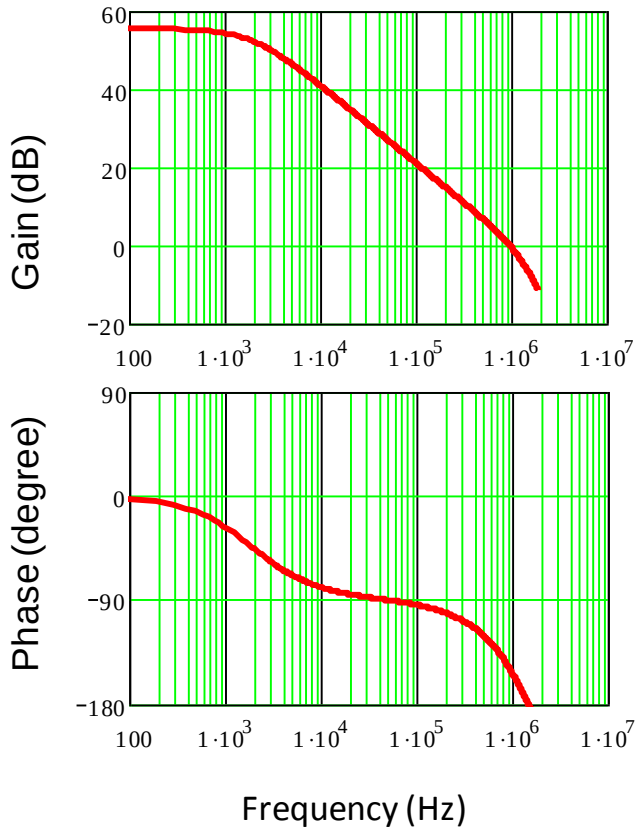

Figure 2. 16 Modeling concept used for ceramic capacitors

The result shows that the bandwidth of ceramic capacitor voltage feedback loop is above the switching frequency. This indicates that the modeling concept will fail and the approximation in Figure 2.7 cannot be used for ceramic capacitors.

2.3 Summary

A circuit model for V^2 control with bulk capacitors is proposed based on the concept of separating inner voltage feedback information. The proposed circuit model makes use of previous circuit model for current mode control and is applicable for different V^2 modulation schemes. The capacitance voltage feedback information is treated using a unit voltage feedback loop. This circuit model relates V^2 control with current mode control. The proposed circuit model is straightforward and easy to use. Modeling results are verified using Simplis simulation.

Chapter 3. Modeling of V^2 Control with Composite Capacitors

3.1 Benefit of Composite Capacitors

For V^2 control structure, different modulation schemes can be used, like constant frequency V^2 control including peak voltage mode control and valley voltage mode control; variable frequency V^2 control including constant on-time V^2 control and constant off-time V^2 control [20]. Among these four schemes, constant frequency peak voltage mode control and constant on-time V^2 control are the two most popular structures. For all these V^2 type structures, sub-harmonic oscillation may happen. It has been discovered that the time constant of output capacitors plays an important role in stabilizing the system [14][19]. It is often required that the output capacitor should have relatively large ESR, or in another word, relatively large time constant [19][37][38]. This requirement has been shown in different product application notes without any explanation. Recently, Dr. Jian Li from CPES, Virginia Tech, gave a theoretical explanation for system instability based on the small signal model in his dissertation "Current-Mode Control: Modeling and its digital application" [14].

Although V^2 control works fine with large ESR output capacitors, this kind of capacitors is not desired from the output voltage ripple and transient voltage variation point of view [39][40][54]. For a DC/DC converter, smaller output voltage ripple is preferred. The equivalent model for the bulk output capacitor branch is shown in Figure

3.1. The impedance curve of the output capacitor branch (R_{C1}=3mΩ, C_{o1}=660μF, L_{C1}=640pH) is also shown.

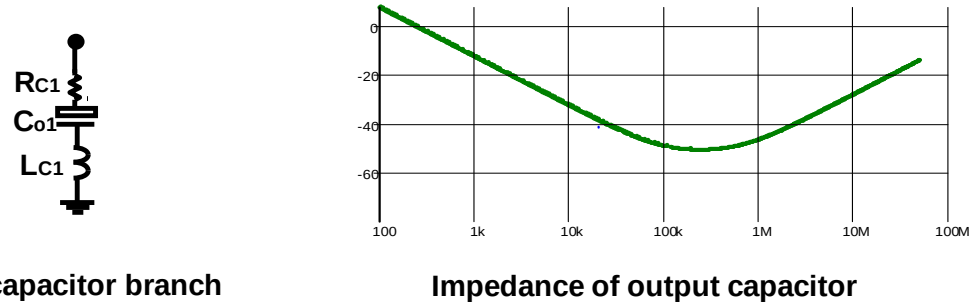

Figure 3. 1 Bulk capacitor branch: model and impedance

Recently several popular types of bulk output capacitors are OSCON capacitors (Aluminum solid capacitor with organic semi-conductive electrolyte), SP-Cap (specialty polymer aluminum electrolytic capacitor). In V^2 control application, their ESRs are usually large enough to maintain a stable system. However, the large ESRs together with their large ESLs will cause the steady state output voltage ripple to be very large. For a buck converter with only bulk output capacitors, the output voltage will contain large portion of ESR and ESL voltages. An example is shown in Figure 3.2. The switching frequency is 300 kHz and 2 SP caps are used with R_{C1}=3mΩ, C_{o1}=660μF, L_{C1}=640pH. As shown in Figure 3.2, the switching ripple is about 60mV. It can also be seen that the ESL effect will introduce a quite large voltage step which is not good from the switching ripple point of view.

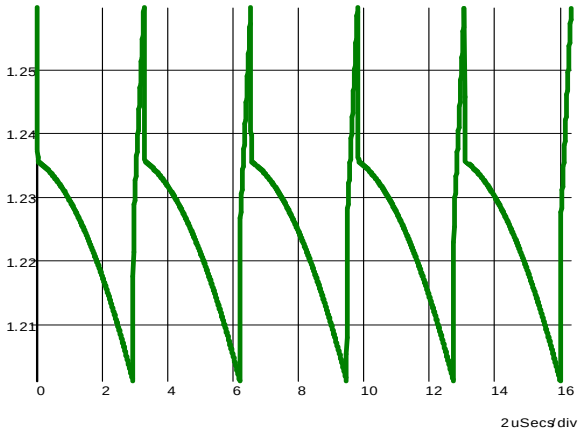

Figure 3. 2 Output voltage switching ripple with bulk capacitors

To ensure the output impedance satisfies the stringent output impedance requirement, many bulk capacitors have to be used in parallel. However, too many bulk capacitors will take large area of valuable motherboard space. An alternative way is to parallel certain amount of ceramic capacitors with the bulk capacitors as shown in Figure 3.3. An example of the impedance curve of the composite capacitor structure is also shown. For comparison purpose, previous impedance curve of bulk capacitor branch is also shown. In this example, we have R_{C1}=3mΩ, C_{o1}=660μF, L_{C1}=640pH, R_{C2} =100uΩ, C_{o2} =300μF and L_{C2} =20pH.

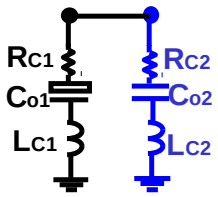

Composite capacitor structure

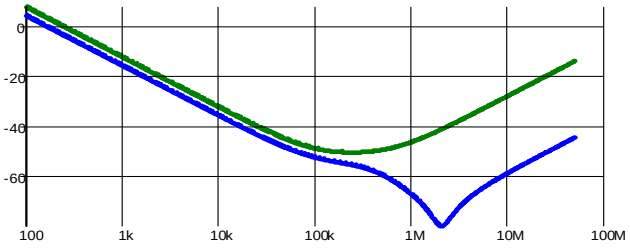

Green: Impedance of bulk capacitor branch

Blue: Impedance of composite capacitors

Figure 3. 3 Composite capacitor structure and impedance

From Figure 3.3, it is apparent that the ESL effect of the green curve is greatly damped by the additional ceramic branch. The final impedance curve will only see a small amount of ESL effect which is coming from the ceramic capacitor branch. Because the ESL effect of the ceramic capacitor branch can only be seen in very high frequency, it has almost no impact on the switching ripple when the switching frequency is in several hundreds of kHz. The output voltage ripple with composite output capacitors is compared with only bulk capacitor case in Figure 3.4.

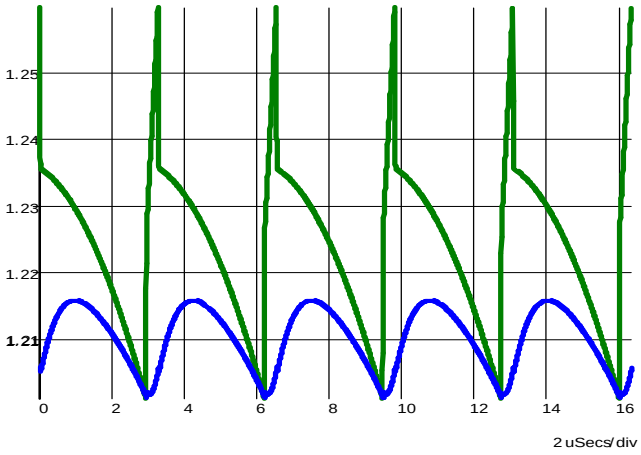

Figure 3. 4 Output voltage ripple comparison

The amount of ceramic capacitance we should add actually is usually based on the output impedance requirement. In DC/DC converter design, besides output voltage ripple requirement, the output impedance is often required to be below a specified value up to certain frequency range. Among all the applications, the VR impedance requirement is the most stringent. In VR application, the frequency limit is 2 MHz which means we should keep the output impedance under the specified value up to that frequency point.

Based on this concept, we review the impedance curve in Figure 3.3. When the required impedance limit is -50dB, it is found that actually in that example it is possible to use less ceramic capacitors. The following impedance curve shows an example when the following parameters are used: R_{C1}=3mΩ, C_{o1}=660μF, L_{C1}=640pH, R_{C2} =250uΩ, C_{o2} =120μF and L_{C2} =50pH. The impedance curve is shown as in Figure 3.5.

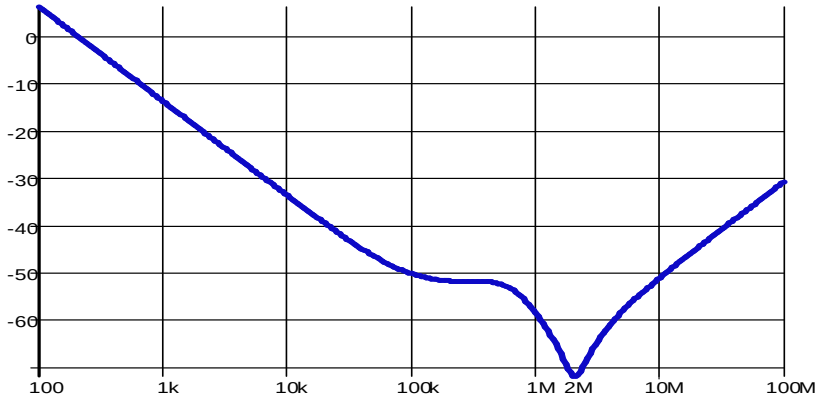

Figure 3. 5 Impedance curve of composite capacitors

For the impedance blow 100 kHz, it is taken care of by the feedback control. So the composite output capacitor structure can fit the DC/DC converter application very well.

For V^2 control with composite capacitors, the resonant frequency of ceramic capacitors is much higher than the switching frequency, so that the remaining ESL effect can be ignored. The V^2 control with composite capacitor structure is shown as Figure 3.6.

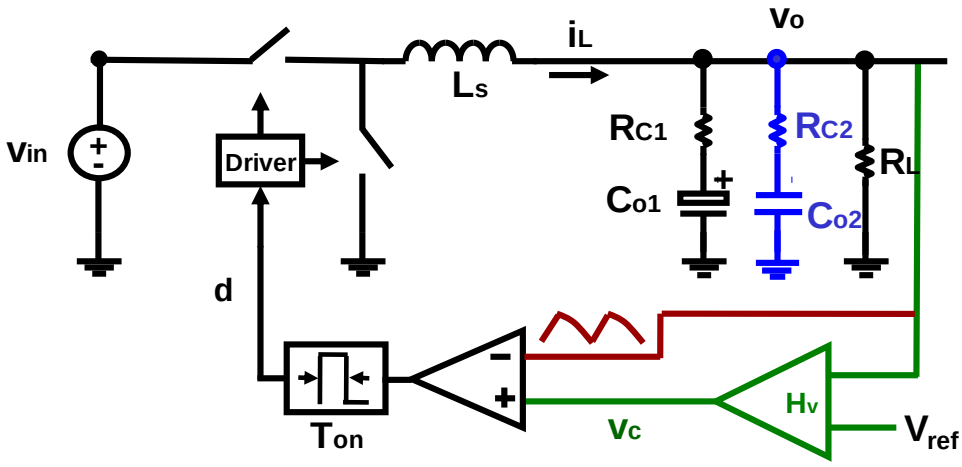

Figure 3. 6 Constant on-time V^2 control with composite capacitors

For V^2 control structure, when various types of output capacitors are used (V^2 control with composite capacitors), sub-harmonic oscillation may happen depending on numbers of ceramic capacitors used.

In this chapter, the new model for V^2 control with composite capacitors is derived in 3.3. The final result is simplified and compared with Simplis simulation result. Comparison of composite capacitor case and single type capacitor case is done in 3.4 to provide physical insight.

3.2 Modeling of V^2 Control with Composite Capacitors

3.2.1 Modeling of V^2 control with composite capacitors

It has been demonstrated the modeling concept proposed in [14] is effective in solving both current mode control and V^2 control. This section tries to extend this modeling concept to V^2 control with composite output capacitors. The time domain waveform of V^2 control with composite capacitors is more complicated than V^2 control

with single type of output capacitors. This section will take constant on time V^2 control with composite capacitors as an example.

In constant on-time V^2 control with composite capacitors, the parallel ceramic capacitors have very small ESR compared with the bulk capacitors. For typical ceramic capacitors, the ESR effect will show only at high frequency around MHz range as shown in Figure 3.5. For a DC/DC converter running at several hundred kHz range, the ceramic capacitors can be approximated as pure capacitance. For small signal analysis, the structure we consider is shown in Figure 3.7. The outer voltage loop is ignored and we focus on the transfer function from control signal to output voltage.

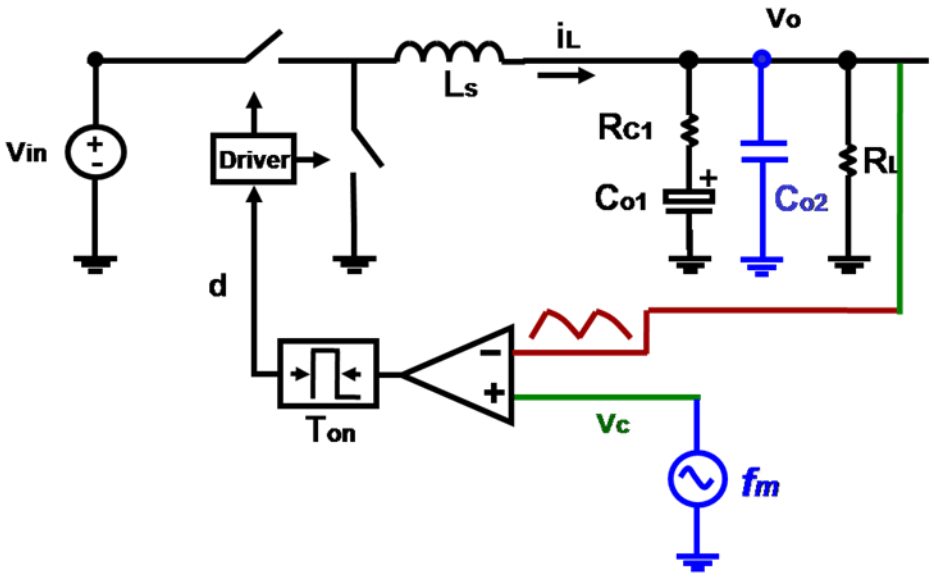

Figure 3. 7 Simplification of V^2 control with composite capacitors

Before applying the describing function method, it is necessary to make several assumptions:

(i) the magnitude of the inductor current slopes during the on-period and the off-period stays constant separately;

(ii) the magnitude of the perturbation signal is very small;

(iii) the perturbation frequency f_m and the switching frequency f_{sw} are commensurable, which means that $N*f_{sw}=M*f_m$, where N and M are positive integers.

By applying a small signal sinusoidal perturbation at the control signal, the off-time T_{off} is modulated. The inductor current, capacitor currents in two branches and output voltage are all modulated. The modulated output voltage will be fed back to the modulator and in turn change the off-time T_{off}.

For small signal modulation, it is important to first calculate the operating point which is the steady state. For a DC/DC converter, when we know the input and output voltage, we know the inductor current waveform which is in a triangular form. However, when composite output capacitors are used, it is not clear how the inductor current distributes between the capacitor branches and load resistor branch. The capacitor current is calculated in Appendix A to provide the steady state information.

When we inject the small signal perturbation at control signal as in Figure 3.7, the perturbed time domain waveform is shown as in Figure 3.8.

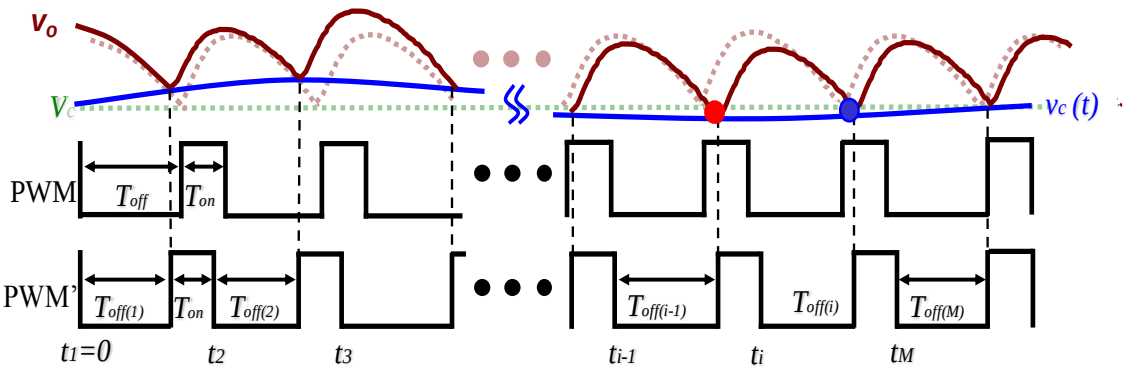

Figure 3. 8 Perturbed output voltage waveform in V^2 control

As shown in Figure 3.8, the output voltage will follow the modulated control signal. Because the on-time T_{on} is constant, the off-time T_{off} is modulated by the perturbation signal $v_c(t)$:

$$v_c(t) = V_c + \hat{v}_c \sin(2\pi f_m \cdot t + \theta) \tag{3.1}$$

where V_c is the steady state DC value of the control signal. $\hat{v}_c$ is the magnitude of the perturbation, and θ is the initial angle. In the following derivation, all the variables in lower case are perturbed variables.

We focus on one switching cycle of the modulated output voltage waveform. At the starting point of this cycle (the red dot in Figure 3.8):

$$v_c(t_{i-1} + T_{off\,(i-1)}) = R_{C1} i_{C1}(t_{i-1} + T_{off\,(i-1)}) + v_{Co1}(t_{i-1} + T_{off\,(i-1)}) \tag{3.2}$$

At the end point of this cycle (the blue dot):

$$v_c(t_i + T_{off\,(i)}) = R_{C1} i_{C1}(t_i + T_{off\,(i)}) + v_{Co1}(t_i + T_{off\,(i)}) \tag{3.3}$$

For the above two equations, they describe a fact that at the decision point, control signal equals to output voltage. i_{c1} is the bulk capacitor current and v_{Co1} is the voltage over bulk capacitance. Output voltage waveform of the bulk capacitor is shown in Figure 3.9 for better understanding.

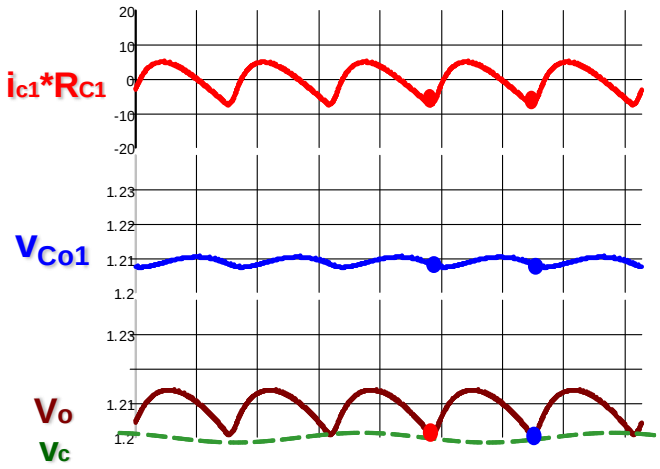

Figure 3. 9 Output voltage waveform of bulk capacitor branch

By subtracting the previous two equations (3.2) and (3.3), the output voltage variation can be related with control signal perturbation.

$$v_c(t_{i-1}+T_{off\,(i-1)})-v_c(t_i+T_{off\,(i)})$$
$$=R_{C1}[i_{C1}(t_{i-1}+T_{off\,(i-1)})-i_{C1}(t_i+T_{off\,(i)})]-\frac{\int_{t_{i-1}+T_{off\,(i-1)}}^{t_i+T_{off\,(i)}} i_{C1}(t)dt}{C_{o1}} \quad (3.4)$$

The left side of the equation is control signal variation over one switching cycle; the right side is the output voltage variation over the same switching cycle. The right side is related with capacitor current under perturbation. The output voltage variation contains two parts: one part is voltage variation over the ESR of the bulk capacitor and the other is voltage variation over the pure bulk capacitance.

To calculate the right side, capacitor current under perturbation is needed. The calculation detail is shown in Appendix B.

Based on the result of Appendix B, the capacitor current perturbation is a function of accumulated off-time variations and control signal perturbation. This capacitor current perturbation can be used to calculate the output voltage perturbation over one switching cycle. Voltage variation over the ESR of bulk capacitor is:

$$\Delta v_{ESR} = R_{C1}[i_{C1}(t_{i-1} + T_{off\,(i-1)}) - i_{C1}(t_i + T_{off\,(i)})] = s_{C1} R_{C1} \Delta T_{off\,(i)} \tag{3.5}$$

Voltage variation over the bulk capacitance is:

$$\begin{aligned} \Delta v_{cap} &= \frac{\int_{t_{i-1}+T_{off\,(i-1)}}^{t_i+T_{off\,(i)}} i_{C1}(t)dt}{C_{o1}} = \frac{s_f T_{sw}}{C_{o1}+C_{o2}} \sum_{0}^{i-1} \Delta T_{off\,(k)} \\ &+ \frac{I_{C1valley}}{C_{o1}} \Delta T_{off\,(i)} + \frac{v_c(t_i + T_{off\,(i)} + \frac{\pi}{2\pi f_m \cdot 2}) - v_c(t_{i-1} + T_{off\,(i-1)} + \frac{\pi}{2\pi f_m \cdot 2})}{2\pi f_m \cdot R_L (C_{o1}+C_{o2})} \end{aligned} \tag{3.6}$$

Substitute equation (3.6) and (3.5) into (3.4)

$$\begin{aligned} & v_c(t_{i-1} + T_{off\,(i-1)}) - v_c(t_i + T_{off\,(i)}) + \frac{v_c(t_i + T_{off\,(i)} + \frac{\pi}{2\pi f_m \cdot 2}) - v_c(t_{i-1} + T_{off\,(i-1)} + \frac{\pi}{2\pi f_m \cdot 2})}{2\pi f_m \cdot R_L (C_{o1}+C_2)} \\ &= R_{C1} s_{C1} \Delta T_{off\,(i)} + R_{C1} \frac{C_{o1}}{C_{o1}+C_{o2}} \Delta T_{off\,(i-1)} + \frac{(s_f \sum_{k=0}^{i-1} \Delta T_{off\,(k)}) T_{sw}}{C_{o1}+C_{o2}} + \frac{I_{C1valley}}{C_{o1}} \Delta T_{off\,(i)} \end{aligned} \tag{3.7}$$

The perturbed duty cycle d(t) and the perturbed inductor current $i_L(t)$ can be expressed by:

$$d(t)\big|_{0 \le t \le t_{M} - T_{off\,(M)} + T_{on}} = \sum_{i=1}^{M} [u(t - t_i - T_{off\,(i)}) - u(t - t_i - T_{off\,(i)} - T_{on})] \tag{3.8}$$

$$i_L(t)\big|_{0\le t\le t_M - T_{off(M)}+T_{on}} = \int_0^t [\frac{V_{in}}{L_s} d(t)\Big|_{0\le t\le t_M - T_{off(M)}+T_{on}} - \frac{V_{in}}{L_s}]dt + i_{L0} \tag{3.9}$$

where, u(t)=1 when t>0, and i_{L0} is the initial value of the inductor current.

Then, the Fourier analysis can be performed on the inductor current:

$$c_{m(iL)} = j2f_m / N \cdot \int_0^{t_M + T_{off(M)} + T_{on}} i_L(t)\big|_{0\le t\le t_M + T_{off(M)} + T_{on}} \cdot e^{-j2\pi f_m t} dt \tag{3.10}$$

where, $c_m(iL)$ is the Fourier coefficient at the perturbation frequency f_m for the inductor current. The off time variation in equation (3.7) can be used to solve equation (3.10). Based on the results in [14] and [35], the Fourier coefficient of inductor current can be calculated as:

$$c_{m(iL)} = \frac{f_s}{s_{C1}} \frac{(1-e^{-2\pi f_m T_{on}})(1-e^{-2\pi f_m T_{sw}})(1+\frac{1}{2\pi f_m \cdot R_L(C_{o1}+C_{o2})})}{(R_{C1}+\frac{I_{C1valley}}{s_{C1}C_{o1}}) - (R_{C1}+\frac{I_{C1valley}}{s_{C1}C_{o1}} - \frac{s_f}{s_{C1}}\frac{T_{sw}}{C_{o1}+C_{o2}})e^{-2\pi f_m T_{sw}}} \frac{V_{in}}{L_s \cdot j2\pi f_m} e^{-j\theta} \tag{3.11}$$

where s_{c1} is the slope of capacitor current at the decision point, $I_{C1valley}$ is the magnitude of capacitor current at the decision point, T_{sw} is the steady state switching period.

Next, the Fourier coefficient $c_m(vo)$ of the output voltage v_o can be calculated based on:

$$c_{m(vo)} = c_{m(iL)} \cdot \frac{R_L(R_{C1}C_{o1} \cdot j2\pi f_m + 1)}{R_L[R_{C1}C_{o1}C_{o2}(j2\pi f_m)^2 + (C_{o1}+C_{o2}) \cdot j2\pi f_m] + R_{C1}C_{o1} \cdot j2\pi f_m + 1} \tag{3.12}$$

The Fourier coefficient at the perturbation frequency f_m for the control signal $v_c(t)$ is $\hat{r} \cdot e^{-j\theta}$, so the describing function from the control to output can be calculated as:

$$\frac{v_{o(f_m)}}{v_{c(f_m)}} = \frac{f_s}{s_{C1}} \frac{(1-e^{-2\pi f_m T_{on}})(1-e^{-2\pi f_m T_{sw}})(1+\frac{1}{2\pi f_m \cdot R_L(C_{o1}+C_{o2})})}{(R_{C1}+\frac{I_{C1valley}}{s_{C1}C_{o1}})-(R_{C1}+\frac{I_{C1valley}}{s_{C1}C_{o1}}-\frac{s_f}{s_{C1}}\frac{T_{sw}}{C_{o1}+C_{o2}})e^{-2\pi f_m T_{sw}}} \frac{V_{in}}{L_s \cdot j2\pi f_m} \times \frac{R_L(R_{C1}C_{o1} \cdot j2\pi f_m + 1)}{R_L[R_{C1}C_{o1}C_{o2}(j2\pi f_m)^2 + (C_{o1}+C_{o2}) \cdot j2\pi f_m] + R_{C1}C_{o1} \cdot j2\pi f_m + 1} \tag{3.13}$$

Note that the results are not applicable to frequencies where $f_m = n*F_{sw}$, where n is a positive integer [14][35]. The influence from the variation of the inductor current slope is ignored since it is much smaller than the influence of the current divider and the capacitor voltage ripple. In the s-domain, the control to output voltage transfer function can be expressed by

$$\frac{v_o(s)}{v_c(s)} = \frac{f_s}{s_{C1}} \frac{(1-e^{-sT_{on}})(1-e^{-sT_{sw}})(1+\frac{1}{s \cdot R_L(C_{o1}+C_{o2})})}{(R_{C1}+\frac{I_{C1valley}}{s_{C1}C_{o1}})-(R_{C1}+\frac{I_{C1valley}}{s_{C1}C_{o1}}-\frac{s_f}{s_{C1}}\frac{T_{sw}}{C_{o1}+C_{o2}})e^{-sT_{sw}}} \frac{V_{in}}{sL_s} \times \frac{R_L(R_{C1}C_{o1} \cdot s + 1)}{R_L[R_{C1}C_{o1}C_{o2}s^2 + (C_{o1}+C_{o2})s] + R_{C1}C_{o1}s + 1} \tag{3.14}$$

This is an exponential expression and can be accurate beyond switching frequency. This model is verified using Simplis simulation. In the simulation setup, the switching frequency is F_{sw}=300kHz, and D=0.1. The simulation result is shown in Figure 3.10.

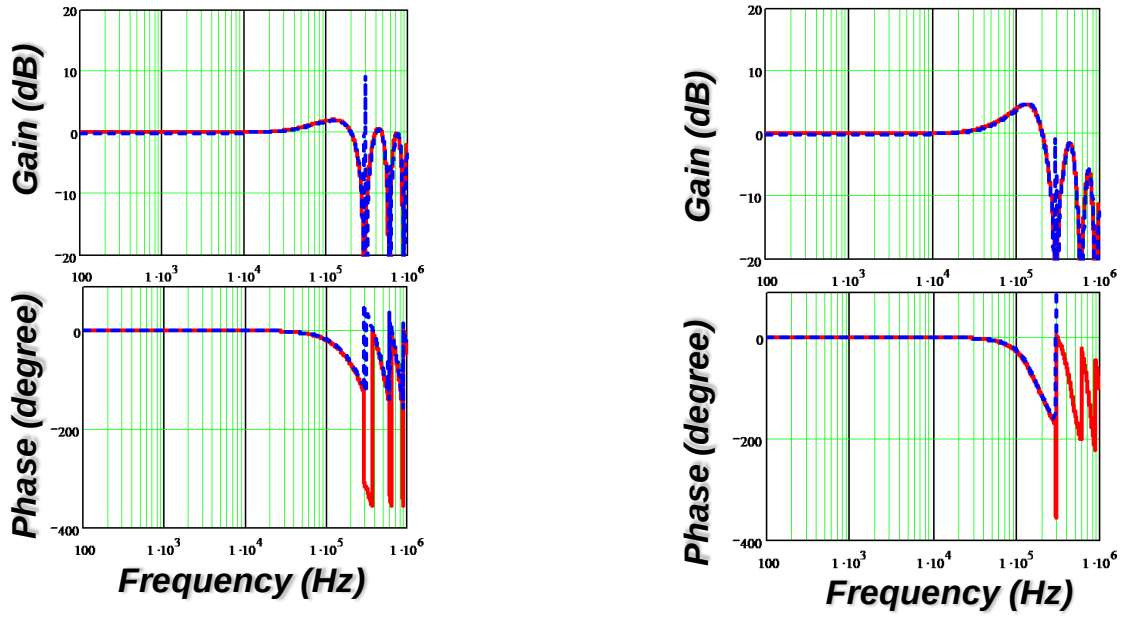

(a) (b)

Red curve: New model; Blue curve: Simplis simulation (≈measurement)

Figure 3. 10 Control to output transfer function comparison (a) R_{C1} =3m, C_{o1} =660μF, C_{o2} =10μF; (b) R_{C1} =3m, C_{o1} =660μF, C_{o2} =300μF;

Although the model in equation (3.14) is very accurate, it is very complicated and difficult to use. The exponential term can be simplified using Padé approximation [9][42]:

$$e^{-T_{sw}} = 1 - \frac{sT_{sw}}{1 + \frac{s}{Q_1\omega_2} + \frac{s^2}{\omega_2^2}} \tag{3.15}$$

where $\omega_2 = \pi/T_{sw}$, and $Q_1 = 2/\pi$. This approximation is valid up to switching frequency. Using equation (3.15), transfer function of (3.14) can be simplified:

$$\frac{v_o(s)}{v_c(s)} \approx \frac{R_{C1}C_{o1}s + 1}{1 + \frac{s}{Q_3\omega_2} + \frac{s^2}{\omega_2^2}} \cdot \frac{1}{1 + R_{C1}\frac{C_{o1}C_{o2}}{C_{o1} + C_{o2}}s} \tag{3.16}$$

where

$$Q_3 = \frac{T_{sw}}{(\frac{R_{C1}C_{o1}^{\ 2}}{C_{o1}+C_{o2}} - \frac{T_{on}}{2})\pi}$$

To understand the modeling result better, we can compare the composite capacitor case with previous single type capacitor case. The previous simplified model for constant on time V^2 control with single type output capacitors in [14] gives a result of second order control to output transfer function:

$$\frac{v_o(s)}{v_c(s)} = \frac{R_{C1}C_{o1}s + 1}{1 + (R_{C1}C_{o1} - \frac{T_{on}}{2})s + \frac{s^2}{\omega_2^{\ 2}}} \tag{3.17}$$

where, T_{on} is the constant on time and $\omega_2=\pi/T_{sw}$. The stability criterion is determined as:

$$R_{C1}C_{o1} > \frac{T_{on}}{2} \tag{3.18}$$

It is shown that when the on time is determined, the output capacitor time constant has to be big enough to ensure the system stability. For OSCON capacitors with parameters: R_{C1}=6mΩ, C_{o1}=560μF, the system is stable; For ceramic capacitors with parameters: R_{C1}=1.4mΩ, C_{o1}=100μF, the system is unstable.

Comparing the equation of (3.16) with equation (3.17), we can see both equations have a double pole located at half of switching frequency. However, the stability criterion for composite capacitor case has been changed to

$$\frac{R_{C1}C_{o1}^{\ 2}}{C_{o1}+C_{o2}} > \frac{T_{on}}{2} \tag{3.19}$$

We define the equivalent ESR for the bulk capacitor branch as:

$$R_{C1equ} = R_{C1}\frac{C_{o1}}{C_{o1}+C_{o2}} \tag{3.20}$$

The stability criterion is changed as:

$$R_{C1equ}C_{o1} > \frac{T_{on}}{2} \tag{3.21}$$

To explain why the equivalent ESR has been decreased, we go back to the fundamental difference of these two structures. In composite output capacitor case, we add a pure capacitance branch in parallel, which will form a current divider circuit with the original bulk capacitor branch. Figure 3.11 shows the time domain waveforms of the two structures.

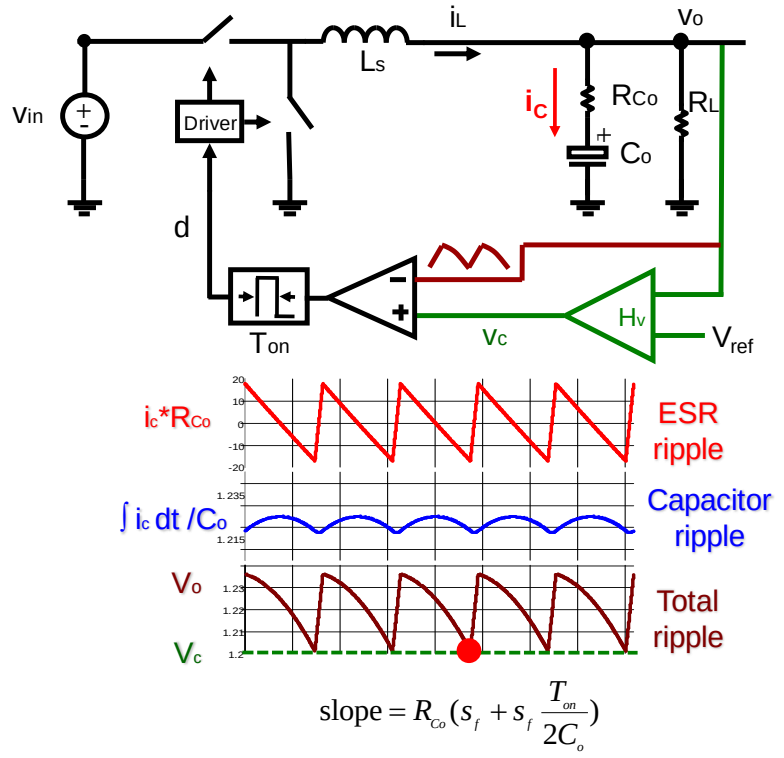

$$slope = R_{Co}(s_f + s_f \frac{T_{on}}{2C_o})$$

(a)

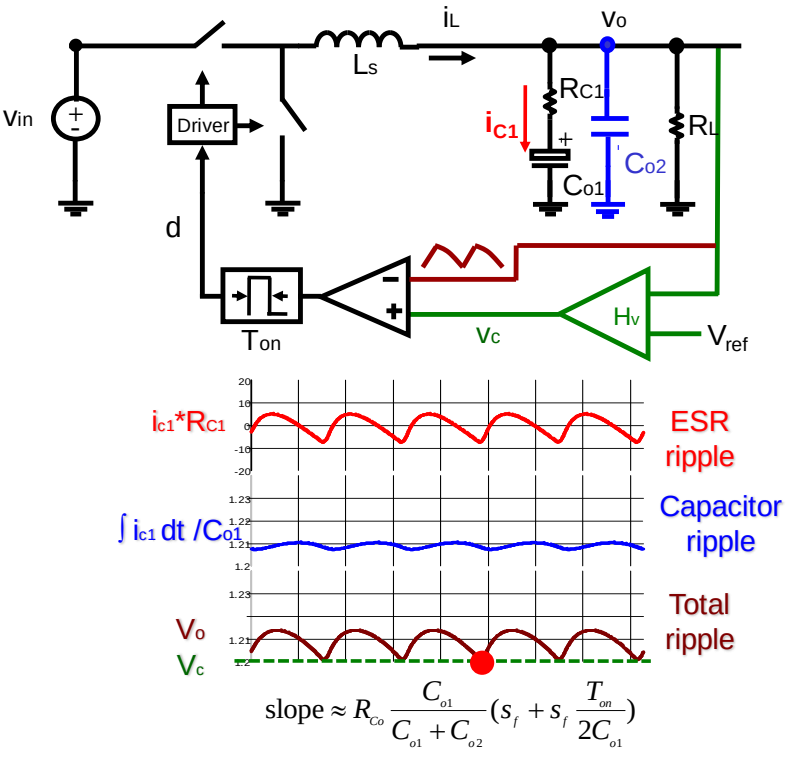

$$slope \approx R_{Co} \frac{C_{o1}}{C_{o1} + C_{o2}}(s_f + s_f \frac{T_{on}}{2C_{o1}})$$

(b)

Figure 3. 11 Slope comparison of single type of capacitors and composite capacitors

At the decision point, the capacitor current slope actually is changed by the current divider. From Figure 3.11 we can see slope of the ESR ripple at decision point for composite capacitor case is smaller than single type output capacitor case.

For composite capacitor case, the capacitor current slope around decision point is s_{c1}. The slope can be simplified as:

$$s_{c1} = -\frac{K_1}{R_{C1}C_{o2}} e^{\frac{-T_{off}}{\tau}} + \frac{C_{o1}}{C_{o1}+C_{o2}} s_f \approx \frac{C_{o1}}{C_{o1}+C_{o2}} s_f \tag{3.22}$$

From equation (3.22), we know at the decision point the capacitor current slope is smaller than single type of output capacitor case. The coefficient is the same as the coefficient in equation (3.20).

Comparing the two transfer functions, we know for composite capacitors case, there is also an additional pole which is caused by the additional ceramic capacitor branch.

From the transfer function of (3.16), we know the more ceramic capacitance we add, the double pole peaking around half of the switching frequency will be higher which means the stability margin is smaller. The ceramic capacitor branch can effectively reduce output voltage switching ripple. However, it will also reduce system stability margin. We should design the capacitance of the ceramic capacitor branch carefully.

The simplified third order transfer function is verified using Simplis simulation as shown in Figure 3.12.

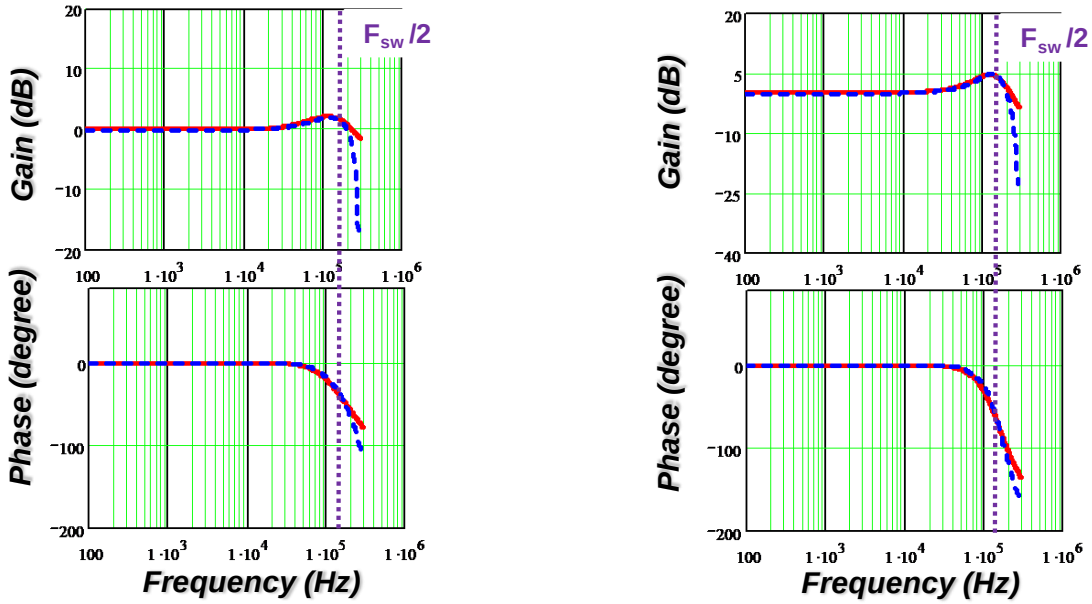

(a) (b)

Red curve: Simplified model; Blue curve: Simplis simulation (≈measurement)

Figure 3. 12 Control to output transfer function comparison (a) R_{C1} =3m, C_{o1} =660µF, C_{o2} =10µF; (b) R_{C1} =3m, C_{o1} =660µF, C_{o2} =300µF;

Although all the derivation is based on constant on time modulation, the modeling process can be applied to other modulation schemes. For constant frequency case, all the derivation is similar and detail is shown in Appendix C.

3.2.2 Experimental verification

The experimental verification is done based on the LM34930 evaluation board from National Semiconductor. The evaluation board is modified to add a pure ceramic capacitor in parallel with original output capacitors. The parameters are: V_{in}=20V, V_o=5V, F_{sw}=800kHz, L_s=10µH, R_L=10Ω, R_{C1} =220mΩ, C_{o1}=4.4µF, C_{o2}=1µF. The control to output transfer function comparison is shown as in Figure 3.17. The proposed model can accurately predict the double pole at half of the switching frequency.

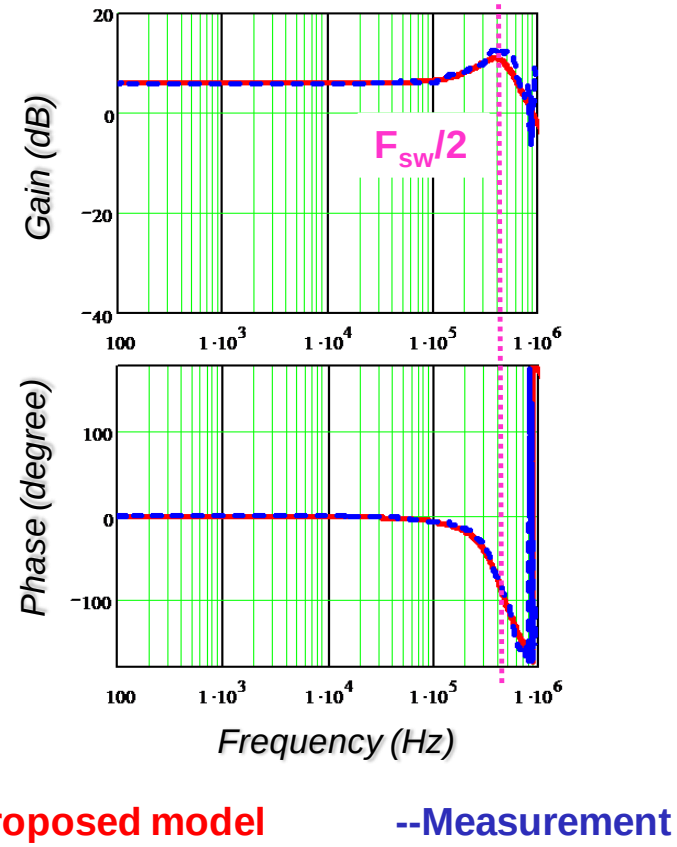

Figure 3. 13 Control to output transfer function comparison

3.3 Methods to Enhance Stability Margin

it is possible for designers to add large amount of ceramic capacitors in parallel to get the desired output impedance characteristic. Nevertheless, the stability margin for V^2 control is decreased as the equivalent ESR is decreased. Two ways are commonly used to enhance the stability margin: one is to add current ramp to output voltage feedback; the other is to add artificial ramp (external ramp) to output voltage feedback.

3.3.1 Adding the inductor current ramp

It is possible to enhance the system stability by introducing inductor current information in the feedback. The structure is shown in Figure 3.14. R_i is the current sensing gain. The additional inductor current information will enhance the effect of ESR of the bulk capacitors.

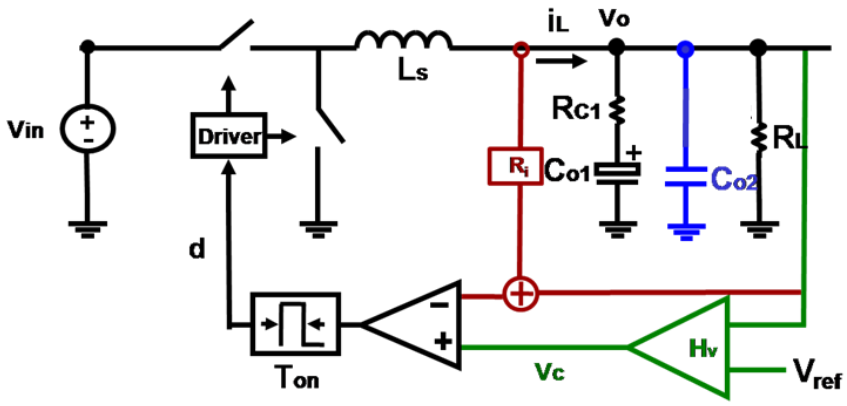

Figure 3. 14 V^2 control with composite capacitors and additional current feedback

Similar modeling process can be carried out. The transfer function from control to output is simplified as below:

$$\frac{v_o(s)}{v_c(s)} \approx \frac{R_{C1}C_{o1}s+1}{1+\frac{s}{Q_4\omega_2}+\frac{s^2}{\omega_2^2}} \cdot \frac{1}{1+R_{C1}\frac{C_{o1}C_{o2}}{C_{o1}+C_{o2}}s} \tag{3.23}$$

where

$$\frac{1}{Q_4\omega_2} = R_i(C_{o1}+C_{o2}) + \frac{R_{C1}C_{o1}^{\ 2}}{C_{o1}+C_{o2}} - \frac{T_{on}}{2} \tag{3.24}$$

The stability criterion is for equation (3.24) to be positive. It is very clear from equation (3.24) that the current sensing gain can increase system stability margin.

Equation (3.24) can also be used to design the current sensing gain to get the desired quality factor.

The transfer function is verified using Simplis simulation as in Figure 3.15. The simplified third order transfer function can be accurate up to half of switching frequency.

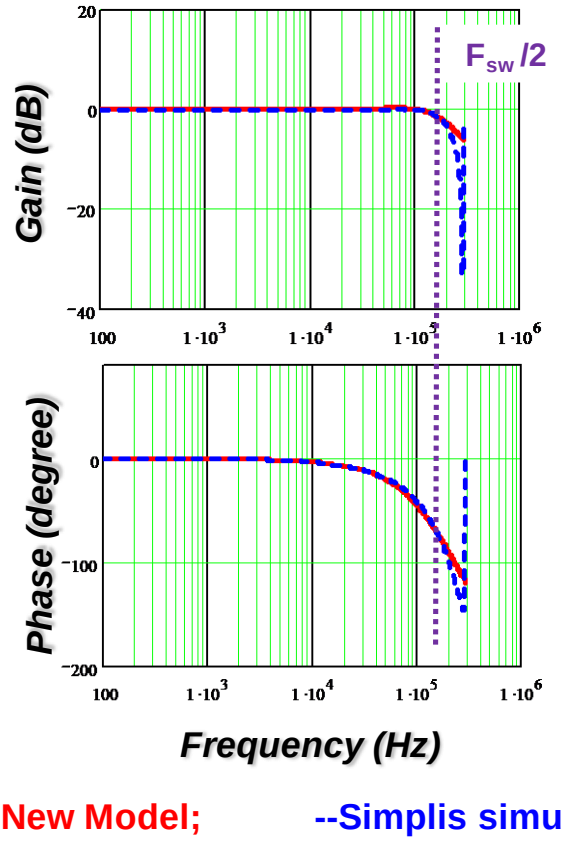

Figure 3. 15 Control to output transfer function with R_i =1m, R_{C1} =3m, C_{o1} =660µF, C_{o2} =300µF, D=0.1, F_{sw} =300kHz

3.3.2 Adding the external ramp

In peak current mode control, external ramp can be used to eliminate the sub-harmonic oscillation. External ramp can also be used in V^2 control as in Figure 3.16.

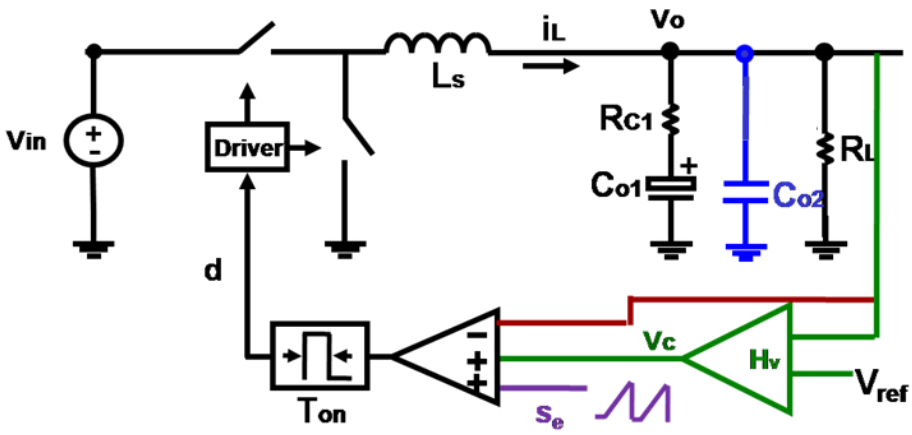

Figure 3. 16 V^2 control with composite capacitors and external ramp

The control to output transfer function can be derived and simplified as

$$\frac{v_o(s)}{v_c(s)} \approx \frac{R_{C1}C_{o1}s+1}{1+\frac{s}{Q_5\omega_2}+\frac{s^2}{\omega_2^2}} \cdot \frac{1}{1+R_{C1}\frac{C_{o1}C_{o2}}{C_{o1}+C_{o2}}s}$$

(3.25)

in which

$$\frac{1}{Q_5\omega_2} = \frac{2s_e}{s_f}(C_{o1}+C_{o2}) + \frac{R_{C1}C_{o1}^{\ 2}}{C_{o1}+C_{o2}} - \frac{T_{on}}{2} \qquad (3.26)$$

This is an approximation used for relatively small external ramp. For large external ramp case, the simplified transfer function will be more complicated. For large external ramp case, the transfer function is shown in Appendix D.

The stability criterion is to make sure the quality factor to be positive based on equation (3.26) and the design criterion is to choose a proper external ramp magnitude to get a desired quality factor.

The transfer function is verified using Simplis simulation as in Figure 3.17. The simplified third order transfer function can be accurate up to half of switching frequency.

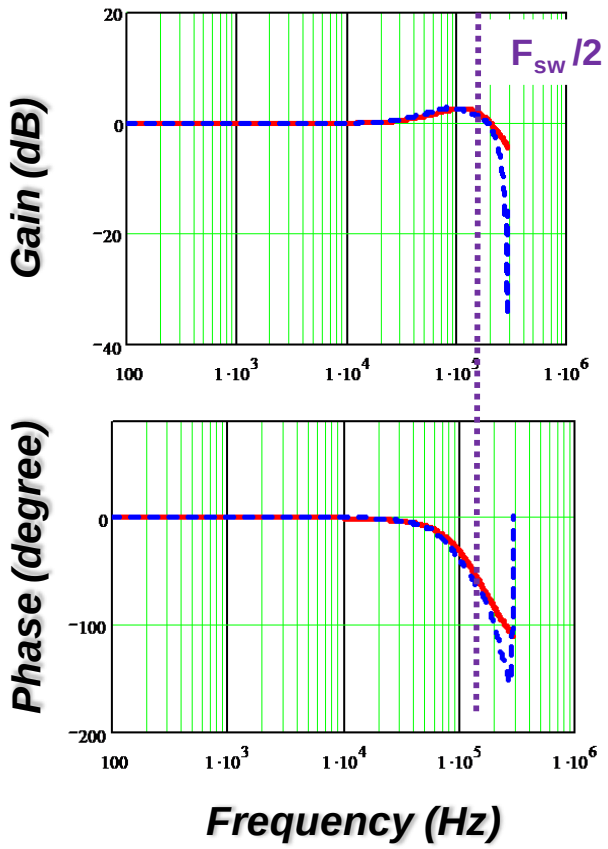

Figure 3. 17 Control to output transfer function with s_e =2mV, R_{C1} =3m, C_{o1} =660µF, C_{o2} =300µF, D=0.1, F_{sw} =300kHz

3.6 Summary

This chapter looks into the modeling for V^2 control with composite capacitors. By adding a ceramic capacitor branch in parallel with the original bulk capacitor branch, the system stability margin is reduced. Adding too many ceramic capacitors will cause system instability. Simulation results are provided to verify the proposed model. To enhance the system stability, inductor current ramp or external ramp can be used.

Chapter 4. Modeling of Average Current Mode Control

4.1 Average Current Mode Control

Average current mode control is widely used in various applications. Without proper design, average current mode control can run into sub-harmonic oscillation just like peak current mode control or V^2 control. However, the modeling of average current mode control is complicated comparing with peak current mode control, because the inductor current feedback loop contains a low pass filter. The structure of average current mode control is shown in Figure 4.1.

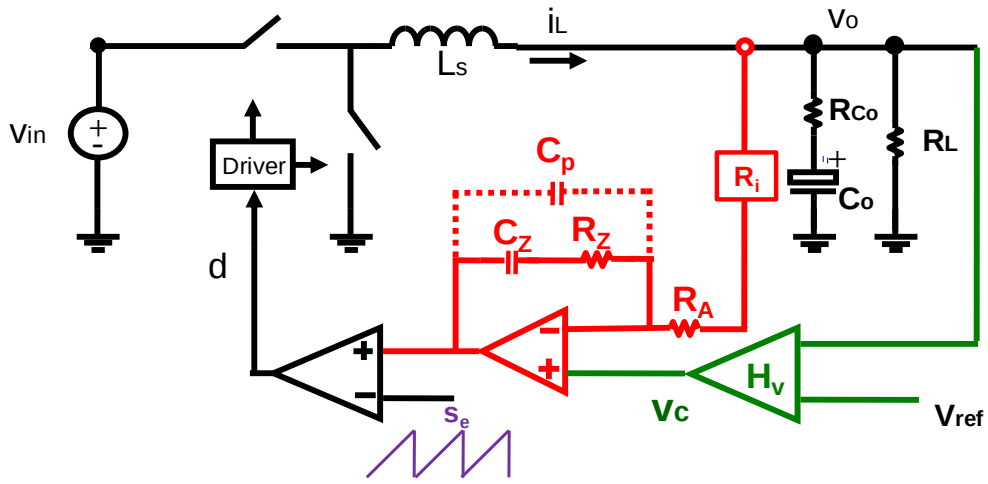

Figure 4. 1 Structure of average current mode control

As shown in Figure 4.1, normally two different compensation structures are used [26]. In peak current mode control, as the current loop doesn't have an integrator, in low frequency the current loop has a finite gain. The average inductor current cannot be controlled very well. By putting an integrator in the current feedback loop, the DC gain of current loop is pushed to infinite. However, the integrator will introduce 90 degree phase drop. To compensate this additional phase drop, a zero is added to the current compensator. An integrator and a zero form one very popular compensation structure in average current mode control. The other popular compensation structure is to add another high frequency pole. This pole can help to attenuate the switching ripple as well as switching noise.

4.2 Modeling of Average Current Mode Control

Following the modeling concept in previous chapter, average current mode control can also be solved using describing function method. However, this chapter tries to simplify the problem by relating the new problem with previous old problems about which we have better understanding.

Based on different compensation structures, the following part will consider the most commonly used two structures and solve them one by one.

4.2.1 Average current mode with PI compensation

First, we look into a simpler compensation structure. The current compensator is composed of an integrator and a zero (PI compensation). The structure is shown as in Figure 4.2.

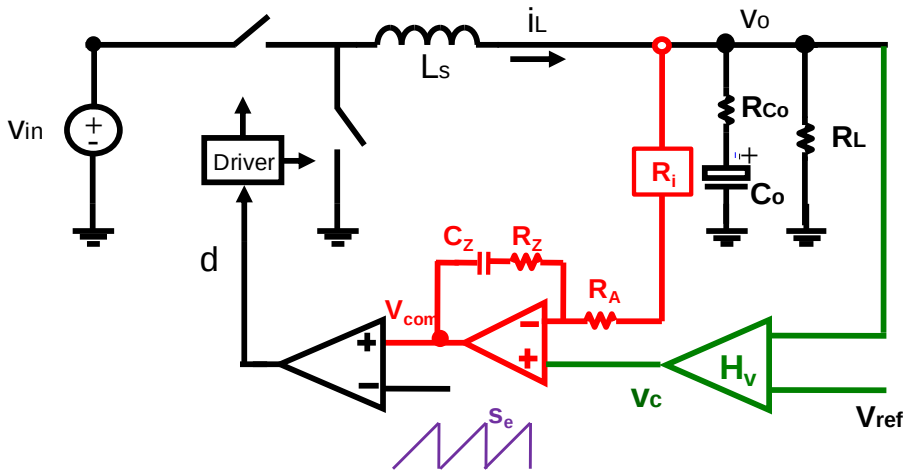

Figure 4. 2 Average current mode control with PI compensation

To understand this control structure, we look into the detail of feedback information. For the current feedback loop, inductor current is sensed and passed through a compensation network. Based on the PI compensation, the compensator output actually contains two parts: one part is proportional with inductor current which is the voltage over the resistor R_Z ; the other part is integration of inductor current ripple which is the voltage over the capacitor C_z. The steady state compensator output voltage waveform is shown as in Figure 4.3.

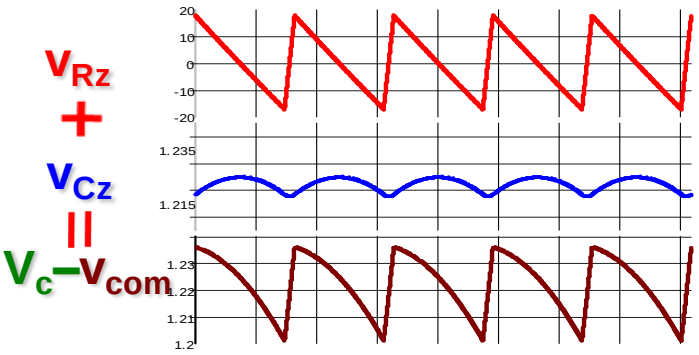

Figure 4. 3 Waveform of compensator output voltage

The compensator output is denoted as v_{com}.

If we recall the feedback information for V^2 control, just as shown in Figure 2.5 in Chapter 2, we know the current compensator output waveform as shown in Figure 4.3 is very similar to output voltage waveform.

For average current mode control with PI compensation, define the current flowing through the compensation network as i_{com}

$$i_{com} = \frac{R_i}{R_A} i_L - \frac{V_c}{R_A} \tag{4.1}$$

In which V_c is the output of voltage compensator output. From equation (4.1), we know compensator current has the same shape as inductor current.

The feedback information in V^2 control is formed by inductor current flowing into two branches: the output capacitor and load resistor. However, in average current mode control, the current compensator structure is similar as the output capacitor branch. For comparison, we purposely add a resistor branch in parallel. The comparison between average current mode control and V^2 control is shown in Figure 4.4. As constant frequency average current mode control is the most widely used structure, constant frequency V^2 control is chosen for comparison. The value of this additional resistor can be very large so that it will not impact the operation.

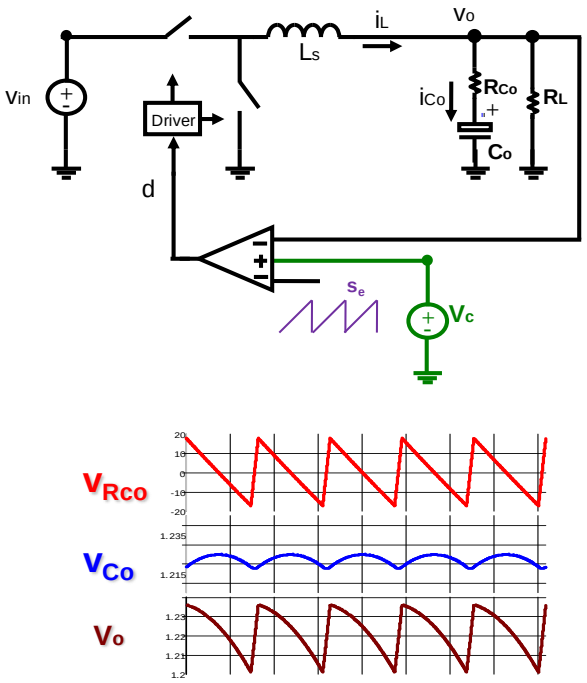

(a)

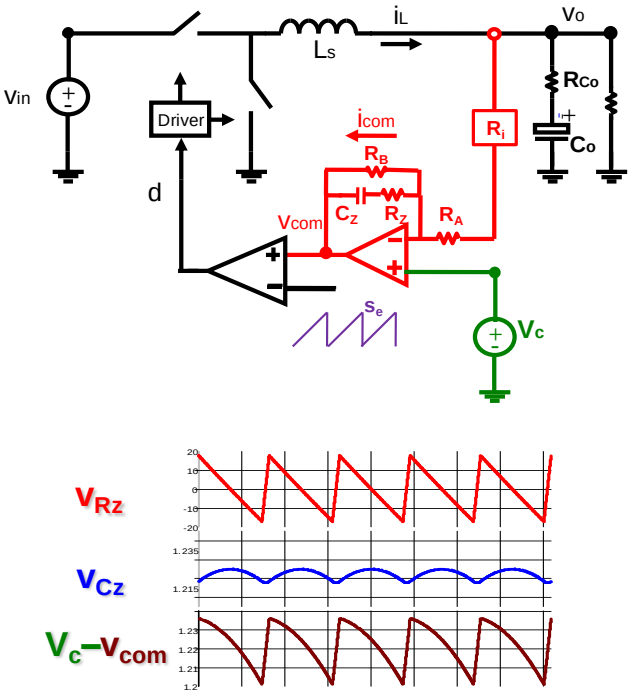

(b)

Figure 4. 4 Time domain waveforms comparison (a) V^2 output voltage (b) Average current mode compensator output

We can clearly see the similarity between v_o waveform and v_{com} waveform. From feedback information point of view, output capacitor and the load resistor work as a compensation network in V^2 control. This load RC compensation network has the same structure as current compensator in average current mode control. Based on the same compensation structures, the small signal behaviors are also similar.

In V^2 control, perturbation is usually injected at the control signal, which is the input of PWM modulator. For comparison, we also inject a small signal perturbation at the input of PWM modulator in average current mode control as shown in Figure 4.5. The perturbation point is denoted as v_{c1}. Then based on the same structures previous modeling result for V^2 can be directly adopted for average current mode control.

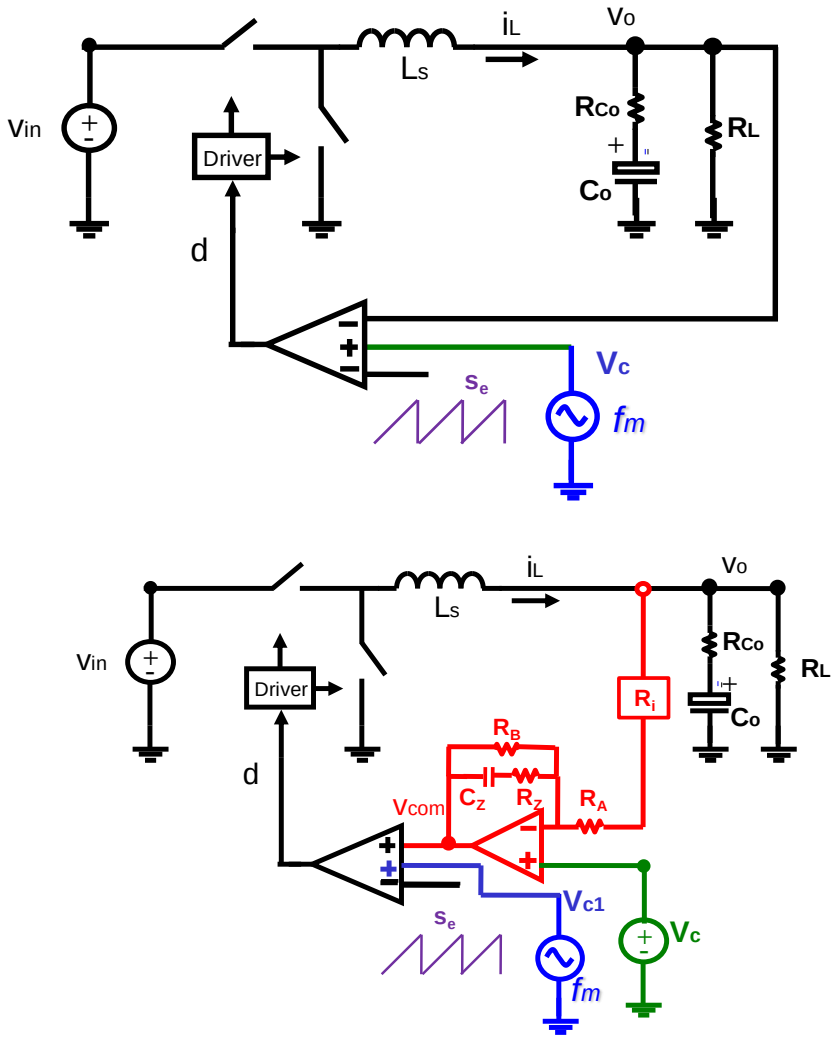

Figure 4. 5 Perturbation injection for V^2 control and average current mode control

The transfer function from control signal v_c to output voltage v_o for V^2 control can be modified to describe the transfer function from v_{c1} to compensator output v_{com} in average current mode control. It should be noted that v_{c1} is added for comparison purpose. In real circuit, there is no such control port. To adopting previous modeling result, some parameters have to be changed for average current mode control. The parameters are listed in the Table 4.1.

V²	$\frac{v_o(s)}{v_c(s)}$	R_{Co}	C_o	$s_n = R_{Co}\frac{V_{in}-V_o}{L_s}$	$s_f = R_{Co}\frac{V_o}{L_s}$
Average current	$\frac{v_{com}(s)}{v_{c1}(s)}$	R_Z	C_Z	$s_n = R_i\frac{R_Z}{R_A}\frac{V_{in}-V_o}{L_s}$	$s_f = R_i\frac{R_Z}{R_A}\frac{V_o}{L_s}$

Table 4. 1 Parameters comparison for V^2 control and average current mode control

The similarity between V^2 control and average current mode control is general for different modulation schemes. As constant frequency average current mode control is the most popular scheme, this section will take constant frequency average current mode control as an example.

Based on previous modeling result for constant frequency V^2 control with single type of output capacitors given in [19], the result is modified to give the relation between v_{c1} and v_{com} in average current mode control.

$$\frac{v_{com}(s)}{v_{c1}(s)} = \frac{(R_Z C_Z s+1)}{(1+\frac{s}{Q_2\omega_2}+\frac{s^2}{\omega_2^2})(1-\frac{s}{Q_2\omega_2}+R_Z C_Z s+\frac{s^2}{\omega_2^2})-(s_f-s_e-\frac{s_f T_{off}}{2R_z C_z})\frac{s^2 T_{sw} R_Z C_Z}{s_n+s_f}} \tag{4.2}$$

where

$$s_n = R_i\frac{R_Z}{R_A}\frac{V_{in}-V_o}{L_s},\ s_f = R_i\frac{R_Z}{R_A}\frac{V_o}{L_s},\ Q_2 = \frac{2}{\pi},\ \omega_2 = \frac{\pi}{T_{sw}}$$

Equation (4.2) describes the transfer function from v_{c1} to v_{com} in average current mode control. This is an intermediate result which related average current mode control and V^2 control. From the transfer function, it is noticed that the additional large resistor R_B will not impact the transfer function and is ignored ever since.

To verify the proposed model for average current mode control, this modeling result is compared with Simplis simulation in Figure 4.6. The parameters used for the simulation are: V_{in} =12V, V_o=1.5V, F_{sw} =300kHz, R_i =10m, R_A =2kΩ, R_z =2kΩ, C_Z=3.5nF, s_e=0.5V.

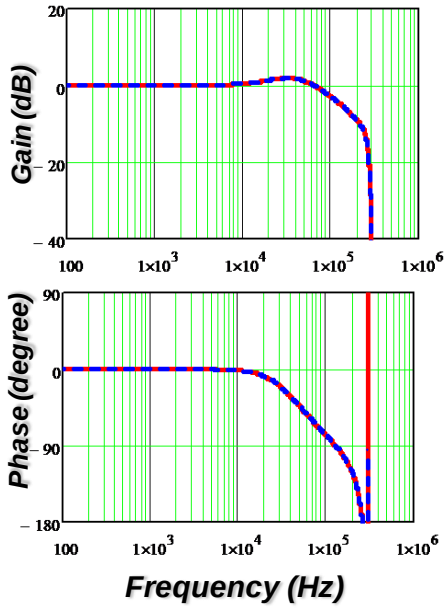

Figure 4. 6 v_{c1} to v_{com} transfer function comparison

The simplified polynomial transfer function of equation (4.2) is accurate up to switching frequency.

For the fourth order transfer function (4.2), it is not easy to analyze. The transfer function can be rewritten as a general form as

$$\frac{v_{com}(s)}{v_{c1}(s)} = \frac{(R_z C_z s + 1)}{(1 + \frac{s}{Q_a \omega_2} + \frac{s^2}{a\omega_2^2})(1 + \frac{s}{Q_b \omega_2} + a\frac{s^2}{\omega_2^2})} \tag{4.3}$$

in which Q_a and Q_b are two unknown quality factors. By equating the coefficients of equation (4.2) and (4.3),

$$\frac{1}{Q_a}+\frac{1}{Q_b}=R_Z C_Z \frac{\pi}{T_{sw}} \tag{4.4}$$

$$\frac{1}{Q_a}\cdot\frac{1}{Q_b}=[R_Z C_Z(\frac{Ds_e}{s_f}+\frac{1}{2}-D)-\frac{T_{sw}}{4}+D\frac{(1-D)T_{sw}}{2}]\frac{\pi^2}{T_{sw}} \tag{4.5}$$

For the system to be stable, Q_a and Q_b have to be positive. That means equation (4.4) and equation (4.5) are both positive. The stability criterion can be calculated as:

$$Y=R_Z C_Z(\frac{Ds_e}{s_f}+\frac{1}{2}-D)-\frac{T_{sw}}{4}+D\frac{(1-D)T_{sw}}{2}>0 \tag{4.6}$$

From equation (4.6) it can be observed that all the parameters: duty cycle *D*, compensator parameters R_Z, C_Z and R_A (within s_f) and external ramp s_e will all impact the system stability. Similar as in peak current mode control, external ramp can be used to get desired stability margin.

From equation (4.3), we can clearly see there are two sets of double poles around half of switching frequency depending on the value of *a*. The two sets of double poles can be clearly seen from Figure 4.6.

Another way to get the stability criterion is based on *Routh-Hurwitz Stability Criterion* [52]. *Routh-Hurwitz stability criterion* can be used for high order polynomial characteristic equations.

Equation (4.6) can also be used as the design criterion. Assume that $Q_a \geq Q_b$, then we want to control Q_a to be small enough so that the whole system will not show large peaking around half of the switching frequency.

$$Q_a = \frac{2}{R_z C_z \frac{\pi}{T_{sw}} - \frac{\pi}{T_{sw}} \sqrt{(R_z C_z)^2 - 2T_{sw} Y}} \tag{4.7}$$

Expression for Y is shown in equation (4.6). The desired quality factor can be designed based on equation (4.7).

After we get the intermediate result of transfer function from v_{c1} to $v_{com,}$ we want to find out the relation between control signal and inductor current (output voltage). Structure of average current mode control with perturbation at control signal is shown in Figure 4.7.

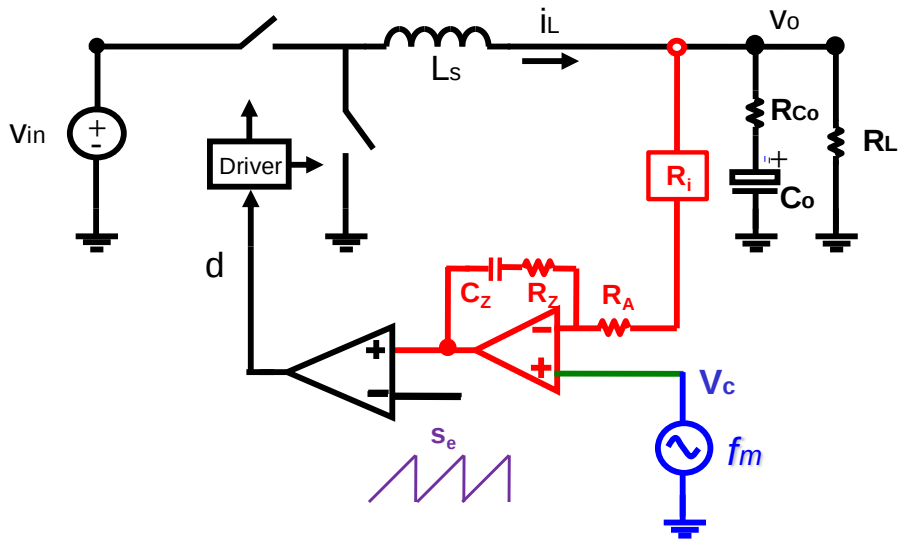

Figure 4. 7 Structure of average current mode control

Based on Figure 4.7, we can easily get relations between v_c and v_{c1}, v_{com} and i_L. These are all linear relations.

$$\frac{v_{c1}(s)}{v_c(s)} = 1 + \frac{R_Z + \frac{1}{sC_Z}}{R_A} \tag{4.8}$$

$$\frac{v_{com}(s)}{i_L(s)} = \frac{R_i}{R_A}(R_Z + \frac{1}{sC_Z}) \tag{4.9}$$

Then, control to inductor current transfer function can be calculated as below:

$$\frac{i_L(s)}{v_c(s)} = \frac{v_{com}(s)}{v_{c1}(s)}(\frac{v_{c1}(s)}{v_c(s)}\frac{i_L(s)}{v_{com}(s)}) = \frac{v_{com}(s)}{v_{c1}(s)}\frac{(R_A + R_Z)C_Z s + 1}{R_i(R_Z C_Z s + 1)} \tag{4.10}$$

This gives the relation between control signal and inductor current. The control to output voltage transfer function is shown as below:

$$\frac{v_o(s)}{v_c(s)} = \frac{i_L(s)}{v_c(s)}\frac{R_L(R_{Co}C_o s + 1)}{(R_L + R_{Co})C_o s + 1} = \frac{v_{com}(s)}{v_{c1}(s)}\frac{(R_A + R_Z)C_Z s}{R_i(R_Z C_Z s + 1)} \cdot \frac{R_L(R_{Co}C_o s + 1)}{(R_L + R_{Co})C_o s + 1} \tag{4.11}$$

To get equation (4.11), there is an underlying assumption that the inductor current slopes are considered as constant. The reason is that when we derive the model for V^2 control, constant current slopes assumption is used. Further discussion about this assumption is shown in Appendix E.

The simplified model has been verified in Simplis simulation as shown in Figure 4.8.

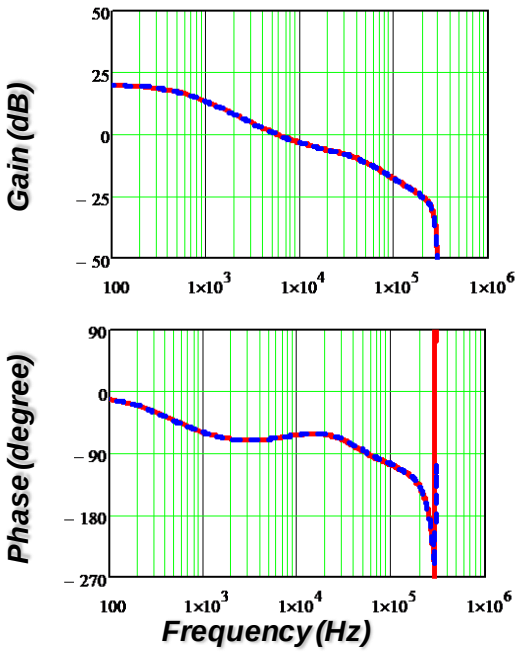

Figure 4. 8 control to output voltage transfer function verification

The model is very accurate comparing with Simplis simulation. However this model shows a transfer function of six orders. This high order transfer function gives designers trouble in understanding the result and designing average current mode control.

We look into the final transfer function (4.14) from control to output voltage. Equation (4.14) can be divided into two parts. The first part is v_{c1} to v_{com} transfer function, which is a fourth order transfer function; the remaining is only two orders related with current compensator and output RC network. The first part can be considered as high frequency part of the transfer function as it is unit gain until around half of switching frequency. We can choose proper external ramp magnitude based on equation (4.7) to get the desired stability margin. A flat curve up to high frequency is preferred for v_{c1} to v_{com} transfer function. Then the total transfer function of control signal to output

voltage is largely depend on the second order part which is mainly the low frequency part. Figure 4.9 is used to show the two parts of the final transfer function.

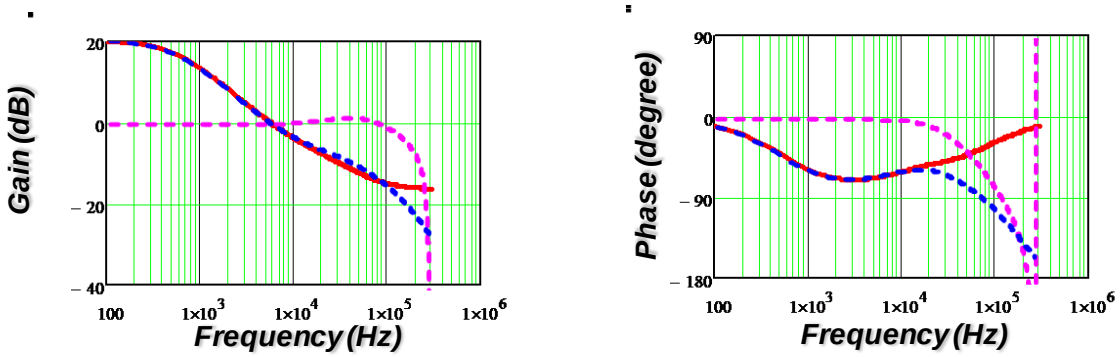

Figure 4. 9 Two parts of the control to output transfer function

In Figure 4.9, the pink curve is the high frequency fourth order part while the red curve is the low frequency second order part and the blue curve is the final transfer function from control to output.

For compensator design of average current mode control, we can based on the low frequency part second order transfer function. After we design the current compensator, external ramp can be designed to get desired stability margin based on the high frequency part transfer function.

The low frequency part second order transfer function is shown as below:

$$G_1(s) = \frac{(R_A + R_Z)C_Z s}{R_i(R_Z C_Z s + 1)} \cdot \frac{R_L(R_{Co} C_o s + 1)}{(R_L + R_{Co})C_o s + 1} \tag{4.15}$$

From the transfer function, we know the current compensator zero becomes a pole in control to output transfer function. If the zero position is set to be the same position as the output capacitor ESR zero, then these two will cancel.

For $R_z C_z = R_{Co} C_o$

$$G_1(s) = \frac{(R_A + R_Z)C_Z s}{R_i} \cdot \frac{R_L}{(R_L + R_{Co})C_o s + 1} \tag{4.16}$$

The low frequency part of control to output voltage transfer function is only a first order transfer function. The remaining pole is determined by the load resistor and output capacitor while the zero is at lower frequency than the output capacitor ESR zero. In this design method, the lower frequency zero will give us less phase drop for control to output voltage transfer function and would benefit the outer voltage loop design.

After we design the compensator based on the low frequency characteristic, the external ramp is chosen to get the desired high frequency characteristic, meaning relatively low peaking around half of switching frequency.

4.2.2 Average current mode with PI and high frequency pole

Another popular compensator structure for average current mode control is to add a small capacitor in parallel as shown in Figure 4.10. The additional small capacitor will introduce a high frequency pole for the current compensator. This high frequency pole is usually located around or higher than half of switching frequency to attenuate switching ripple and switching noise.

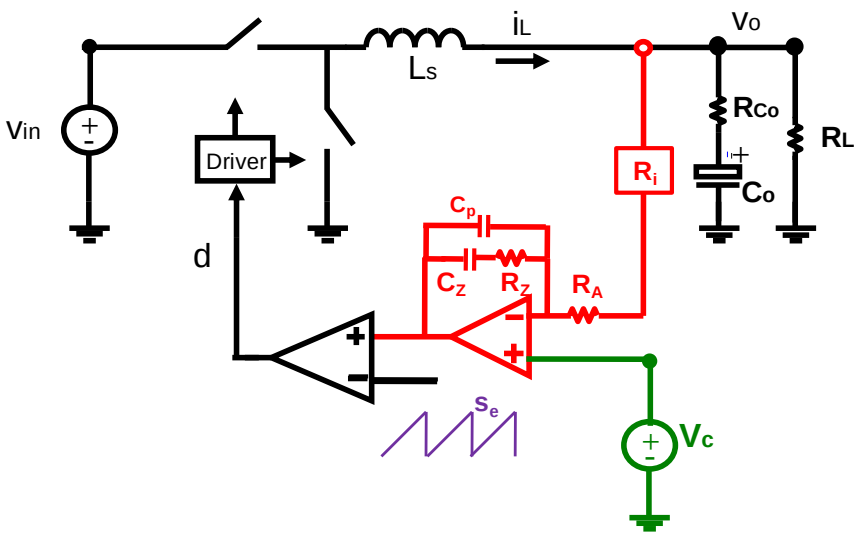

Figure 4. 10 Average current mode control with PI and high frequency pole

Following the same concept as in previous section for average current mode control with PI compensation, this average current mode control structure is also compared with V^2 control to find the similarity. This time, the V^2 control with composite output capacitors as shown in Chapter 3 is considered. The structure of V^2 control with composite output capacitors is shown as Figure 4.11.

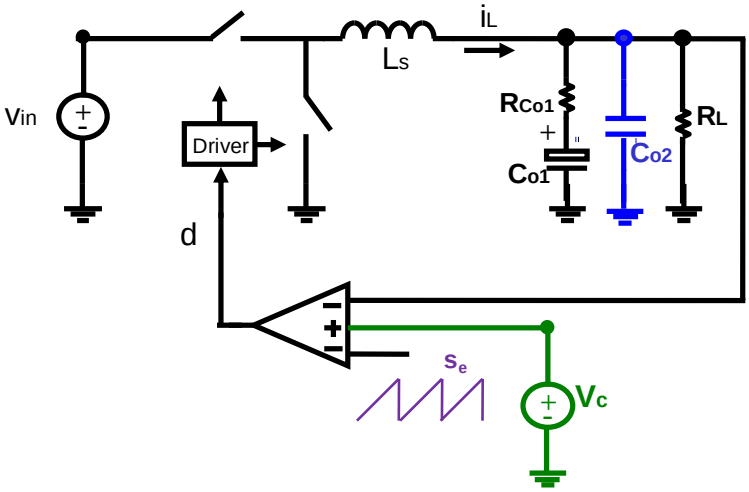

Figure 4. 11 Constant frequency V^2 control with composite capacitors

Similarity is identified between current compensator network in average current mode control and output capacitor network in V^2 control. Again the load resistor has little impact on small signal transfer function. Previous modeling result for constant frequency V^2 control with composite capacitors is used in average current mode control for transfer function from v_{c1} to $v_{com.}$ (v_{c1} is a perturbation source at the input of PWM modulator and v_{com} is the output of current compensator)

$$\frac{v_{com}(s)}{v_{c1}(s)} = \frac{R_Z C_z s + 1}{(1 + \frac{s}{Q_2 \omega_2} + \frac{s^2}{\omega_2^2})(1 + A_2 \cdot s + \frac{s^2}{\omega_2^2}) + B_2 \cdot T_{sw} s^2} \cdot \frac{1}{1 + \frac{R_Z C_Z C_P s}{C_Z + C_P}} \tag{4.17}$$

where

$$A_2 = \frac{s_{C1}}{s_n + s_f} R_z C_p + \frac{R_z C_z^2}{C_z + C_p} - \frac{T_{sw}}{2}, \quad B_2 = \frac{s_{C1}}{s_n + s_f} R_z C_z - \frac{R_z C_z^2}{C_z + C_p} + \frac{s_e}{s_n + s_f} R_Z (C_z + C_p)$$

$$s_{C1} = [\frac{(s_n + s_f)(e^{-\frac{T_{on}}{\tau}} - e^{-\frac{T_{sw}}{\tau}})}{e^{-\frac{T_{sw}}{\tau}} - 1} + s_n] \frac{C_{o1}}{C_{o1} + C_{o2}}, \quad \tau = \frac{R_{Co1} C_{o1} C_{o2}}{C_{o1} + C_{o2}}$$

$$s_n = R_i \frac{R_Z}{R_A} \frac{V_{in} - V_o}{L_s}, \; s_f = R_i \frac{R_Z}{R_A} \frac{V_o}{L_s}$$

This transfer function from v_{c1} to v_{com} is verified using Simplis simulation in Figure 4.12. The parameters used in simulation are: V_{in} =12V, V_o=1.5V, F_{sw} =300kHz, R_i =10m, R_A =2kΩ, R_z =2kΩ, C_Z=3.5nF, C_p=0.3n, s_e=0.5V.

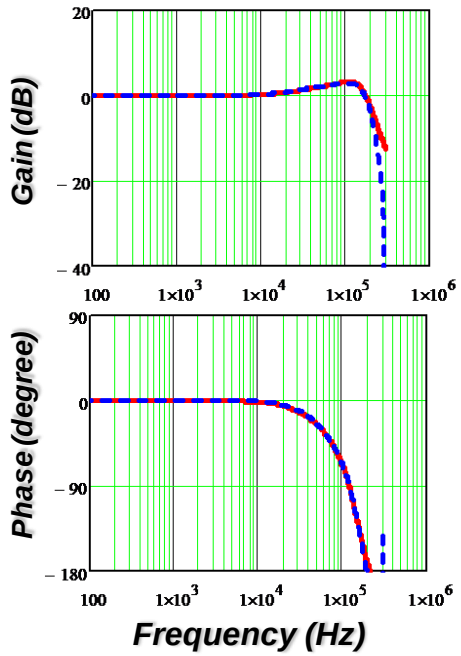

Figure 4. 12 v_{c1} to v_{com} transfer function comparison

Based on the transfer function from v_{c1} to v_{com} the stability criterion can be derived either based on the factorization of the fifth order transfer function or based on *Routh-Hurwitz criterion* as shown in previous section.

The stability criterion is shown as:

$$[1-2e^{-\frac{DT_{sw}}{R_Z C_p}}-2D]R_Z C_Z+\frac{R_A}{R_i}s_e C_Z\frac{2L_s}{V_{in}}-\frac{T_{sw}}{2}>0 \tag{4.18}$$

Just as before, all the compensation parameters, external ramp and duty cycle will impact the stability margin. The external ramp can be controlled to get the desired stability margin.

After we get the transfer function from v_{c1} to v_{com}, it is also easy to get the relation between control signal and output voltage. The structure is shown as in Figure 4.13.

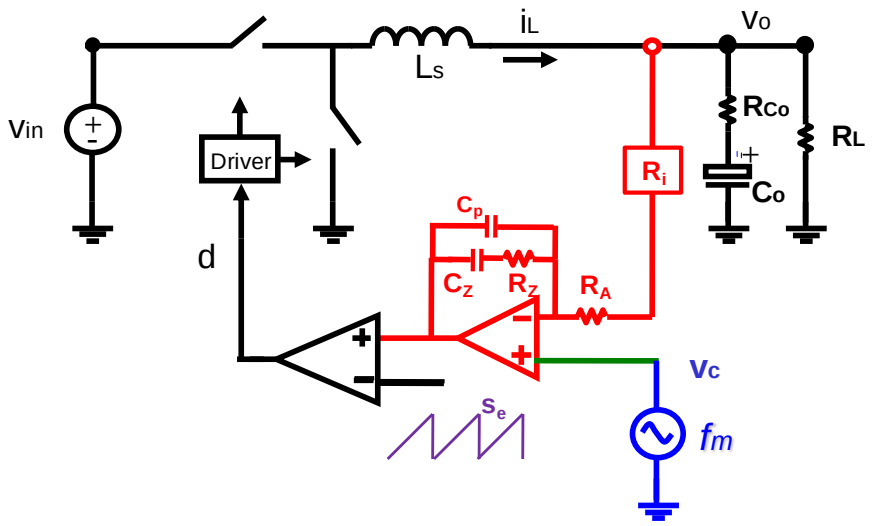

Figure 4. 13 Control to output voltage transfer function

In previous section, it has been proved that the output voltage variation effect is very small. In this structure of current compensator, the transfer function of control to output is shown as:

$$\frac{v_o(s)}{v_c(s)} = \frac{v_{com}(s)}{v_{c1}(s)}\left(\frac{R_A R_Z C_Z C_p s^2 + sC_p R_A + sC_Z R_A}{R_i(R_Z C_Z s+1)} + \frac{1}{R_i}\right)\frac{R_L(R_{Co}C_o s+1)}{(R_L+R_{Co})C_o s+1} \tag{4.19}$$

The control to output voltage transfer function can be verified using Simplis simulation as in Figure 4.14.

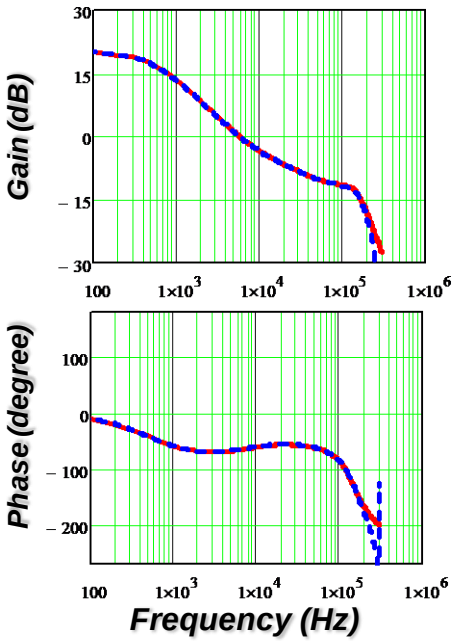

Figure 4. 14 Control to output transfer function comparison

Comparing with previous section of average current mode control with PI compensation, the structure of average current mode control with high frequency pole gives even more complicated small signal transfer function. The final result from control signal to output transfer function is 7th order and some of the coefficients are in exponential form. However, the previous argument still holds that we can use the low frequency part to design the compensator and use external ramp to get the desired stability margin.

4.2.3 Comparison of two compensation structures

For the two most popular compensation structures, the main difference is that whether there is a high frequency pole or not. After we get the modeling result, we can try to find out the effect of this high frequency pole.

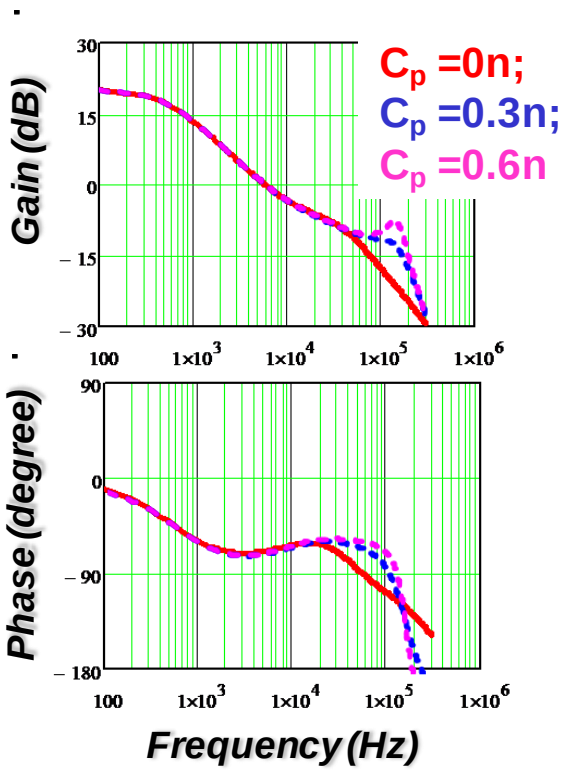

Figure 4. 15 Effect of the high frequency pole in current compensator

Figure 4.15 gives three examples for average current mode control with different high frequency pole positions. By adding more capacitance in parallel, the additional pole will move to lower frequency. However, by doing that, the peaking at half of switching frequency as shown in Figure 4.15 will become higher which indicates lower stability margin.

For the red curve in Figure 4.15, we can design the control to output voltage transfer function to get almost all the properties we want. That means for average current mode control, a PI compensation is enough.

4.2.4 Experimental verification

The experimental verification is done based on the MAX5066 evaluation board from Maxim. The parameters are: V_{in}=10V, V_o=1.3V, F_{sw}=450kHz, L_s=800nH, C_o=400μF, R_L =1Ω. For the compensation network, R_Z =2.55kΩ, C_z=6.8nF.

Experimental results with different values for C_p are shown in Figure 4.16. The experiment results agree with the model results very well.

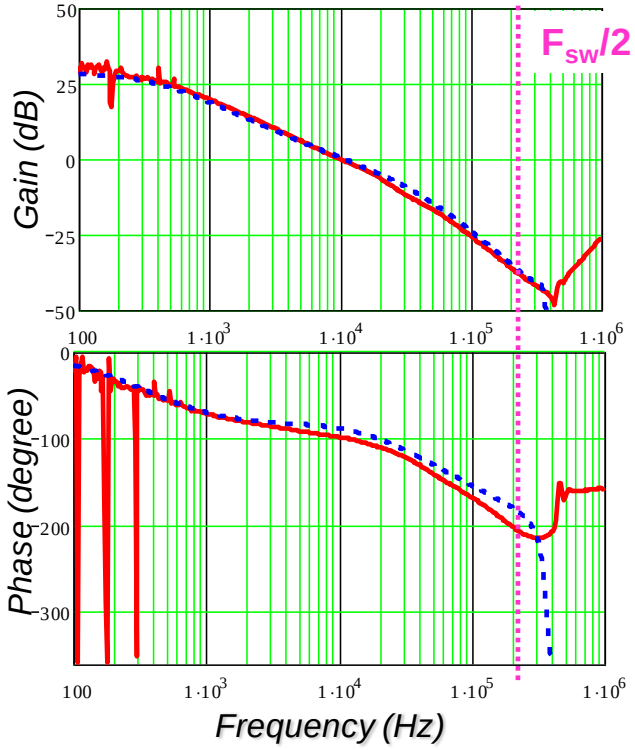

(a)

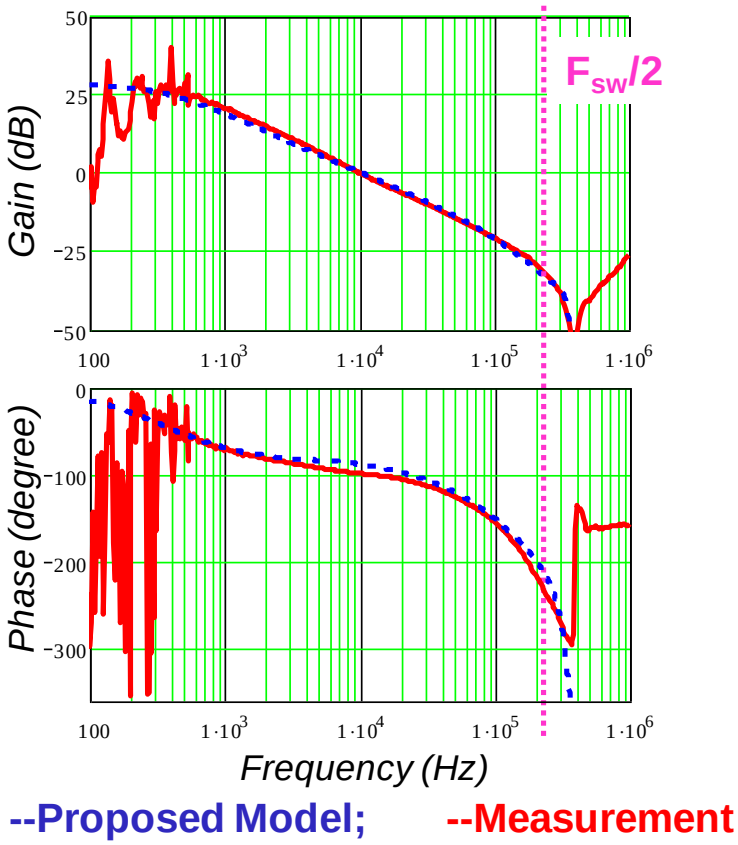

(b)

Figure 4. 16 Control to output transfer function comparison: (a) C_p=0; (b) C_p=150pF

4.3 Extension to Other Average Current Mode Control Scheme

All the derivation in this Chapter is based on the similarity between average current mode control and V^2 control. The similarity is between current compensation network and output capacitor network structures. It is not limited by modulation schemes. In fact the similarity can apply to either constant frequency or variable frequency case. For average current mode control with constant on time modulation, previous modeling result for constant on time V^2 control can be adopted as shown in Figure 4.17.

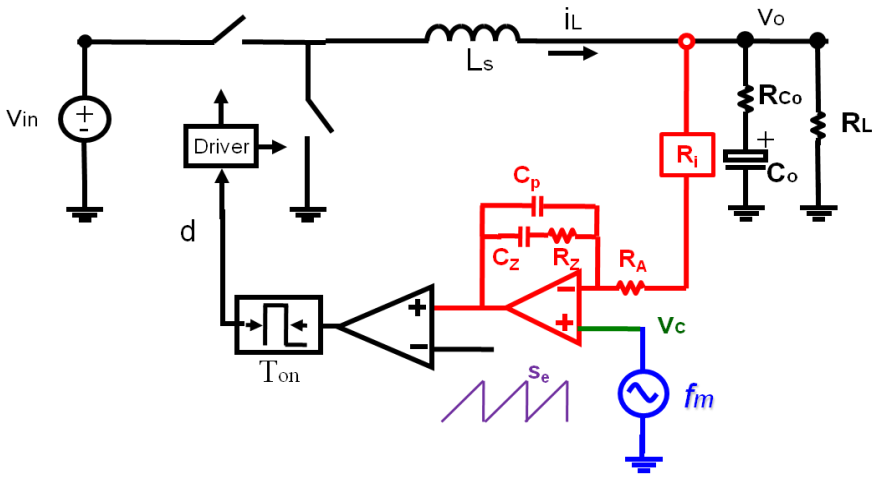

(a)

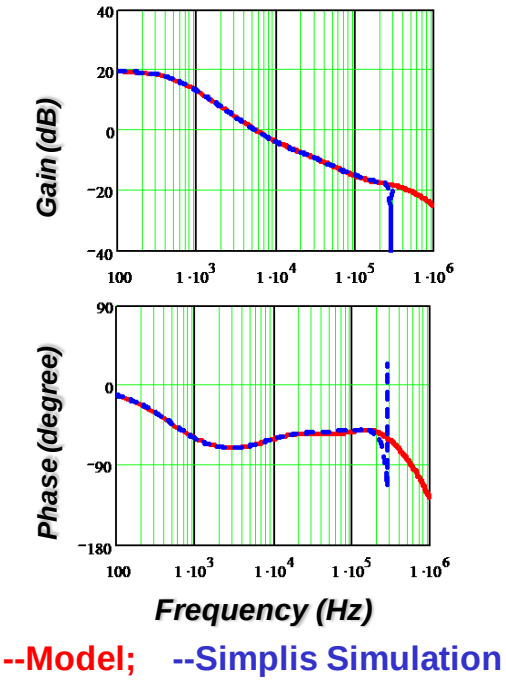

(b)

Figure 4. 17 (a)constant on time average current mode control (b) control to output voltage transfer function

4.4 Summary

The model for average current mode control is derived based on similarity between average current mode control and V^2 control. Previous modeling result for V^2 is utilized. The small signal model can be accurate beyond half of switching frequency. The results have been verified using Simplis simulation and measurements. In average current mode control, it is not desired to add a high frequency pole in current compensator from stability point of view.

Chapter 5. Conclusion

5.1 Summary

With the development of control techniques, various control methods are used nowadays. Some of the feedback loops are becoming more and more nonlinear, such as different types of current mode control and V^2 control. This thesis tries to solve two of the remaining modeling problems: V^2 control with composite capacitors and average current mode control.

For V^2 control with single types of output capacitors, a circuit model is proposed based on the concept of separating the feedback information in inner voltage feedback loop. Previous equivalent circuit model for current mode control is used. The equivalent circuit model for V^2 control reveals the relation between V^2 control and current mode control. V^2 control can be considered as current mode control with a direct capacitor voltage feedback loop.

For V^2 control with composite capacitors, the model is derived based on describing function method. Comparing with V^2 control with single type of output capacitors, the output voltage time domain waveform is much more difficult to describe. The final transfer function from control signal to output voltage is simplified and compared with single type of output capacitor case. It is shown from the modeling result that the additional ceramic branch will reduce the effect of bulk capacitor ESR and reduce system stability margin.

For average current mode control, similarity is found between average current mode control and V^2 control. V^2 control modeling result is utilized for average current mode control. Although the model for average current mode control is complicated, stability criterion and design method are proposed. A low frequency model can be used to design the current compensator and stability criterion can be used to design the external ramp in average current mode control. The small signal model also shows that the high frequency pole in current compensator is not good for system stability.

5.2 Future Works

Although the describing function method is very powerful technique for modeling of nonlinear systems, the process is complicated and difficult to follow. Equivalent circuit model can be a good way to understand the complicated small signal behavior. Chapter 2 makes an attempt to use equivalent circuit to model V^2 control. However, this work is still not finished. It is possible to get an equivalent circuit model for all kinds of V^2 control.

As the average modeling concept will fail for systems with highly nonlinear loops and time domain describing is too complicated, it is possible to extend the average modeling concept to multi-frequency modeling concept as in [53]. Multi-frequency modeling concept can be extended to current mode control and V^2 control.

Appendix A. Steady State Capacitor Current Calculation

The following part will solve the steady state time domain waveform expression for capacitor currents. This will form the basis for further perturbed time domain calculation.

In steady state, we first consider the current divider formed by the two capacitor branches. As the load resistor is relatively large, it is assumed that all of the AC part of inductor current will flow through the two capacitor branches as shown in Figure A.1. In steady state capacitor current calculation, all the frequency components considered is multiples of switching frequency. For these high frequency components, it is reasonable to assume them all flowing through the two capacitor branches.

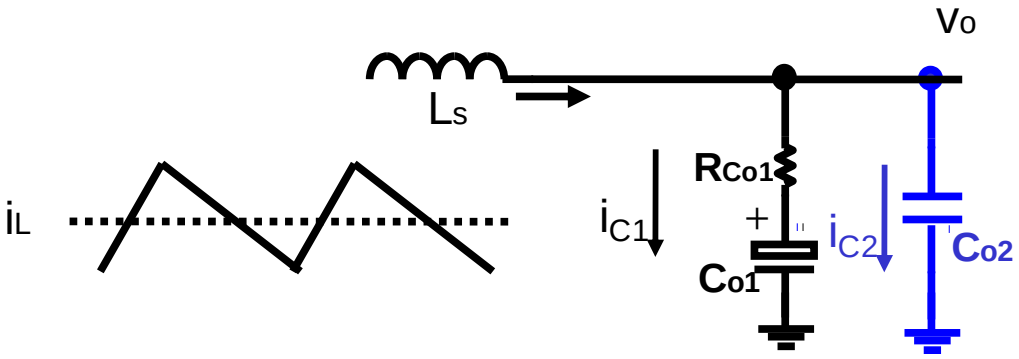

Figure A. 1 current divider formed by two capacitor branches

In Figure A.1, the input current is the AC portion of the inductor current. We know the input current waveform and we know the parameters of the two capacitor branches. We can certainly solve the capacitor current in each branch. In this section, all the variables in lower case are steady state variables.

According to KVL:

$$v_{cap2} = R_{C1} i_{C1} + v_{cap1} \tag{A.1}$$

In which, v_{cap1} and v_{cap2} are the voltages over C_{o1} and C_{o2}.

According to KCL:

$$i_{C1} + i_{C2} = i_L - i_o \tag{A.2}$$

In steady state,

$$i_{C1} + i_{C2} = i_{LAC} \tag{A.3}$$

Substitute (3.2) into (3.4), in steady state, during top switch on-time,

$$i_{C1} + \frac{C_{o2}}{C_{o1}} i_{C1} + R_{C1} C_{o2} \frac{d(i_{C1})}{dt} = s_n t - \frac{I_{pp}}{2} \tag{A.4}$$

during top switch off-time,

$$i_{C1} + \frac{C_{o2}}{C_{o1}} i_{C1} + R_{C1} C_{o2} \frac{d(i_{C1})}{dt} = \frac{I_{pp}}{2} - s_f t \tag{A.5}$$

where $s_n = (V_{in} - V_o) / L_s$, $s_f = V_o / L_s$, L_s is the inductance of the inductor, I_{pp} is the peak to peak inductor current ripple.

As in steady state, the inductor current value at the starting point and the end point of a switching cycle should be the same, based on equation (A.4) and (A.5), the capacitor current in the bulk capacitor branch can be calculated as:

During top switch on-time, current in bulk capacitor branch

$$i_{C1}(t) = -\frac{C_{o1}}{C_{o1}+C_{o2}} K e^{-\frac{t}{\tau}} - \frac{R_{C1} C_{o1}^{\ 2} C_{o2}}{(C_{o1}+C_{o2})^2} s_n - \frac{C_{o1}}{C_{o1}+C_{o2}} \frac{I_{pp}}{2} + \frac{C_{o1}}{C_{o1}+C_{o2}} s_n t \tag{A.6}$$

During top switch off-time, current in bulk capacitor branch

$$i_{C1}(t) = -\frac{C_{o1}}{C_{o1}+C_{o2}} K_1 e^{-\frac{t}{\tau}} + \frac{R_{C1} C_{o1}^{\ 2} C_{o2}}{(C_{o1}+C_{o2})^2} s_f + \frac{C_{o1}}{C_{o1}+C_{o2}} \frac{I_{pp}}{2} - \frac{C_{o1}}{C_{o1}+C_{o2}} s_f t \tag{A.7}$$

where

$$\tau = \frac{R_{C1} C_{o1} C_{o2}}{C_{o1}+C_{o2}}, \quad K = \tau(s_f + s_n)\frac{1-e^{-\frac{T_{off}}{\tau}}}{e^{-\frac{T_{sw}}{\tau}}-1}, \quad K_1 = \tau(s_f + s_n)\frac{-1+e^{-\frac{T_{on}}{\tau}}}{e^{-\frac{T_{sw}}{\tau}}-1}$$

For the capacitor current information, two quantities are of the most importance: the current slope and magnitude at the end of off time where the switch action is determined. According to the capacitor current expressions (A.6) and (A.7), the current slope at the end of off time can be expressed as following

$$s_{c1} = -\frac{K_1}{R_{C1} C_{o2}} e^{\frac{-T_{off}}{\tau}} + \frac{C_{o1}}{C_{o1}+C_{o2}} s_f \tag{A.8}$$

The current magnitude at the end of off time is shown as below

$$I_{valley1} = \frac{C_{o1}}{C_{o1}+C_{o2}} K_1 e^{-\frac{T_{off}}{\tau}} - \frac{R_{C1} C_{o1}^{\ 2} C_{o2}}{(C_{o1}+C_{o2})^2} s_f + \frac{C_{o1}}{C_{o1}+C_{o2}} \frac{I_{pp}}{2} \tag{A.9}$$

All the above calculation is considering the bulk capacitor branch, the other branch current can also be easily derived. After we get the steady state capacitor current, we can easily calculate the steady state output voltage.

Appendix B. Perturbed State Capacitor Current Calculation

This section will focus on the capacitor current calculation under perturbation.

We assume the control signal perturbation is injected at a particular switching cycle. The off time variation of the first perturbed cycle is denoted as $\Delta T_{off(1)}$. As the inductor current slopes are assumed as constant, the inductor current perturbation in the second cycle ($t_1+T_{off(1)}<t< t_2+T_{off}$) is

$$\Delta i_{L(2)} = \Delta i_{C1} + \Delta i_{C2} = s_f \Delta T_{off(1)} \tag{B.1}$$

When we consider the perturbed state, the load resistor branch can no longer be ignored. For low frequency perturbation input, the load resistor branch can show smaller impedance than the two capacitor branches. So the load resistor branch will show its impact in low frequency range when the impedance of load resistor is smaller or comparable with the two capacitor branches .

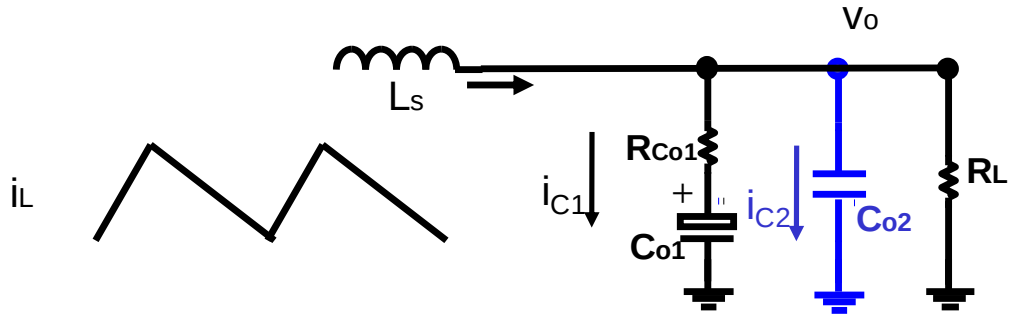

Figure B. 1 Load RC network in perturbed state

As shown in Figure B.1, the input of the load circuit is the inductor current with perturbation. The inductor current contains DC information, modulation frequency and switching frequency harmonics. The DC information will all go into load resistor. When the modulation frequency is low, the modulation frequency will distribute within these three branches. In low frequency range, we assume the output voltage perturbation will follow the control signal perturbation as shown in Figure 3.12, the output current perturbation is

$$\Delta i_o \approx \frac{\Delta v_c}{R_L} \tag{B.2}$$

In equation (B.2), R_L is the load resistor.

Based on Figure B.1, inductor current and load current will both impact the capacitor currents. Equations (B.1) and (B.2) are the two perturbation sources when we calculate the capacitor currents under perturbation. Equation (B.1) considers the modulation signal from two capacitor branches. Equation (B.2) considers the modulation signal from load resistor branch. Based on superposition theory, they can be considered one by one.

The bulk capacitor branch capacitor current perturbation at the end of first cycle (time instant: $t_1+T_{off(1)}$) with an off time variation of $\Delta T_{off(1)}$ ($T_{off(1)}=T_{off}+\Delta T_{off(1)}$) is:

$$\Delta i_{C1(1)} = s_{C1}\Delta T_{off\,(1)} \tag{B.3}$$

It is only determined by the capacitor current slope at the decision point and off time variation.

When we consider the perturbation source from the inductor current perturbation of equation (B.1), we can calculate the capacitor current perturbation during the second cycle ($t_1+T_{off(1)}<t< t_2+T_{off}$) after the perturbation injection.

$$\Delta i_{C1(2)} = (-\frac{K_1}{R_1 C_{o2}} e^{-\frac{T_{off}}{\tau}}) e^{-\frac{t}{\tau}} \Delta T_{off(1)} + \frac{C_{o1}}{C_{o1}+C_{o2}} s_f \Delta T_{off(1)} \tag{B.4}$$

The capacitor current perturbation contains two parts: one part is decaying with time while the other part is constant. Assume the decaying part can be ignored after one cycle, then for period i ($t_{(i-1)}+T_{off(i-1)}<t< t_i+T_{off}$), the capacitor current perturbation is:

$$\Delta i_{C1(i)} = (-\frac{K_2}{R_{C1} C_{o2}} e^{-\frac{T_{off}}{\tau}}) e^{-\frac{t}{\tau}} \Delta T_{off(i-1)} + \frac{C_{o1}}{C_{o1}+C_{o2}} s_f \sum_0^{i-1} \Delta T_{off(k)} \tag{B.5}$$

For equation (B.5), capacitor current perturbation also has two part: one part is decaying and one part is constant. For most of V^2 implementation, due to stability concern, ceramic capacitance is small, so that the time constant τ is much smaller than the off time. In that case, previous equation can be simplified to ignore the decaying term:

$$\Delta i_{C1(i)} \approx \frac{C_{o1}}{C_{o1}+C_{o2}} s_f \sum_0^{i-1} \Delta T_{off(k)} \tag{B.6}$$

When we add large ceramic capacitance in parallel, the aforementioned approximation of ignoring the decaying term will introduce some inaccuracy. For most cases, equation (B.6) is a good approximation.

Considering the other perturbation source coming from the load current of equation (B.2), the total capacitor current perturbation can be expressed as

$$\Delta i_{C1(i)} \approx \frac{C_{o1}}{C_{o1}+C_{o2}} s_f \sum_{0}^{i-1} \Delta T_{off(k)} + \frac{C_{o1}}{C_{o1}+C_{o2}} \frac{\Delta v_c}{R_L} \tag{B.7}$$

Appendix C. Constant Frequency V^2 Control with Composite Capacitors

This appendix provides the detail modeling derivations for constant frequency peak voltage type V^2 control with composite capacitors.

The assumptions are the same as constant on time V^2 case in Chapter 3. The modeling structure is shown in Figure C.1. A small signal perturbation is injected at the control signal.

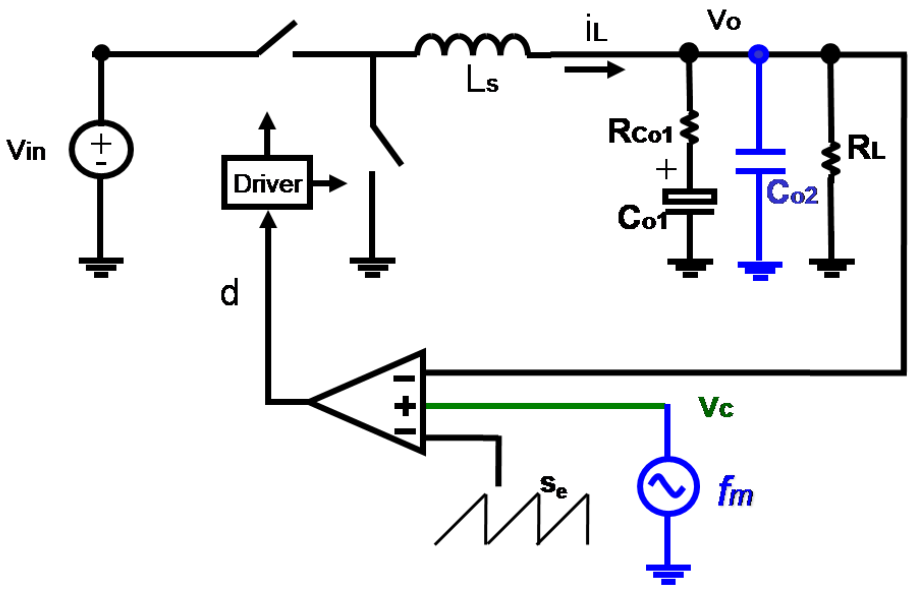

Figure C. 1 Modeling of constant frequency V^2 control with composite capacitors

The first step is still to calculate the steady state capacitor current. The time domain capacitor current expression is important for further perturbation calculation.

According to the calculation in Appendix A, equation (A.6) and (A.7) are repeated as (C.1) and (C.2). These two equations describe the bulk capacitor current during on time and off time.

During switch on-time,

$$i_{C1}(t) = -\frac{C_{o1}}{C_{o1}+C_{o2}} K e^{-\frac{t}{A}} - \frac{R_{C1} C_{o1}^{\ 2} C_{o2}}{(C_{o1}+C_{o2})^2} s_n - \frac{C_{o1}}{C_{o1}+C_{o2}} \frac{I_{pp}}{2} + \frac{C_{o1}}{C_{o1}+C_{o2}} s_n t \tag{C.1}$$

During switch off-time:

$$i_{C1}(t) = -\frac{C_{o1}}{C_{o1}+C_{o2}} K_1 e^{-\frac{t}{A}} + \frac{R_{C1} C_{o1}^{\ 2} C_{o2}}{(C_{o1}+C_{o2})^2} s_f + \frac{C_{o1}}{C_{o1}+C_{o2}} \frac{I_{pp}}{2} - \frac{C_{o1}}{C_{o1}+C_{o2}} s_f t \tag{C.2}$$

where,

$$A = \frac{R_{C1} C_{o1} C_{o2}}{C_{o1}+C_{o2}}, \quad K = A(s_f + s_n)\frac{1-e^{-\frac{T_{off}}{A}}}{e^{-\frac{T_{sw}}{A}}-1}, \quad K_1 = A(s_f + s_n)\frac{-1+e^{-\frac{T_{on}}{A}}}{e^{-\frac{T_{sw}}{A}}-1}$$

For constant frequency V^2 control, the decision point is at the end of switch on time. The capacitor current slope and magnitude at that instant are shown as below:

$$s_{c1} = \frac{K}{R_{C1} C_{o1}} e^{-\frac{T_{on}}{A}} + \frac{C_{o1}}{C_{o1}+C_{o2}} s_n \tag{C.3}$$

$$I_{peak} = -\frac{C_{o1}}{C_{o1}+C_{o2}} K e^{-\frac{T_{on}}{A}} - \frac{R_{C1} C_{o1}^{\ 2} C_{o2}}{(C_{o1}+C_{o2})^2} s_n + \frac{C_{o1}}{C_{o1}+C_{o2}} \frac{I_{pp}}{2} \tag{C.4}$$

When we inject the small signal perturbation at control signal, the perturbed time domain waveform is shown in Figure A.2. Figure A.2 shows a case with external ramp.

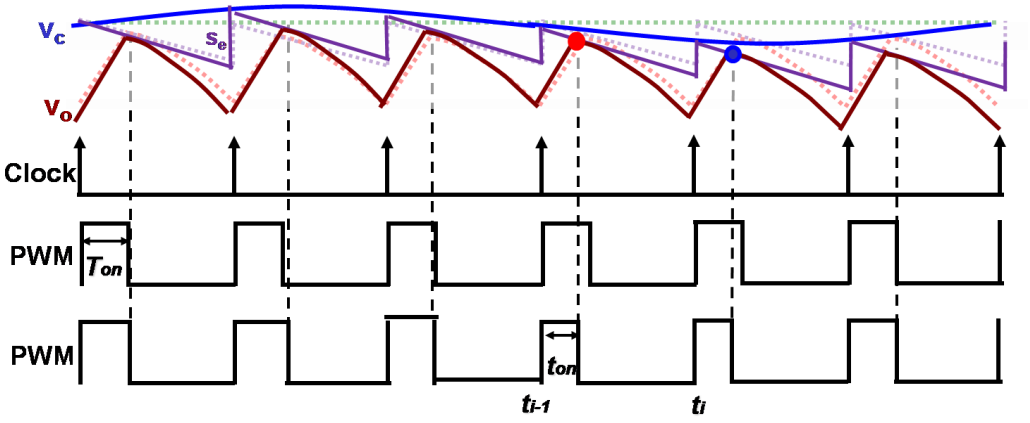

Figure C. 2 Perturbed output voltage waveform in V^2 control

As shown in Figure C.2, the output voltage will follow the modulated control signal. The switch on time is modulated by the perturbation signal $v_c(t)$:

$$v_c(t) = V_c + \hat{v}_c \sin(2\pi f_m \cdot t + \theta) \tag{C.5}$$

where V_c is the steady state DC value of the control signal. $\hat{v}_c$ is the magnitude of the perturbation, and θ is the initial angle.

We focus on one switching cycle in the modulated output voltage waveform. At the starting point of this cycle (the red dot in Figure A. 2):

$$v_c(t_{i-1} + T_{on(i-1)}) = R_{C1} i_{C1}(t_{i-1} + T_{off\,(i-1)}) + v_{Co1}(t_{i-1} + T_{off\,(i-1)}) + s_e T_{on(i-1)} \tag{C.6}$$

At the end point of this cycle (the blue dot):

$$v_c(t_i + T_{on(i)}) = R_{C1} i_{C1}(t_i + T_{on(i)}) + v_{Co1}(t_i + T_{on(i)}) + s_e T_{on(i)} \tag{C.7}$$

For the above two equations, they describe the fact that at the decision point, control signal equals to output voltage.

By subtracting the previous two equations (C.7) and (C.6), the output voltage variation can be related with control signal variation.

$$v_c(t_{i-1}+T_{on(i-1)})-v_c(t_i+T_{on(i)}) = R_{C1}[i_{C1}(t_{i-1}+T_{on(i-1)})-i_{C1}(t_i+T_{on(i)})]-\frac{\int_{t_{i-1}+T_{on(i-1)}}^{t_i+T_{on(i)}} i_{C1}(t)dt}{C_{o1}}+s_e(T_{on(i-1)}-T_{on(i)})$$

(C.8)

The left side of the equation is control signal variation over one switching cycle; the right side has two parts: one part is the output voltage variation over the same switching cycle and the other part is related with external ramp. The output voltage variation contains two parts: one part is voltage variation over the ESR of the bulk capacitor and the other is voltage variation over the pure capacitance.

To calculate the right side, capacitor current under perturbation is needed. So the following part will focus on the capacitor current calculation under perturbation.

We assume the control signal perturbation is injected at a particular switching cycle. The on time variation of the first perturbed cycle is denoted as $\Delta T_{on(1)}$. The inductor current perturbation is

$$\Delta i_L = \Delta i_{C1} + \Delta i_{C2} = s_n \Delta T_{on(1)} \quad \text{(C.9)}$$

The output load current will also be modulated. We assume the output voltage perturbation will follow the control signal perturbation as shown in Figure C.2, the output current perturbation is

$$\Delta i_o \approx \frac{\Delta v_c}{R_L} \tag{C.10}$$

In equation (C.10), R_L is the load resistor.

Similar as in Appendix B, inductor current and load current will both impact the capacitor current. Equations (C.9) and (C.10) are the two perturbation sources when we calculate the capacitor current perturbation. Based on superposition theory, they can be considered one by one.

The bulk capacitor branch capacitor current perturbation with an on time variation of $\Delta T_{on(1)}$ is:

$$\Delta i_{C1(1)} = s_{C1} \Delta T_{on(1)} \tag{C.11}$$

When we consider the perturbation source from the inductor current perturbation of equation (C.9), we can calculate the capacitor current perturbation at the second cycle after the perturbation injection.

$$\Delta i_{C1(2)} = (\frac{K_2}{R_{C1} C_{o2}} e^{-\frac{T_{on}}{A}} - \frac{C_{o1}}{C_{o1} + C_{o2}} s_f) e^{-\frac{t}{A}} \Delta T_{on(1)} + \frac{C_{o1}}{C_{o1} + C_{o2}} (s_n + s_f) \Delta T_{on(1)} \tag{C.12}$$

The capacitor current perturbation contains two parts: one part is decaying with time while the other part is constant. Assume the decaying part can be ignored after one cycle, then for period i, the capacitor current perturbation is:

$$\Delta i_{C1(i)} \approx (\frac{K_2}{R_{C1}C_{o2}} e^{-\frac{T_{on}}{A}} - \frac{C_{o1}}{C_{o1}+C_{o2}} s_f) e^{-\frac{t}{A}} \Delta T_{on(i-1)} + \frac{C_{o1}}{C_{o1}+C_{o2}} (s_n + s_f) \sum_{k=1}^{i-1} \Delta T_{on(k)} \quad \text{(C.13)}$$

Considering the other perturbation source coming from the load current of equation (C.10), the total capacitor current perturbation can be expressed as

$$\Delta i_{C1(i)} \approx (\frac{K_2}{R_{C1}C_{o2}} e^{-\frac{T_{on}}{A}} - \frac{C_{o1}}{C_{o1}+C_{o2}} s_f) e^{-\frac{t}{A}} \Delta T_{on(i-1)} + \frac{C_{o1}}{C_{o1}+C_{o2}} (s_n + s_f) \sum_{k=1}^{i-1} \Delta T_{on(k)} + \frac{C_{o1}}{C_{o1}+C_{o2}} \frac{\Delta v_c}{R_L}$$

(C.14)

From expression of (C.14), the capacitor current perturbation is a function of accumulated on-time variations and control signal perturbation. The most adjacent cycle also has a decaying effect on capacitor current perturbation. This capacitor current perturbation can be used to calculate the output voltage perturbation over one switching cycle. Voltage variation over the ESR of bulk capacitor is:

$$\begin{aligned} \Delta v_{ESR} &= R_{C1}[i_{C1}(t_{i-1} + T_{on(i-1)}) - i_{C1}(t_i + T_{on(i)})] \\ &= (\frac{K_2}{C_{o2}} e^{-\frac{T_{on}}{A}} - \frac{R_{C1}C_{o1}}{C_{o1}+C_{o2}} s_f)(e^{-\frac{T_{sw}}{A}} - 1)\Delta T_{on(i-1)} + s_{C1} R_{C1} \Delta T_{on(i)} \end{aligned} \quad \text{(C.15)}$$

Voltage variation over the bulk capacitance is:

$$\Delta v_{cap} = \frac{\int_{t_{i-1}+T_{off(i-1)}}^{t_i+T_{off(i)}} i_{C1}(t)dt}{C_{o1}} = \frac{(s_n + s_f)T_{sw}}{C_{o1}+C_{o2}} \sum_0^{i-1} \Delta T_{on(k)} + (\frac{K_2}{R_{C1}C_{o1}C_{o2}} e^{-\frac{T_{on}}{A}} - \frac{s_f}{C_{o1}+C_{o2}}) A(1-e^{-\frac{T_{sw}}{A}}) \Delta T_{on(i-1)}$$

$$+ \frac{I_{peak}}{C_{o1}} \Delta T_{on(i)} + \frac{v_c(t_i + T_{on(i)} + \frac{\pi}{2\pi f_m \cdot 2}) - v_c(t_{i-1} + T_{on(i-1)} + \frac{\pi}{2\pi f_m \cdot 2})}{2\pi f_m \cdot R_L(C_{o1}+C_{o2})} \tag{C.16}$$

Substitute equation (C.15) and (C.16) into (C.8)

$$v_c(t_{i-1} + T_{on(i-1)}) - v_c(t_i + T_{on(i)}) + \frac{v_c(t_i + T_{on(i)} + \frac{\pi}{2\pi f_m \cdot 2}) - v_c(t_{i-1} + T_{on(i-1)} + \frac{\pi}{2\pi f_m \cdot 2})}{2\pi f_m \cdot R_L(C_{o1}+C_{o2})}$$

$$= s_{C1} R_{C1} \Delta T_{on(i)} + \frac{I_{peak}}{C_1} \Delta T_{on(i)} + \frac{(s_n + s_f)T_{sw}}{C_1 + C_2} \sum_0^{i-1} \Delta T_{on(k)}$$

$$-(\frac{K_2 C_1}{C_2(C_1+C_2)} e^{-\frac{T_{on}}{A}} - \frac{R_1 C_1^2}{(C_1+C_2)^2} s_f)(1-e^{-\frac{T_{sw}}{A}}) \Delta T_{on(i-1)} \tag{C.17}$$

Equation (C.17) gives the time domain relation of control signal variation and on time variation. Based on similar process as in Chapter 3 or [14][19], transfer function can be derived using Fourier analysis.

Control to output transfer function is:

$$\frac{v_o(s)}{v_c(s)} = \frac{F_{sw}(1-e^{-sT_{sw}})(1-e^{-sT_{sw}})}{R_{C1}s_{C1} + \frac{I_{peak}}{C_{o1}} + (\frac{(s_n+s_f)T_{sw}}{C_{o1}+C_{o2}} - R_{C1}s_{C1} - \frac{I_{peak}}{C_{o1}} - A_2)e^{-sT_{sw}} + A_2 e^{-2sT_{sw}}} \frac{V_{in}}{sL_s} \tag{C.18}$$

$$\times (1 + \frac{1}{sR_L(C_{o1}+C_{o2})}) Z_o(s)$$

where,

$$A_2 = (\frac{KC_{o1}}{C_{o2}(C_{o1}+C_{o2})} e^{-\frac{T_{on}}{A}} - \frac{R_{C1}C_{o1}^{\ 2}}{(C_{o1}+C_{o2})^2} s_f)(1-e^{-\frac{T_{sw}}{A}})$$

The complicated transfer function is accurate beyond switching frequency. Using Padé approximation to simplify equation (C.18):

$$\frac{v_o(s)}{v_c(s)} = \frac{R_{C1}C_{o1}s+1}{(1+\frac{s}{Q_1\omega_2}+\frac{s^2}{\omega_2^{\ 2}})(1+A_3 s+\frac{s^2}{\omega_2^{\ 2}})+B_3 T_{sw} s^2} \cdot \frac{1}{1+\frac{R_{C1}C_{o1}C_{o2}s}{C_{o1}+C_{o2}}} \quad \text{(C.19)}$$

where,

$$Q_1 = \frac{2}{\pi},\ \omega_2 = \frac{\pi}{T_{sw}},\ A_3 = \frac{s_{C1}}{s_n+s_f} R_{C1}C_{o2} + \frac{R_{C1}C_{o1}^{\ 2}}{C_{o1}+C_{o2}} - \frac{T_{sw}}{2},$$

$$B_3 = \frac{s_{C1}}{s_n+s_f} R_{C1}C_{o1} - \frac{R_{C1}C_{o1}^{\ 2}}{C_{o1}+C_{o2}} + \frac{s_e}{s_n+s_f}(C_{o1}+C_{o2})$$

Appendix D. Constant On Time V^2 Control with External Ramp

In Chapter 3, it is briefly discussed for constant on time V^2 control adding external ramp case. With composite output capacitors and small external ramp, the control to output transfer function can be simplified to third order as in (3.25). However, when external ramp is not small, this simplification is not valid.

According to similar derivation process as in Chapter 3, the accurate model for constant on time V^2 control with external ramp is shown as:

$$\frac{v_o(s)}{v_c(s)} = \frac{f_s}{s_{C1}} \frac{(1-e^{-sT_{on}})(1-e^{-sT_{sw}})(1+\frac{1}{s\cdot R_L(C_{o1}+C_{o2})})}{(R_{C1}+\frac{I_{C1valley}}{s_{C1}C_{o1}}+\frac{s_e}{s_{C1}})-(R_{C1}+\frac{I_{C1valley}}{s_{C1}C_{o1}}+\frac{2s_e}{s_{C1}}-\frac{s_f}{s_{C1}}\frac{T_{sw}}{C_{o1}+C_{o2}})e^{-sT_{sw}}+\frac{s_e}{s_{C1}}e^{-2sT_{sw}}} \frac{V_{in}}{sL_s} \times \frac{R_L(R_{C1}C_{o1}\cdot s+1)}{R_L[R_{C1}C_{o1}C_{o2}s^2+(C_{o1}+C_{o2})s]+R_{C1}C_{o1}s+1} \tag{D.1}$$

According to Padé approximation, transfer function of (B.1) can be simplified as:

$$\frac{v_o(s)}{v_c(s)} \approx \frac{(R_{C1}C_{o1}s+1)(1+\frac{s}{Q_1\omega_2}+\frac{s^2}{\omega_2^2})}{(1+\frac{s}{Q\omega_2}+\frac{s^2}{\omega_2^2})(1+\frac{s}{Q_1\omega_2}+\frac{s^2}{\omega_2^2})+\frac{s_e}{s_f}T_{sw}(C_{o1}+C_{o2})s^2} \cdot \frac{1}{1+R_{C1}\frac{C_{o1}C_{o2}}{C_{o1}+C_{o2}}s} \tag{D.2}$$

where

$$Q_3 = \frac{T_{sw}}{(\frac{R_{C1}C_{o1}^{\ 2}}{C_{o1}+C_{o2}} - \frac{T_{on}}{2})\pi}$$

$$Q_1 = \frac{2}{\pi}, \quad \omega_2 = \frac{\pi}{T_{sw}}$$

Appendix E. Current Slope Variation in Average Current Mode Control

As the transfer function for average current mode control is coming from the modeling result of V^2 control, the assumption of constant current slopes are inherited. For rigorous derivation, the slope variation should be considered for control to output voltage transfer function.

To incorporate the impact coming from output voltage variation, a perturbation source is added at the output voltage part to examine the response of inductor current. The structure is shown as in Figure E.1.

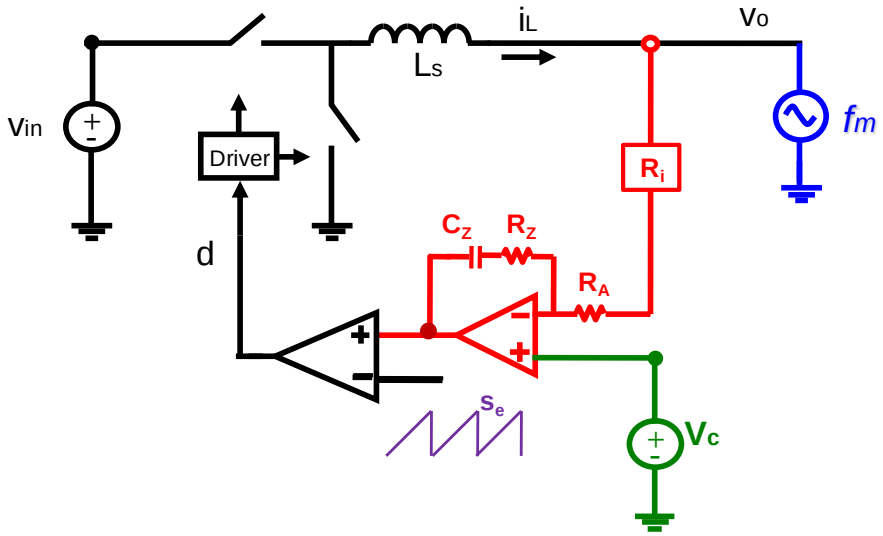

Figure E. 1 Effect of output voltage variation

Based on describing function method similar as shown in [13][14], voltage variation impact on inductor current is calculated as below:

$$FB(s) = \frac{i_L(s)}{v_o(s)} \approx -\frac{2s_e + s_n - s_f}{s_n + s_f} \frac{T_{sw}}{2L_s} \frac{R_z C_z s}{R_z C_z s + 1} \tag{E.1}$$

This effect is considered as a feedback term in control to inductor current and output voltage transfer functions [3][9].

Average current mode control with real load capacitor network is shown in Figure E.2. In Figure E.2, perturbation is injected at control signal port.

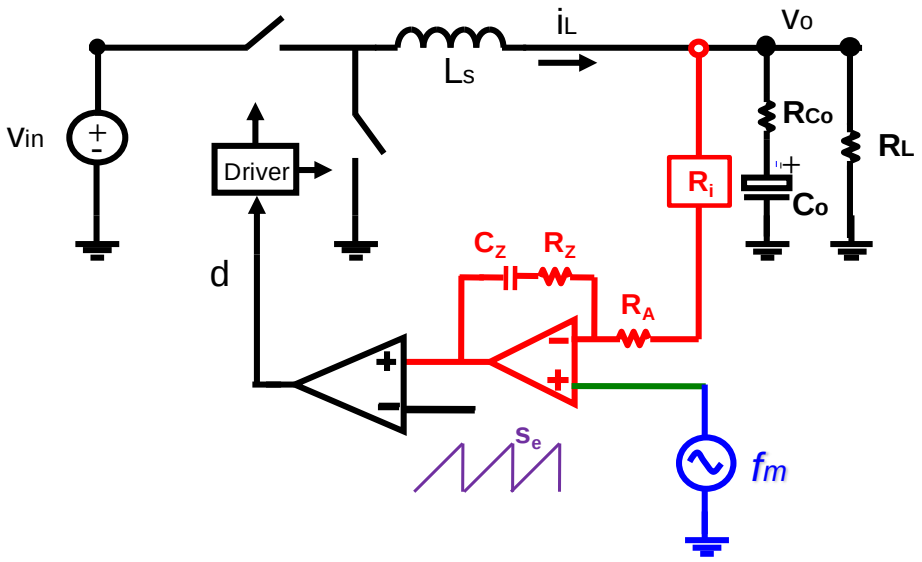

Figure E. 2 Average current mode control with load RC network

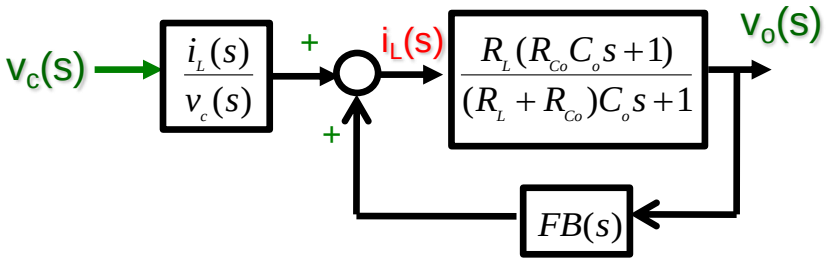

Figure E. 3 Complete model for average current mode control

Figure E.3 shows the concept of incorporating the output voltage variation effect as a feedback term. So the complete transfer function from control signal to output voltage is:

$$\frac{v_o(s)}{v_c(s)} = \frac{\frac{i_L(s)}{v_c(s)}\frac{R_L(R_{Co}C_o s+1)}{(R_L+R_{Co})C_o s+1}}{1-FB(s)\frac{R_L(R_{Co}C_o s+1)}{(R_L+R_{Co})C_o s+1}} \tag{E.2}$$

The feedback term coming from output voltage variation makes the transfer function very complicated. We look into transfer function (E.2) and try to simplify the result. The magnitude of the feedback effect in the denominator is examined:

$$FB(s)\frac{R_L(R_{Co}C_o s+1)}{(R_L+R_{Co})C_o s+1} = -\frac{2s_e+s_n-s_f}{s_n+s_f}\frac{T_{sw}}{2L_s}\frac{R_z C_z s}{R_z C_z s+1}\frac{R_L(R_{Co}C_o s+1)}{(R_L+R_{Co})C_o s+1} \tag{E.3}$$

Bode plot of equation (E.3) is shown as below:

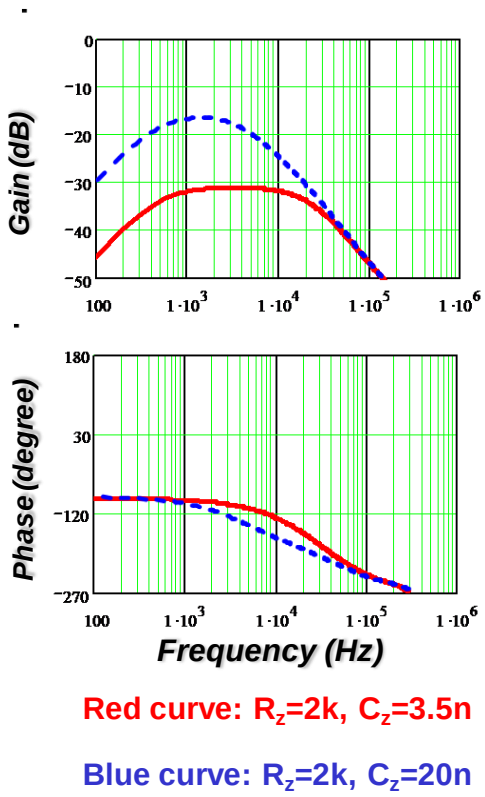

Figure E. 4 Impact of the feedback effect coming from output voltage variation

From Figure E.4, we know the impact from output voltage variation is small because the gain is much smaller than 0dB. However, the feedback term may have small impact in low frequency range when the compensator zero is in very low frequency range just as the blue curve in Figure E.4.

To simplify the modeling result of control to output voltage transfer function, the feedback term from output voltage is ignored. Equation (E.3) can be simplified as the same as (4.11):

$$\frac{v_o(s)}{v_c(s)} \approx \frac{i_L(s)}{v_c(s)} \frac{R_L(R_{Co}C_o s+1)}{(R_L+R_{Co})C_o s+1} = \frac{v_{com}(s)}{v_{c1}(s)} \frac{(R_A+R_Z)C_Z s}{R_i(R_Z C_Z s+1)} \cdot \frac{R_L(R_{Co}C_o s+1)}{(R_L+R_{Co})C_o s+1} \quad \text{(E.4)}$$

References

[1] Shi-Ping Hsu, A. Brown, L. Rensink, R. Middlebrook, “Modeling and analysis of switching dc to dc converters in constant frequency current programmed mode,” PESC 79 Record, pp 284-301

[2] Fred C. Lee, M. F. Mahmoud, Y. Yu, J. C. Kolecki, “Analysis and design of a standardized control module for switching regulators”, IEEE 1982

[3] R. D. Middlebrook, “Topics in Multiple-Loop Regulators and Current Mode Programming,” in *proc. IEEE PESC’85*, pp. 716-732

[4] R.D. Middlebrook, “Modeling Current-Programmed Buck and Boost Regulators,” *IEEE Trans. Power Electron.*, Vol. 4, pp. 36-52, January 1989.

[5] B. Holland, “Modelling , Analysis and Compensation of the Current-Mode Converter,” in *proc. POWERCON’84*, paper H-2.

[6] A. S. Kislovski, “Current-Mode Control: A Unified Model for Open-loop Stability,” in proc. IEEE APEC’91, pp. 459-465.

[7] V. Voqkrian, “Analysis of current-mode controlled PWM converters using the model of the current-controlled PWM switch,” in *proc. PCIM Con’90*.

[8] R. Redl and N. O. Sokal, “Current-mode control, five different types, used with the three basic classes of power converters: small-signal ac and large-signal dc characterization, stability requirements, and implementation of practical circuits,” in *Proc. IEEE PESC’85*, pp. 771-785.

[9] R. B. Ridley, “A new, continuous-time model for current-mode control,” *IEEE Trans. Power Electron.,* vol. 6, no. 2, pp. 271-280, April 1991.

[10] R. B. Ridley, “A new continuous-time model for current-mode control with constant frequency, constant on-time, and constant off-time, in CCM and DCM,” in *proc. IEEE PESC’90*, pp. 382- 389.

[11] W. Tang, F. C. Lee, R. B. Ridley, and I. Cohen, “Charge control: modeling, analysis, and design,” *IEEE Trans. Power Electron.,* vol. 8, pp. 396-403, Oct. 1993.

[12] W. Tang, F. C. Lee, and R. B. Ridley, “Small-signal modeling of average current-mode control,” *IEEE Trans. Power Electron.,* vol. 8, pp. 112-119, April 1993.

[13] Jian Li, Fred C. Lee, “New modeling approach and equivalent circuit representation for current mode control” *IEEE Trans*, 2010

[14] Jian Li, “Current mode control: modeling and its digital application”. PH. D. dissertation, 2009

[15] D. Goder and W. R. Pelletier, “V^2 architecture provides ultra-fast transient response in switch mode power supplies," in p*roc. HFPC’96*, pp. 19-23.

[16] D. Goder, “Switching regulators,” U.S. Patent, 5,770,940, 1998.

[17] W. Huang and J. Clarkin, “Analysis and design of multiphase synchronous buck converter with enhanced V^2 control,” in *Proc. HFPC’00*, 2000, pp. 74–81.

[18] S. Qu, “Modeling and design considerations of V^2 controlled buck regulator,” in *Proc. IEEE APEC’01,* Anaheim, California, pp. 507–513.

[19]Jian Li, Fred C. Lee, “Modeling of V^2 current mode control”, IEEE Trans, 2010

[20] R. Redl, J. Sun, “Ripple-based control of switching regulators-An overview”, IEEE Trans, 2009

[21] Maxim, Max17000 datasheet

[22] Texas Instruments, TPS51116 datasheet

[23] National semiconductor, LM2696 datasheet

[24] Intersil Corporation, ISL6237 datasheet

[25] On semiconductor, CS5157 datasheet

[26] Lloyd Dixon, “Average current mode control of switching power supplies”, Unitrode application note, 1990

[27] Jay Rajagopalan, Fred C. Lee, Paolo Nora, “A general technique for derivation of average current mode control laws for single-phase-power-factor-correction circuits without input voltage sensing”, IEEE Trans, 1999

[28] Maxim, MAX16818 datasheet

[29] Linear Tech, LT3743 datasheet

[30] G. C. Verghese, C. A. Bruzos, K. N. Mahabir, "Averaged and sampled-data models for current mode control: A reexamination", PESC 1989

[31] Jian Sun, Richard M. Bass,"A new approach to averaged modeling of PWM converters with current-mode control", IECON 1997

[32] A. R. Brown and R. D. Middlebrook, “Sample-Data Modeling of Switched Regulators,” *IEEE Power Electronics Specialists Conference*, 1981 Record, pp. 349-369.

[33] D. M. Mitchell, “Pulse width modulator phase shift.” *IEEE Trans. Power Electron.*, vol. AES-16, pp. 272-278, May 1980.

[34] R. D. Middlebrook, “Predicting modulator phase lag in PWM converter feedback loops,” In *proc. POWERCON’ 81*, paper H-4.

[35] J. Sun, “Small-signal modeling of variable-frequency pulsewidth modulators,” *IEEE Trans. Aerosp.*, vol 38, pp. 1104-108, July 2002.

[36] Feng Yu, Fred C. Lee, "Design oriented model for constant on-time V^2 control", *IEEE ECCE* 2009

[37] Jian Sun, "Characterization and performance comparison of ripple-based control for voltage regulator modules", *IEEE trans* 2006

[38] Yu-Huei Lee, Shih-Jung Wang, Ke-Horng Chen, "Quadratic differential and integration technique in V^2 control buck converter with small ESR capacitor", *IEEE Trans*, 2010

[39] Julu Sun, “Investigation of Alternative Power Architectures for CPU Voltage Regulators,” Ph.D. Dissertation, Virginia Tech 2008.

[40] Julu Sun, Ming Xu and Fred C. Lee, “High Power Density, High Efficiency System Two-stage Power Architecture for Laptop Computers,” in *IEEE PESC* 2006.

[41] Pengjie Lai,"Improvement of Sigma Voltage Regulator-A new power architecture", Master thesis, Virginia Tech, 2010

[42] J. Lam, “Balanced realization of Padé approximants of e-*sT*,” *IEEE Trans. Automat Contr*., vol. 36, no. 9, pp. 1096-1100, Sep. 1991.

[43] Puqi Li, “Modeling average-current-mode-controlled multi-phase buck converters”, PESC 2008

[44] Philip Cooke, “Modeling average current mode control”, APEC 2000

[45] Chunxiao Sun, Brad Lehman, Rosa Ciprian, “Dynamic modeling and control in average current mode controlled PWM DC/DC converters”, PESC 1999

[46] Maxim, “DC-DC controllers use average-current-mode control for infotainment applications”, Application note 3939

[47] Jian Sun, Richard M. Bass, “Modeling and practical design issues for average current control”, APEC 1999

[48] Chunxiao Sun, Brad Lehman, Jian Sun, “Ripple effects on small signal models in average current mode control”, APEC 2000

[48] Young-Seok Jung, Jun-Young Lee, Myung-Joong Youn, “A new small signal modeling of average current mode control”, PESC 1998

[49] Puqi Li, Tony O’Brien, John Lee, John Beecroft, “A unified small signal analysis of DC-DC converters with average current mode control”, ECCE 2009

[50] K. D. Purton, R. P. Lisner, “Average current mode control in power electronic converters-analog versus digital”, AUPEC 2002

[51] Kaiwei Yao,”High-frequency and high-performance VRM design for the next generations of processors”, Ph.D dissertation, Virginia Tech, 2004

[52] Richard C. Dorf, Robert H. Bishop (2001). *Modern Control Systems, 9th Edition*. Prentice Hall. ISBN 0-13-030660-6.

[53] Yang Qiu, “High-frequency modeling and analyses for buck and multiphase buck converters”, Ph. D dissertation, Virginia Tech, 2005

[54] Jia Wei, "High frequency high efficiency voltage regulators for future microprocessors", Ph. D dissertation, Virginia Tech, 2004